MICHIGAN STATE UNIVERSITY

CYCLOTRON PROJECT*

Effects of Field Imperfections on Radial Stability

M. M. Gordon and W. S. Hudec

November 1961

Department of Physics

East Lansing, Michigan

---

*Research Supported in part by U. S. Atomic Energy Commission Contract AT(11-1)-872

EFFECTS OF FIELD IMPERFECTIONS ON RADIAL STABILITY

by

M.M. Gordon and W.S. Hudec*

November 1961
Department of Physics
East Lansing, Michigan

Research Supported in part by U.S. Atomic Energy Commission Contract AT (1101) - 872

* Parts of this report represent work done for the M.S. degree thesis requirements.

TABLE OF CONTENTS

Note: All figures pertaining to a given chapter are located, in order, at the end of the chapter.

INTRODUCTION AND SUMMARY

In a medium energy three-sector cyclotron the value of ν_r is always close to unity. As a result of the $\nu_r=3/3$ non-linear resonance [1,2]* the radial motion of the particles has stability limits which may be rather stringent. A substantial amount of computer calculation has been carried out on machines of this type which indicate that these stability limits are sufficiently large for machines with weak-spiral [3,4]. A theoretical analysis of the orbit properties in a three-sector cyclotron, including the 3/3 non-linear resonance, has been carried out by Smith and Garren [5], and by Verster and Hagedoorn [6]. The results of this work are in good agreement with data obtained from computer studies [7,8].

Since the radial stability of the particles is rather limited, and since ν_r is close to unity, it is clear that the situation could be severely aggravated by the presence of relatively weak imperfection fields ("field bumps"). The present report presents the results of a study made of this problem. These results should be

---

* References will be given in square brackets, and all references will be listed at the end of this report.

helpful in establishing limits on the size of imperfection fields of particular types which can be tolerated for a given three-sector geometry. At the same time, these results re-emphasize the importance of using a three-sector geometry with as little spiral as possible.

A theoretical treatment of the effects of a field bump on the N/3 resonance was first given by L.J. Laslett and K.R. Symon [9] and by Laslett and S.J. Wolfson [10] at MURA in connection with a scheme for achieving beam injection into a synchrotron. A subsequent analysis was carried out by M.M. Gordon of the effects of a one-sector and two-sector field bump on the 3/3 resonance, which was less quantitative than the present work reported here, but which also included in the calculation the effects on the three outer stable fixed points associated with the edge region of the magnetic field [11]. The purpose of that work was to help clarify and interpret the results of the computer studies on a resonant beam extraction scheme being investigated at this laboratory [12]. Further analyses of this problem have been carried out by T.K. Khoe [13] and L. Teng [14]. The results of the present study can also be used for calculation of the strength and angular position of a field bump required for effective resonant beam extraction, provided ν_r is sufficiently close to unity

such that the three unstable fixed point orbits are substantially closer to the equilibrium orbit than are the three outer stable fixed point orbits. The extension of the present results so as to incorporate the three outer stable fixed points into the theory should be fairly straightforward.

The two main perturbations of the radial oscillations produced by field imperfections are the one-sector perturbation and the two-sector gradient perturbation. The effect of these perturbations is to reduce the size of the stability limits; and when sufficiently strong, to completely destroy the stability. In the absence of any field imperfections, the stability limits are defined by the three unstable fixed point orbits associated with the 3/3 resonance. These perturbations cause one or more of these unstable fixed point orbits and the equilibrium orbit to move toward each other; the new stability limit is then defined by the displaced equilibrium orbit and the nearest unstable fixed point orbit. When the field imperfection is strong enough to cause the equilibrium orbit to merge with one of the unstable fixed point orbits, the stability limit goes to zero. An alternative picture of how the loss of stability arises is that the imperfection field produces a shift in the equilibrium

orbit and a change in the linear oscillation frequency about this orbit which tends toward the $\nu_r=2/2$ stop-band. A one-sector perturbation is produced mainly by the field imperfection component having frequency n=1, and to a lesser extent by those components having frequencies n=2 and n=4 through coupling with the three-sector structure of the equilibrium orbit and of the alternating-gradient modulation of the linear oscillations. The two-sector gradient perturbation is produced mainly by the imperfection field harmonic with n=2, and again, to a lesser extent by those harmonics with n=1 and n=5. The one-sector perturbation produced by the harmonics given above can arise not only from the values themselves but also from their first derivatives; in the same way, the two-sector gradient perturbation can result not only from the first derivative of the field harmonics but also from the zeroth and second derivatives.

There are two properties of the main three-sector field which determine the sensitivity of the orbits to field imperfections of a given size. These are the values of (ν_r-1) and the values of a quantity called A_o, which is essentially the (first harmonic) amplitude of the displacement of one of the unstable fixed point orbits from the equilibrium orbit in the absence of any field

imperfections. In the case of a one-sector perturbation, the magnitude of the field imperfection which will completely destroy the stability ("critical bump strength") is essentially proportional to $(\nu_r-1)A_o$; and for a two-sector gradient perturbation, the critical bump strength is essentially proportional to (ν_r-1). Thus if one or both of the parameters is small, the radial stability will be quite sensitive to small field imperfections of the kind described above. The values of (ν_r-1) for a three-sector geometry with weak-spiral are consistently larger, though not by a large factor, than those of a comparable three-sector geometry with moderate-spiral; moreover, the values of A_o in the former case are significantly greater than those in the latter case. As a result, a three-sector field with moderate-spiral is very sensitive to relatively small field imperfections; in the case of a tight-spiral design, the situation would be completely intolerable. H.G. Blosser and K. Kosaka [15] carried out a series of computer studies in the spring of 1961 at this laboratory on the relative merits of two different three-sector fields, one with weak-spiral and one with moderate-spiral; in the course of these investigations, an exploratory study was made of the effects of a flat one-sector bump on stability which brought out the

essential features of the results noted above. It was these exploratory computer results which furnished the direct motivation for the work presented here.

In Chapter I a discussion is presented of the three-sector fields (B26.29A and B26A1) upon which the computer results of this study given in Chapter III are based. One of these fields (B26.29A) is essentially the same as the weak-spiral three-sector field used in many other studies at this laboratory [16]; the other field (B26A1) of moderate-spiral was so constructed that it has half the flutter of B26.29A and a compensating increase in spiral so as to yield comparable values for ν_z. Output data from the Equilibrium Orbit Code [17,18] is presented giving essential properties of the equilibrium orbit and of the linear radial and axial oscillations about this orbit as a function of energy. These data are not significantly different for the two fields considered. Additional data from the Fixed Point Code [17] is also presented which leads to the evaluation of the radial stability limits as a function of energy in the absence of a field bump; in this case the stability limits for the weak-spiral field (B26.29A) are substantially larger at almost all energies than for the moderate-spiral field (B26A1).

The theory of the effects of field imperfections is

presented in Chapter II. Instead of the usual radial displacement variable $x=x(\theta)$, the theory in section 1 of Chapter II is formulated in terms of the variable $y=y(\phi)$ which reduces the linear oscillations to simple harmonic motion of frequency ν_r. It is then shown that the predominant first harmonic component of $x(\theta)$ is to a good approximation equal to the first harmonic component of $y(\phi)$; as a result, the theory is then formulated entirely in terms of the first harmonic (or "quasi-first harmonic") component of $y(\phi)$. The non-linear resonance driving force associated with the 3/3 resonance is introduced in a simple, semi-empirical way such that the correct first harmonic component for the unstable fixed point orbits is obtained. The one-sector and two-sector gradient perturbation forces are then introduced into the differential equation for $y(\phi)$ and the resultant equations for the first harmonic component of the displaced fixed point orbits are then derived as well as the equation for the approximate invariant associated with the motion of the phase space points. In section 2 of this chapter the effect of the one-sector perturbation acting by itself is considered. Explicit equations are obtained for the displacement of the fixed point orbits as a function of the perturbation strength, in the two extreme cases of

"pure one-corner opening" and "pure two-corner opening" of the stability triangle. Equations for the critical bump strengths and values for the required phases of the perturbation are obtained in each case. In section 3 of Chapter II the same results are derived for a two-sector gradient perturbation acting by itself. In section 4 a simple, semi-quantitative result is obtained for the critical perturbation strengths when both the one-sector and two-sector gradient perturbations are present simultaneously. This result is based on the calculation of the linear oscillation frequency about the displaced equilibrium orbit. All these theoretical considerations are based on a representation of the perturbations by a strength and phase parameter; in section 5 it is shown how these parameters can be evaluated in terms of the physical properties of a given field bump and explicit formulae are given for carrying this out.

In Chapter III results of computer computations relative to the effects of certain field bumps on the fields B26.29A and B26A1 are presented and a comparison is made with the theoretical predictions of Chapter II. The following four types of field bumps are considered: 1. a flat one-sector bump; 2. a flat two-sector bump; 3. a flat four-sector bump; and 4. a two-sector gradient

bump. For each type of field bump a series of static (non-accelerated) phase plots are given for different bump strengths which exhibit the changes in fixed point locations and the stability limits. For ease of comparison all phase plots are at the same energy for each field so chosen such that the stability limits are near their maximum in the absence of any field perturbations. For each of these field bumps the predictions of the theory are in reasonably good quantitative agreement in practically all cases with the computer results as concerns:
1. the corners of the stability triangle which open;
2. the relative displacement of the fixed points; and also 3. the critical bump strengths required. In addition, for the flat one-sector bump a detailed comparison is carried out between the computed first harmonic components of the fixed point orbits and the theoretical predictions of section 2, Chapter II. In this case the quantitative agreement between theory and computer results is very good.

In the Appendix of this work some of the results of Chapter II are extended to include a cyclotron field having four-sector geometry.

A note of thanks is in order to Mr. Stan Steinberg for his skillful help with some of the computer calculations.

CHAPTER I

THREE-SECTOR FIELD INFORMATION

Following a brief exposition of the field notation and cyclotron units used in this report, this chapter presents a discussion of the genesis of the two different three-sector fields which are used in the computer studies to be described in Chapter III. One of the fields (B26.29A) is a weak-spiral geometry closely related to the fields used in other studies at this laboratory; the other field (B26A1) corresponds to a moderate-spiral geometry, which is introduced for comparative purposes. Both fields have been limited to just one harmonic in addition to the average field. Output data from the Equilibrium Orbit (E.O.) Code is presented giving the radial and axial focusing frequencies (ν_r and ν_z), the mean radius of the equilibrium orbit (R) and the fractional phase slip per turn ($\Delta\phi/2\pi$), all as a function of energy (E). Further data is presented from the Fixed Point Code giving the (r, p_r) coordinates of the three unstable fixed point orbits relative to the E.O. (at $\theta=0$) again as a function of energy. Using this data phase space diagrams are then given which show the evolution of the triangular stability region with energy; it is

clear from these diagrams that the stability limits for the weak-spiral field are substantially larger than those for the moderate-spiral field at practically all energies.

1. Median Plane Magnetic Field Notation.

In polar coordinates, the median plane magnetic field in a sector-focused cyclotron is specified by:

$$B(r,\theta) = B_o(r) + B_f(r,\theta), \qquad (1.1)$$

where $B_o(r)$ is the average magnetic field and $B_f(r,\theta)$ is the flutter field which averages to zero over θ. For a three-sector geometry, the flutter field may be expressed as follows:

$$B_f(r,\theta) = \sum_{n>o} B_n(r) \cos 3n [\theta - \zeta_n(r)], \qquad (1.2)$$

where $B_n(r)$ is the amplitude of the nth harmonic and $\zeta_n(r)$ is the spiral angle for that harmonic. To accomodate the computer codes used at Michigan State University, this expression is rewritten as follows:

$$B_f(r,\theta) = \sum_{n>o} [H_n(r) \cos 3n\theta + G_n(r) \sin 3n\theta],$$

where $H_n(r)$ and $G_n(r)$ the Fourier coefficients of the nth harmonic, are then given by:

$$H_n(r) = B_n(r) \cos 3n\zeta_n(r), \quad G_n(r) = B_n(r) \sin 3n\zeta_n(r). \qquad (1.3)$$

2. Cyclotron Units.

Output data from the computer programs to be described in this report are all in cyclotron units except for the kinetic energy (E) which is in Mev. The unit of magnetic field b is given as:

$$b = \frac{m_o \omega}{e},$$

where b is the value of the isochronous magnetic field at r=0, $\omega = 2\pi\nu_o$ where ν_o is the frequency of the r-f system, and m_o and e are the rest mass and charge of the particle (in this case the proton). The field unit b is obtained from a combination of measured magnetic field values and the isochronous $B_o(r)$ as derived from the Isochronism Code [18,19]. The cyclotron length unit a is defined as:

$$a \equiv c/\omega,$$

where c is the speed of light; therefore, $ba = (m_o c)/e$. For the fields under consideration, b = 13.63 kilogauss is the cyclotron field unit; therefore, the cyclotron length unit is given by:

$$a = 90.4".$$

b = 13.63 kilogauss	= 1 cyclotron unit
a = 90.4"	= 1 cyclotron unit

All field and length units used in this report are expressed in terms of b and a and are called cyclotron units (abbreviated "c.u."). All momenta (e.g., p_r and p_x) in this report are in $m_o c$ units.

3. Field Data on B26.29A and B26A1.

This report employs two fields, B26.29A and B26A1. Consider first the field B26.29A; this measured field was obtained from B26, a field which has been studied a great deal at Michigan State University, and which is described in detail elsewhere [16]. The Fourier coefficients, $H_n(r)$ and $G_n(r)$, from B26 were "smoothed" by a process used and perfected at ORNL [20]; this "smoothing" process eliminated the small fluctuations in the flutter amplitude caused by measuring errors. Then, the values of $B_o(r)$ were made highly isochronous; the new field was designated B26.29. The field to be considered here, B26.29A, is identical to B26.29 except all harmonics higher than the first have been removed in order to save computer time.

In order to justify the removal of the higher harmonics in the field B26.29A, a comparison was made of pertinent orbit properties for this field and for the original field B26.29. Below is part of the print-out of the E.O. Code data from B26.29 and B26.29A; the data indicates the

small effect the removal of the higher harmonics has on such results.

	E(Mev)	R	$\frac{\Delta\phi}{2\pi}$	ν_r	ν_z
B26.29	20	+.20212	+.00004413	+1.05513	+0.25102
B26.29A	20	+.20206	-.00006334	+1.05638	+0.25326

A further comparison of the similarity in results from B26.29 and B26.29A may be obtained from the two quantities x and p_x defined as:

$$x = r - r(E.O.), \text{ and } p_x = p_r - p_r(E.O.),$$

where the (r,p_r) coordinates are those for one of the fixed points and $r(E.O.)$ and $p_r(E.O.)$ are the corresponding coordinates for the E.O. At 20 Mev, the following results are obtained for the two fields.

	x	p_x
B26.29	+.05515	+.05245
B26.29A	+.05713	+.04794

A comparison of the E.O. Code data and Fixed Point Code data at other energies yields similar relative results for B26.29 and B26.29A. It was concluded that removal of the higher harmonics in B26.29 would have little effect as far as the features of interest in this study are concerned.

Field B26.29A has a total spiral angle of approximately 20° over the pole radius of 32"; this is considered a weak-spiral geometry. Further investigation of B26.29A leads to the conclusion that axial focusing is produced mainly by the strong flutter field which at its maximum is about .4 the magnitude of $B_o(r)$; very little (less than 10%) of the axial focusing is due to the spiral. Fig. 1 shows $B_o(r)$, $B_1(r)$, and $\zeta_1(r)$ for B26.29A as a function of radius in c.u. The figure shows that $\zeta_1(r)$ is very nearly linear over the radius of the pole tip.

As was previously mentioned, B26.29A derived most of its axial focusing from a strong flutter field. It was decided to construct a second field (labeled B26A1) with half the flutter and a compensating increase in spiral in order to evaluate the effect of spiral on the features of interest. Unlike B26.29A, B26A1 obtains a good part of its axial focusing from its moderate-spiral angle pitch. A comparison of the results from the two fields, both with and without a field bump present, shows clearly the effect of spiral or radial stability.

The field B26A1 like B26.29A had its origin in B26. To obtain $B_1(r)$ for B26A1, all the $B_1(r)$ values in B26 were arbitrarily reduced by a factor of one-half. To compensate for the loss in focusing due to the decrease in

the flutter amplitude, the spiral angle $\zeta_1(r)$ was increased. From Fig. 1, it is seen that $\zeta_1(r)$ for B26.29A is nearly linear with r over most of the machine; because of this, a function $\zeta_1(r)$ was chosen for B26A1 that is nearly linear with r and at the same time goes to zero as r^2 at the center of the machine; this function is given as follows:

$$\zeta_1(r) = \frac{\zeta_o r^2}{\sqrt{r^2+g^2}}, \qquad (1.4)$$

where ζ_o is a parameter determining the strength of the spiral and g is a parameter presumably related to the gap width. To have $\zeta_1(r)$ nearly linear with r to relatively small r values, g was arbitrarily chosen as: g=.01c.u. The following approximate formula was used to calculate ζ_o:

$$\nu_z^2 = -r^2 + 1/2\ (B_1/B_o)^2\ [1 + 2(\zeta_o r)^2], \qquad (1.5)$$

where r is in c.u. (this is a much simplified version of the "smooth approximation" formula). Since ν_z increases with r in this case it was somewhat arbitrarily decided to set ν_z=.2 for r=.3 in this formula and solved for the resultant value of ζ_o; the value so obtained was:

$$\zeta_o = 5.91.$$

The resultant $\zeta_1(r)$ was then used to determine $H_1(r)$ and

$G_1(r)$ using the relations in Eq. (1.3) and the value of $B_1(r)$ obtained from the field data. These Fourier coefficients were then used in the Isochronism Code to determine an isochronous $B_o(r)$; the resulting functions $B_o(r)$, $B_1(r)$ and $\zeta_1(r)$ are shown in Fig. 2 as a function of radius. It is these functions which specify the moderate-spiral field B26A1 considered in this report. Note that the value of ν_z given by the above formula is not very accurate; however it provides a reasonably accurate method of determining ζ_o, the actual value of which is justified only by the resultant values of ν_z obtained from the E.O. Code (discussed below) which are considered quite satisfactory.

Figs. 1 and 2 show that the values of $B_o(r)$ for the two fields are very nearly the same and that $B_1(r)$ in B26A1 is one-half the flutter amplitude used in B26.29A. Also the value $d\zeta_1/dr$ is about 6.5 times greater in magnitude for field B26A1. It was quite by accident that $d\zeta_1/dr$ has opposite signs so that the two fields have opposite spiral directions; however, the direction of the spiral has no effect on the data associated with the E.O. and fixed points. The radius of the pole tip is indicated in both figures.

4. Equilibrium Orbit Code Data.

Fig. 3 is a plot of an exact ν_z as a function of energy for B26A1 and B26.29A. The sharp rise in ν_z at low energies (small radius values) is due to the rapid rise in the flutter amplitude near the center of the machine; this holds true for B26A1 and B26.29A. The rapid rise in the flutter amplitude near the center of the machine is followed by a flattening in $B_1(r)$ and then, a sharp drop in $B_1(r)$ near the edge of the magnet for both fields. Corresponding to the flattening of $B_1(r)$, the ν_z curve for B26.29A is also flat because the spiral is quite small; in the case of B26A1, ν_z rises slowly from 10 Mev to 30 Mev because of the substantial linear spiral in this case. In the case of both fields, a sharp rise is noted in ν_z near the edge of the magnet; this rise in ν_z is due primarily to the drop in $B_o(r)$ near the edge of the magnet (see Figs. 1 and 2). The values of ν_z for B26A1 are consistently lower than those of B26.29A; however, the axial focusing in the case of B26A1 is clearly adequate.

Fig. 4 is a plot of (ν_r-1) as a function of energy for both fields. The rapid rise in (ν_r-1) at small radii is due to the rapid rise in $B_1(r)$ near the center of the machine; this rapid rise is most significant for the field

B26.29A. The sharp drop in (ν_r-1) at high energies is due mainly to the decrease in $B_o(r)$ near the edge of the magnet and is evident for both fields. For B26A1, (ν_r-1) has nearly a constant slope from 6 Mev to 30 Mev; this is due to k (introduced below) being nearly linear with energy here and also to the fact that the linear spiral contributes a significant term to ν_r which is likewise linear with energy. A corresponding rise in ν_r-1 is not noticed for B26.29A because the spiral is small and the main contribution to ν_r comes from the large (relatively flat) $B_1(r)$ in the intermediate region of the machine. Note that the values of (ν_r-1) for B26.29A are consistently larger than those for B26A1; this difference is quite significant in the low energy region as far as radial stability (with and without a field bump) is concerned.

Over the range of r values where $B_o(r)$ is isochronous,

$$E \cong 1/2\ m_o c^2(v^2/c^2) \cong 938.2\ \text{Mev}\ (1/2\ R^2), \qquad (1.6)$$

since $v/c \cong R(\text{c.u.})$ is not too large. Eq. (1.6) states that over the isochronous part of the field, the energy is approximately linear with the square of the mean radius of the E.O. Fig. 5 is a plot of R^2 versus energy for both

fields using the data from the E.O. Code and also a straight line obtained by assuming Eq. (1.6) is exactly correct; the nearly linear dependence between energy and R^2 is quite evident.

The E.O. Code also prints out the fractional phase slip per revolution. Below is the average value of the fractional phase slip per revolution for B26A1 and B26.29A over the energy range from 0 Mev to 30 Mev. For energies greater than this, the fields are not isochronous and the phase slip increases rapidly; that is, the Isochronism Code renders $B_o(r)$ isochronous only out to a pre-assigned radius (r=.26), thereafter, $B_o(r)$ falls off with r as determined by the model magnet measurments (see Figs. 1 and 2).

	Average Fractional Phase Slip Turn $\left\lvert\frac{\Delta\bar{\phi}}{2\pi}\right\rvert$
B26.29A	5.00×10^{-5}
B26A1	2.43×10^{-4}

The fractional phase slip per revolution is nearly four times greater in B26A1 but is still quite small. In both cases, the degree of isochronism is quite good enough for the purpose of the investigations carried out in this report.

5. Fixed Point Data.

Since ν_r is close to unity, the significant fixed point orbits are those orbits which close smoothly on themselves after one revolution; that is, the particle is in the fixed point orbit if and only if the values of (r, p_r) at the beginning and end of one revolution are the same. The E.O. is distinguished from other fixed point orbits in that it is periodic in one-sector (in the absence of a field bump).

The Fixed Point Code is the same as the E.O. Code except for the addition of an overwrite. To find a fixed point at one energy, the code must be given an initial reasonably good guess for (r, p_r). If one fixed point is to be found at a number of energies, a minimum of two guesses must be given the code. The code will use the first guess to determine the one fixed point at the first energy; it then uses the second guess to find the fixed point at the second energy; the code then extrapolates from the values found to determine a guess for the fixed point at the third and all subsequent energies. The Fixed Point Code prints out at equally spaced energies the same data about the fixed point orbit as the E.O. Code prints out for the E.O. (see above).

This report is concerned with the three unstable fixed points in (r, p_r) phase space because the triangular region determined by these three fixed points as vertices approximately outlines the stable region in this phase space; the E.O. fixed point lies close to the center of this triangular region. Any particle started with a (r, p_r) value well within this triangle will remain near the E.O. on all subsequent revolutions. All particles given initial conditions outside the triangular region will, on subsequent revolutions, tend eventually to move further and further from the E.O.; these particle orbits are, for practical purposes "unstable". Because of the three-sector symmetry of the magnetic field, only one unstable fixed point need be found at a given energy; the other two unstable fixed points can then be found with the General Orbit Code [21,18] by integrating the equations of motion for one revolution and printing out the (r, p_r) values once per sector. The error in the (r, p_r) values found by the Fixed Point Code and E.O. Code is less than 10^{-7}.

In discussing the fixed point orbits, it is convenient to introduce the coordinates x and p_x defined by:

$$x = r - r\ (\text{E.O.}) \text{ and, } p_x = p_r - p_r\ (\text{E.O.}).$$

Introduction of x and p_x places the E.O. at the origin in phase space. Fig. 6 and 7 are plots of x versus p_x for the three unstable fixed points for B26.29A at a sequence of energies covering the range of the machine; Figs. 8 and 9 are the corresponding plots for B26A1. The data for these plots was obtained from the output of the Fixed Point Code and General Orbit Code as described above. In the figures, lines were drawn connecting the fixed points at a given energy; the triangular region enclosed by the lines is the approximate stable region for that energy as noted above. The figures show how the stability limits depend on energy. The figures also show that the area of the stable region expands from zero to a maximum and then shrinks to zero again.

Fig. 10 shows the difference in size of the stable region for the two fields at comparable energies (see also Figs. 14 and 15 for static phase plots at these energies). At these energies, the distance to the fixed points is about 3 times greater for B26.29A than for B26A1. Theoretical formulae for the unstable fixed points have been worked out by Smith and Garren [5] and Verster and Hagedoorn [6]. These authors have shown that $(\nu_r - 1)$ is a factor upon which the extent of the stable region depends; the other factors involve the derivatives of

$G_1(r)$ and $H_1(r)$ and are such that for a given (ν_r-1), introduction of spiral causes a decrease in stability limits. Since for the two cases depicted in Fig. 10, (ν_r-1) differs by no more than 35% for the two fields, it can be concluded that the large difference in stability limits is primarily due to the difference in spiral. The effect of spiral on stability has been investigated for many machines with the same general result.

Figs. 6, 7, 8 and 9 indicate that the stability limits are large enough for both fields such that the beam could be successfully accelerated from the center to the extraction radius. Introduction of a bump field into the equations of motion reduces the stability limit and no conclusion on the relative performance of the two fields is possible until the effects of the bump field are investigated.

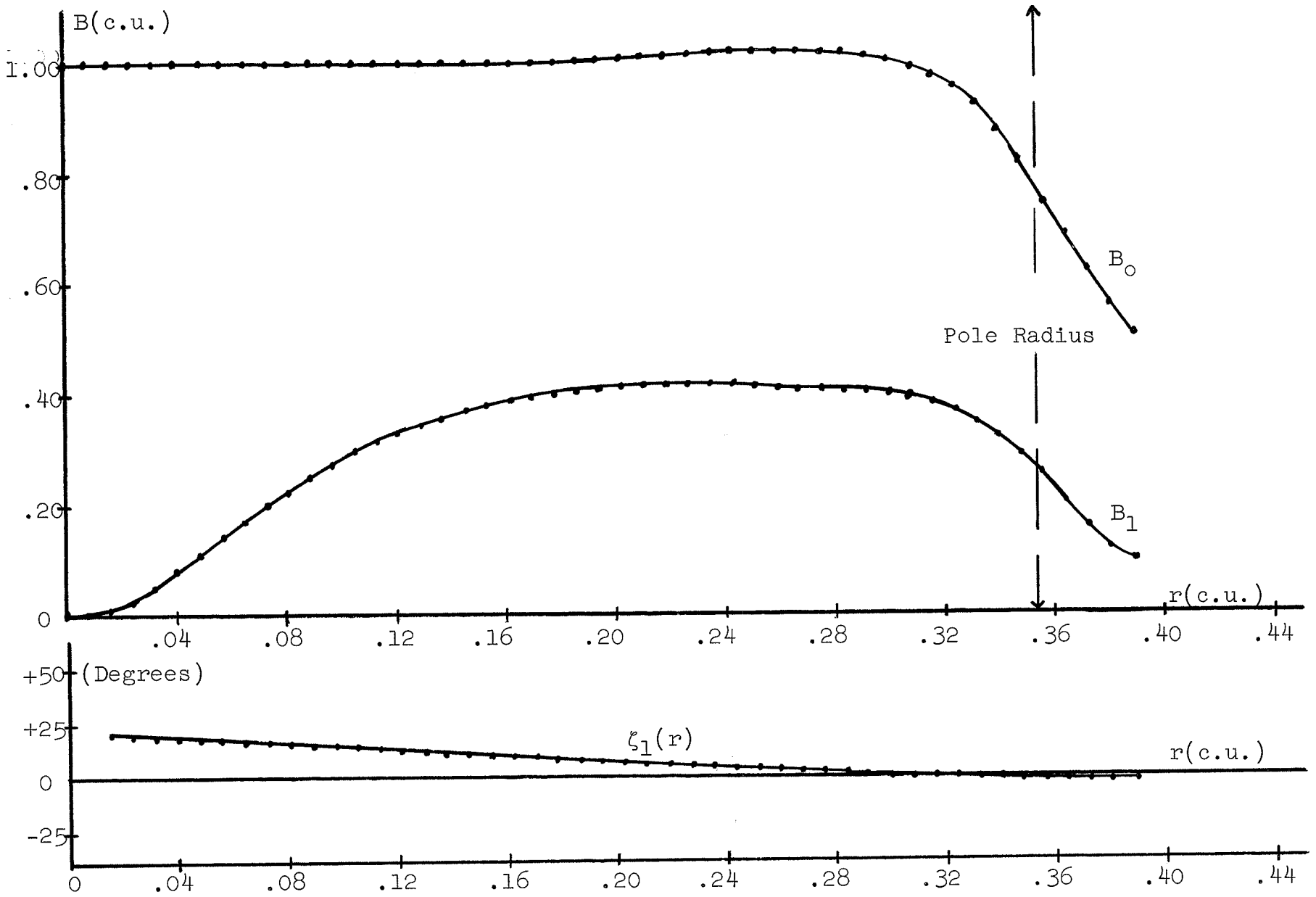

Figure 1: Average magnetic field B_o, amplitude of three-sector component B_1 and spiral angle ζ_1 as a function of r(c.u.) for field B26.29A.

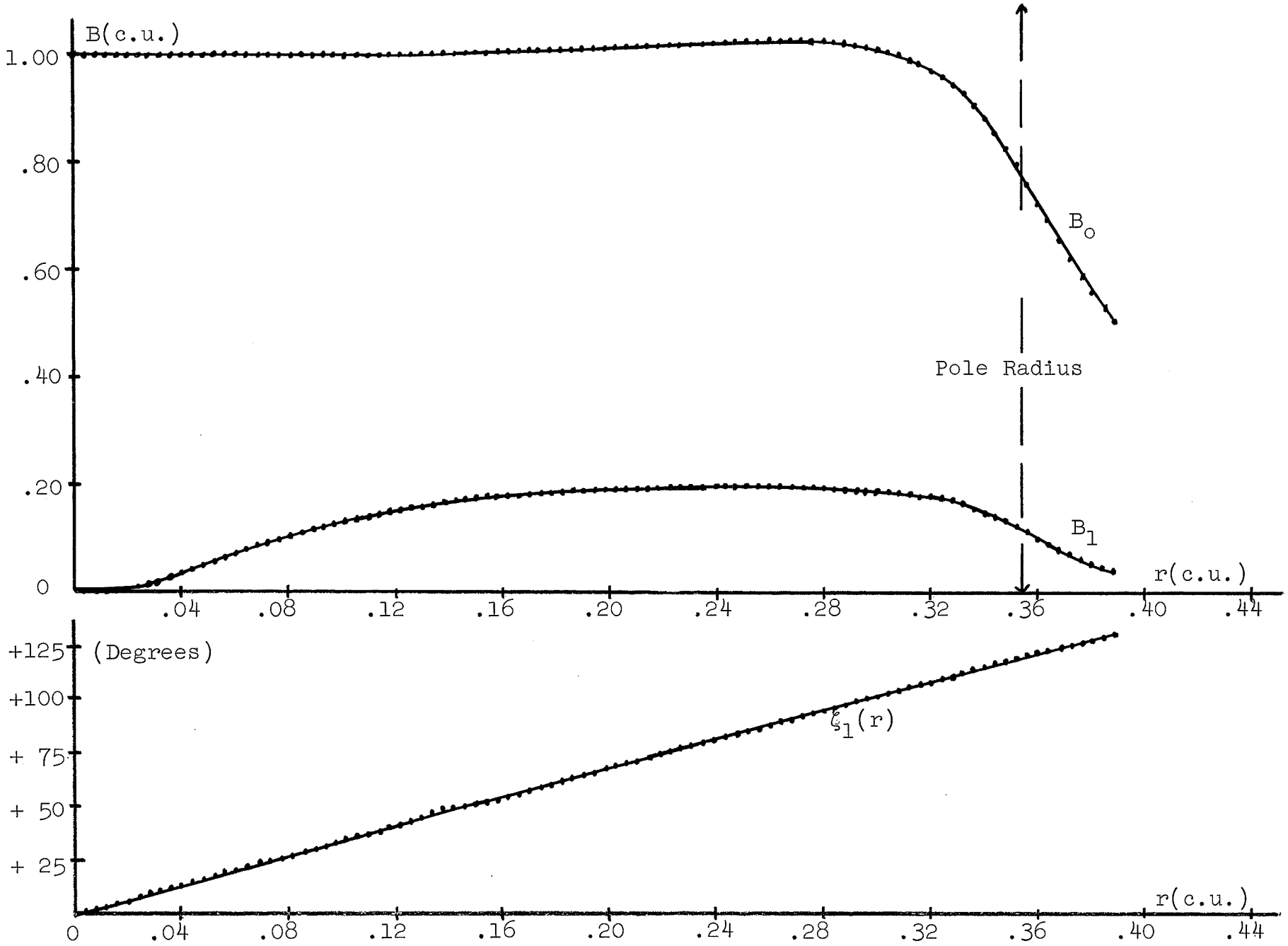

Figure 2: Average magnetic field B_o, amplitude of three-sector component, B_1 and spiral angle ζ_1 as a function of r(c.u.) for field B26A1.

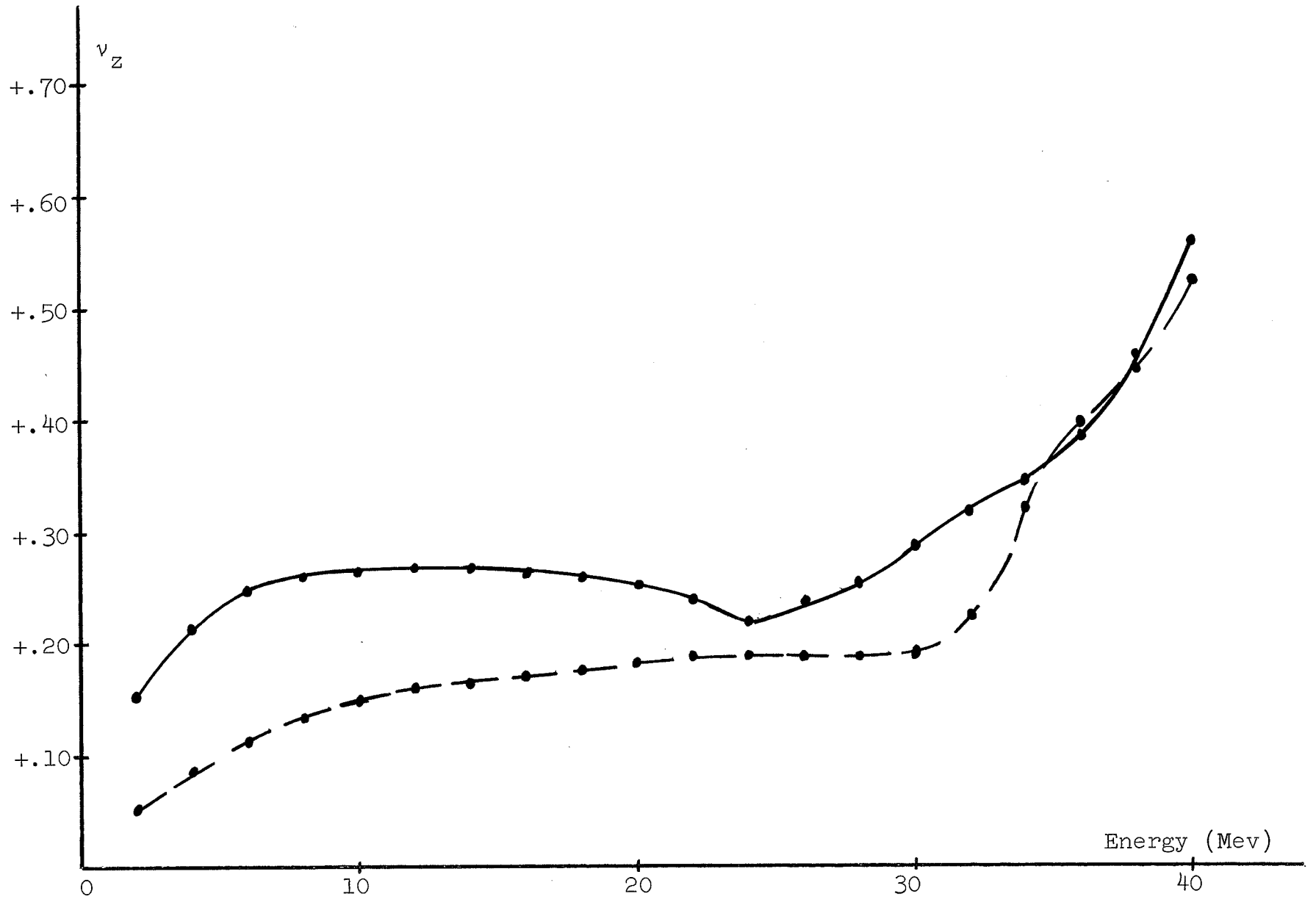

Figure 3: Axial oscillation frequency ν_z as a function of energy for field B26.29A (solid line) and for field B26A1 (broken line).

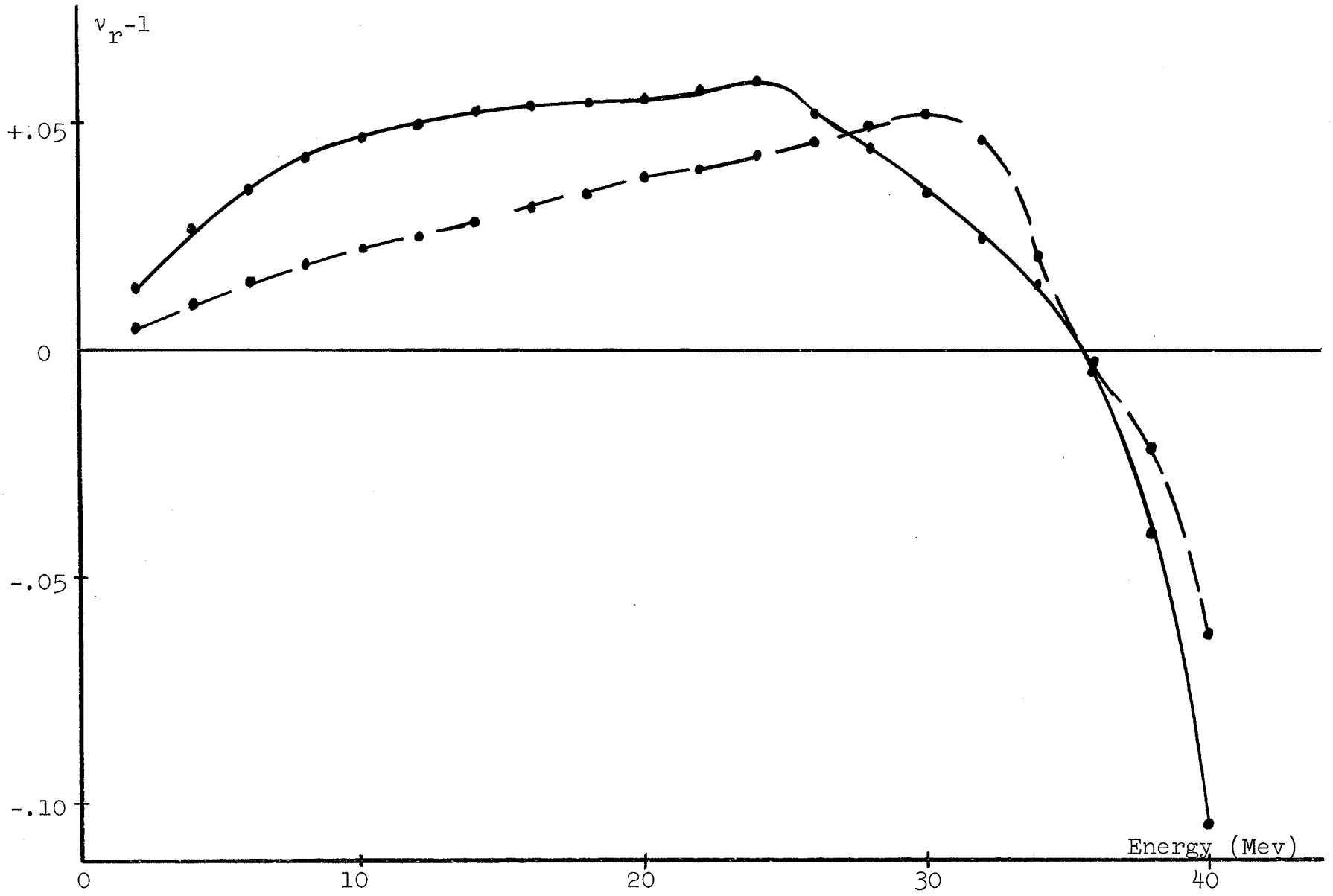

Figure 4: (ν_r-1) as a function of energy for field B26.29A (solid line) and for field B26A1(broken line).

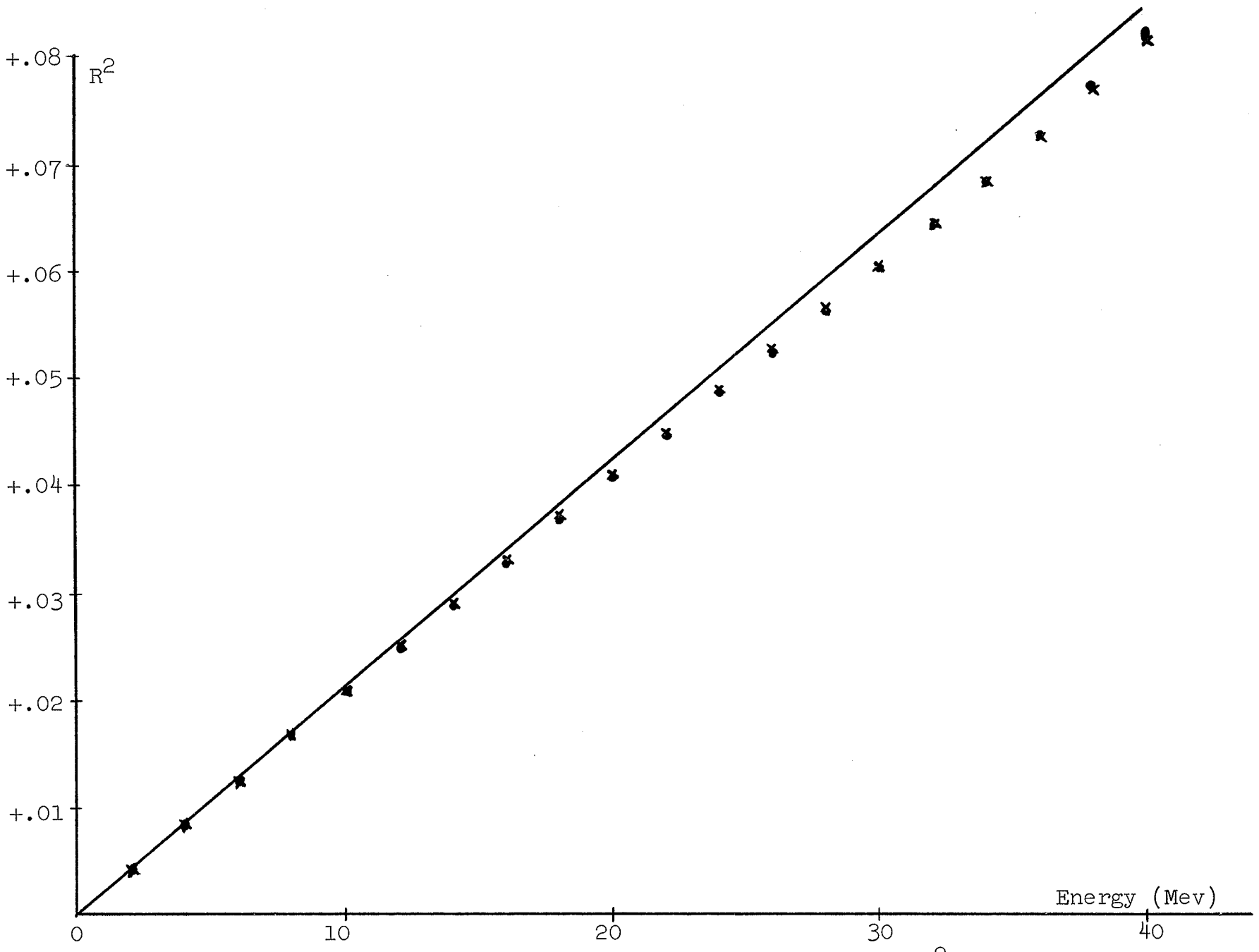

Figure 5: Square of the mean radius of the equilibrium orbit (R^2) as a function of energy for field B26.29A (dots) and for field B26A1 (x's).

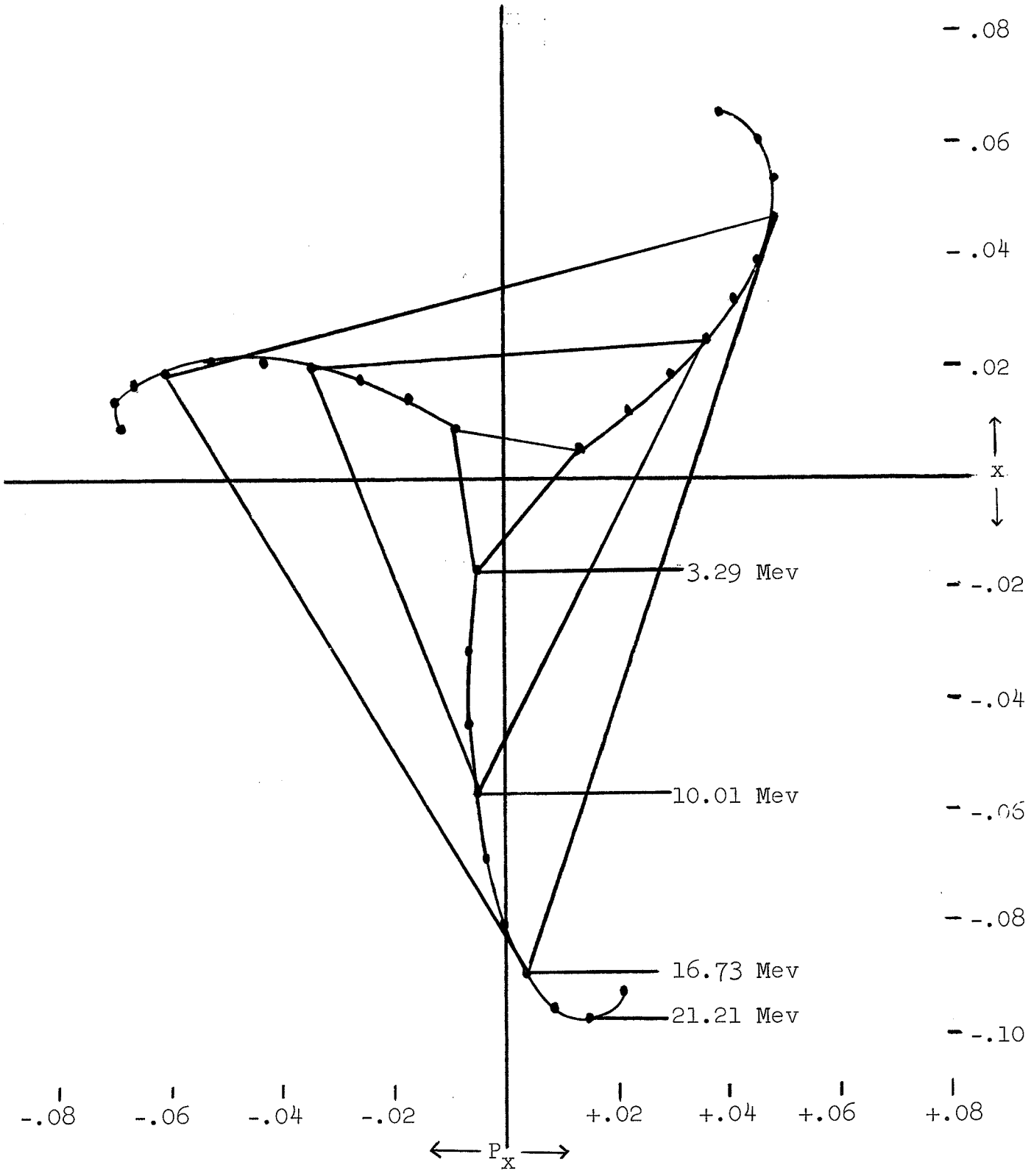

Figure 6: x vs. p_x phase space diagram showing three unstable fixed points (dots) and approximate stability limit for field B26.29A from 3.29 Mev to 23.45 Mev in steps of 2.24 Mev.

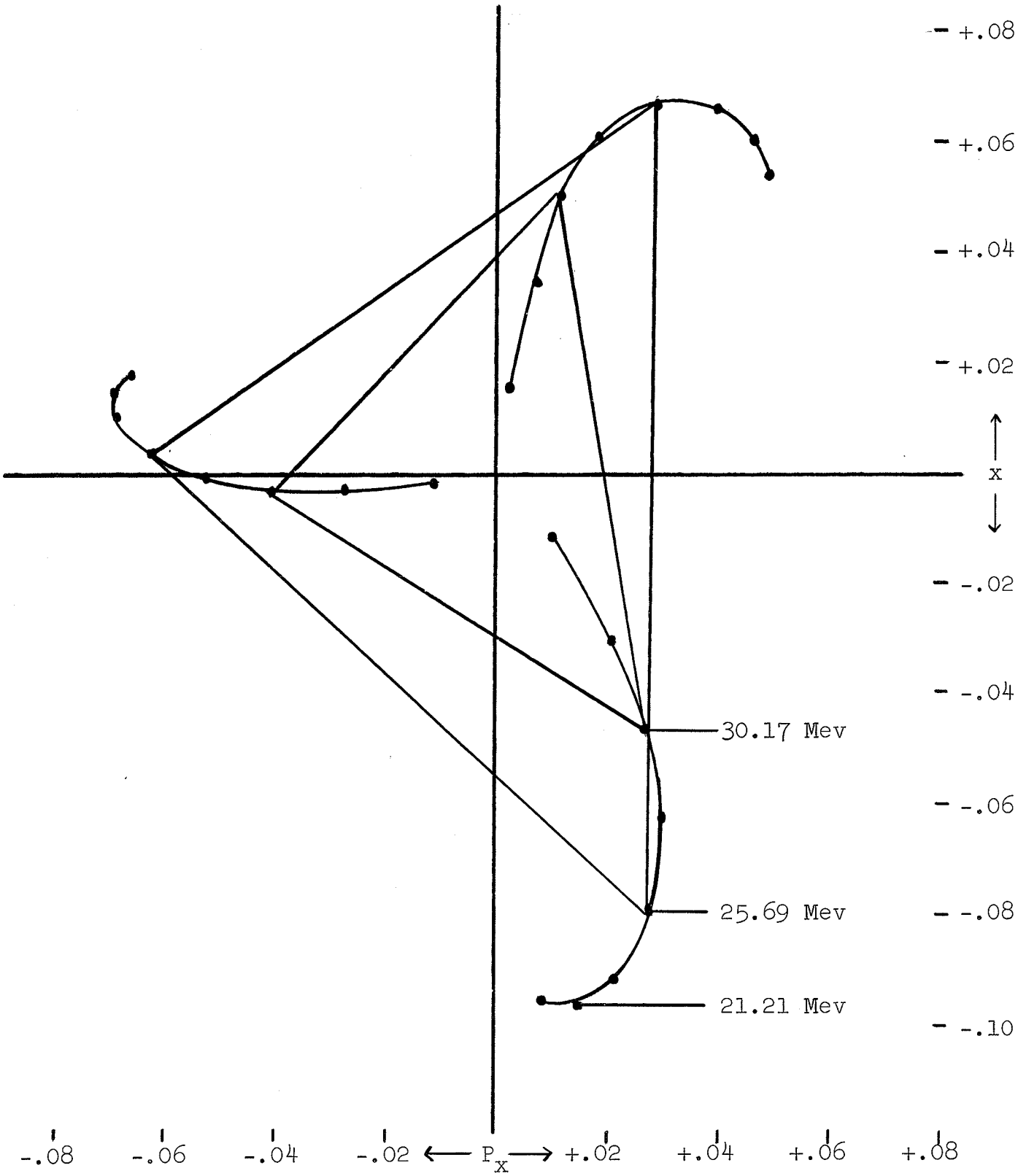

Figure 7: x vs. p_x phase space diagram showing three unstable fixed points (dots) and approximate stability limit for field B26.29A from 18.97 Mev to 34.65 Mev in steps of 2.24 Mev.

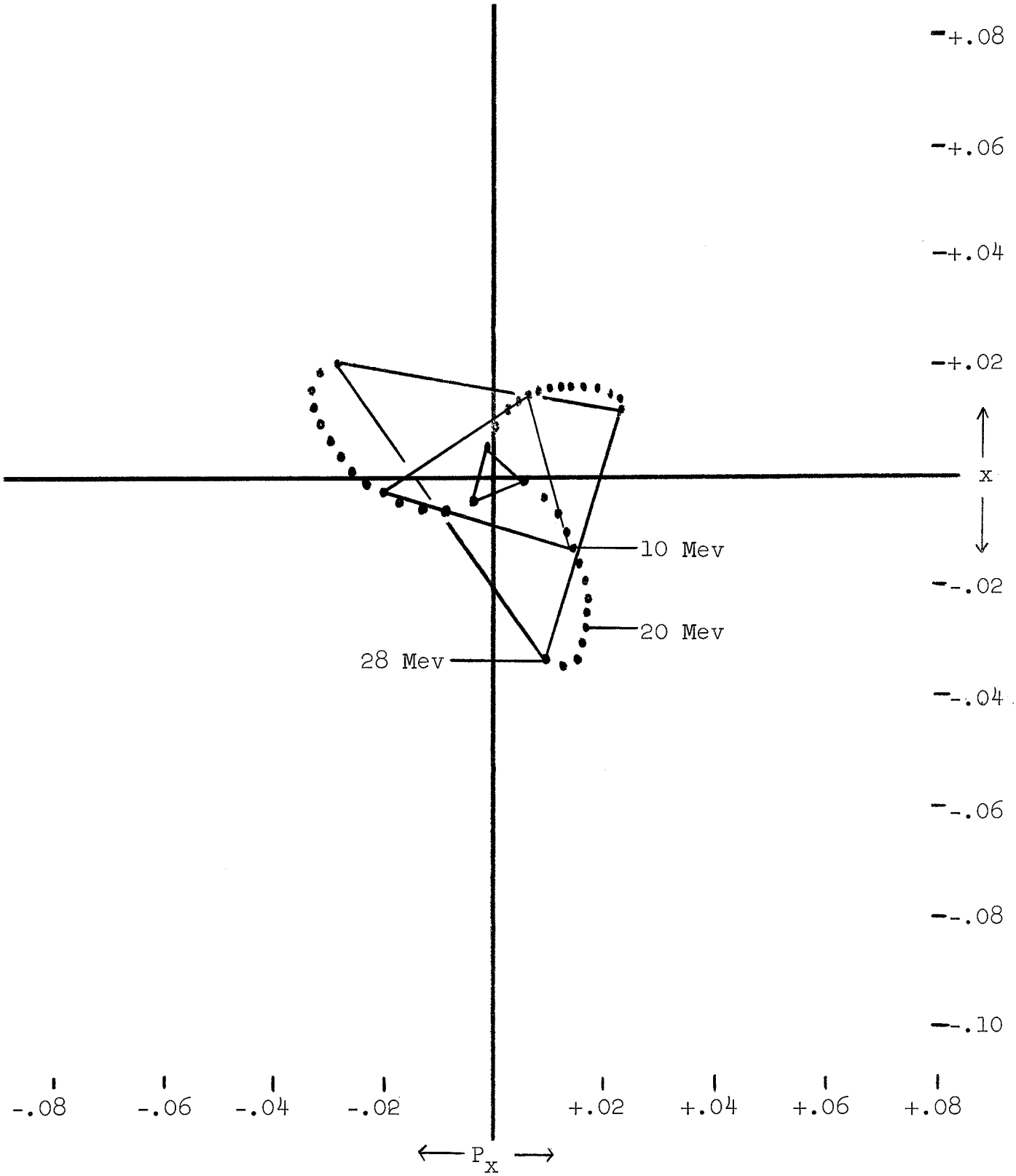

Figure 8: x vs. p_x phase space diagram showing three unstable fixed points (dots) and approximate stability limit for field B26A1 from 2 Mev to 28 Mev in steps of 2 Mev.

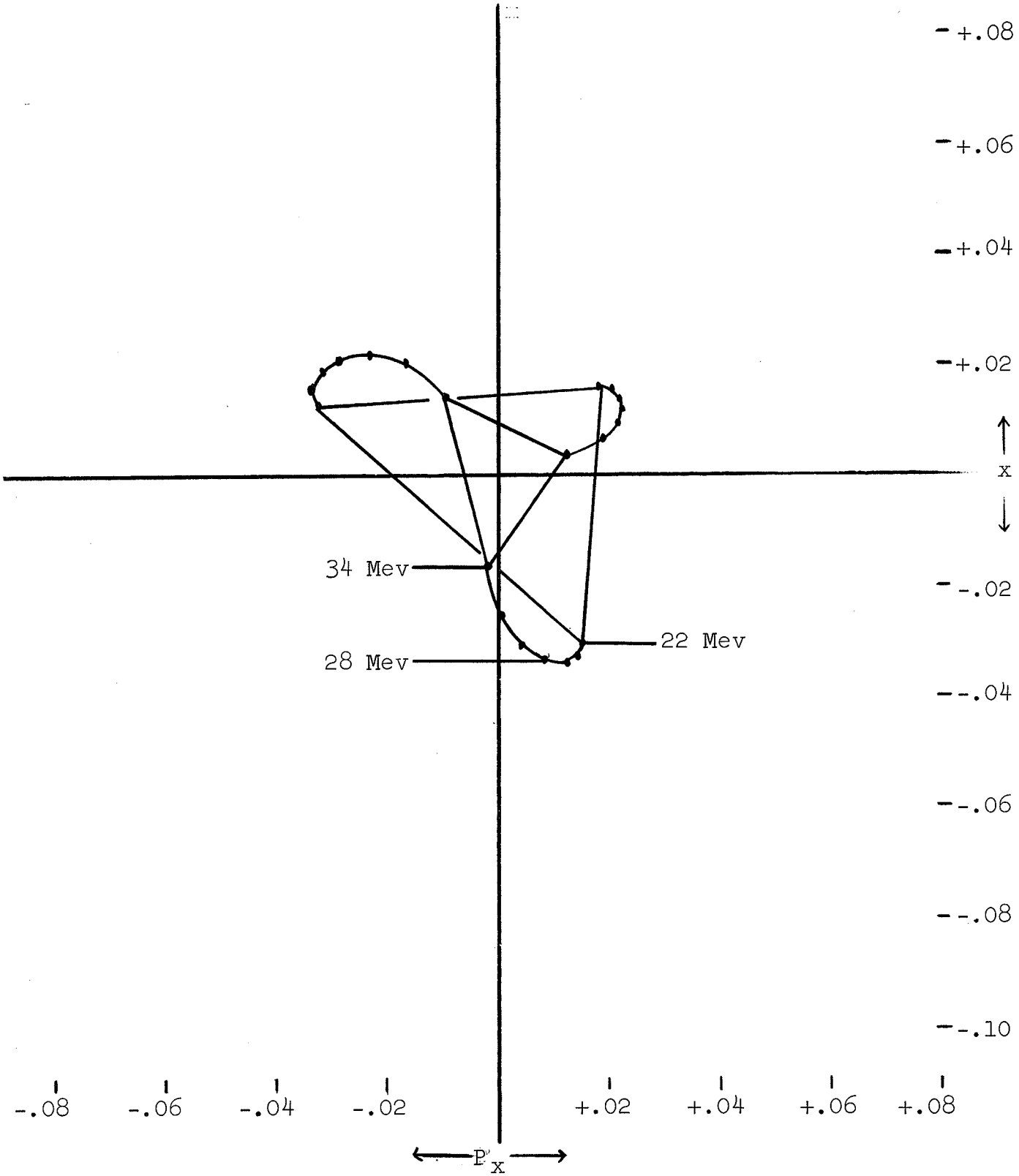

Figure 9: x vs. p_x phase space diagram showing three unstable fixed points (dots) and approximate stability limit for field B26A1 from 22 Mev to 34 Mev in steps of 2 Mev.

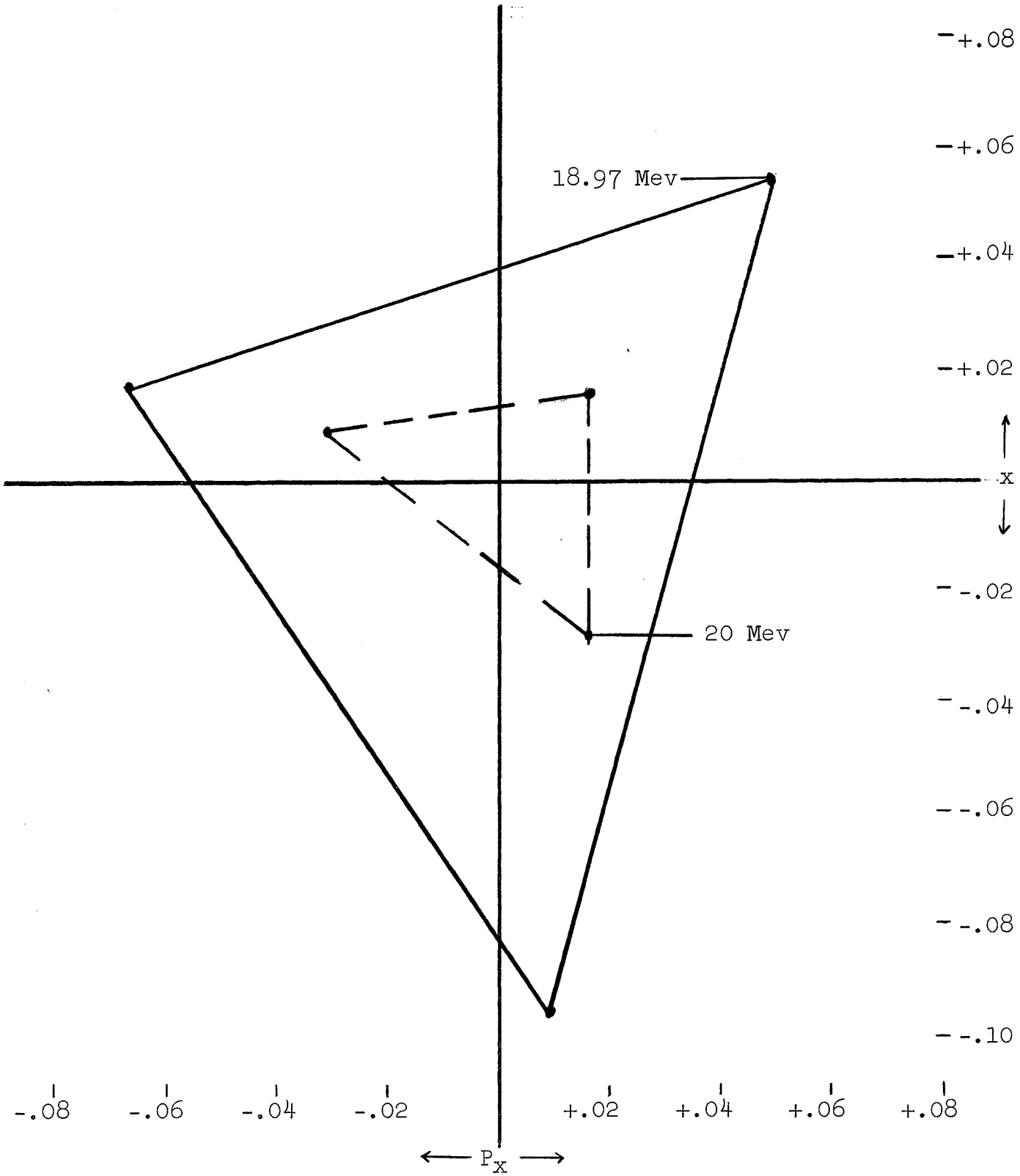

Figure 10: Comparison of stable region for field B26.29A (solid line) and field B26A1 (broken line) at 18.97 Mev and 20 Mev respectively; the dots represent the three unstable fixed points.

CHAPTER II

THEORY OF THE EFFECTS OF FIELD IMPERFECTIONS

1. Basic Equations.

If a charged particle is moving in a magnetic field, and at right angles to the field, the momentum of the particle is given by:

$$p = eB(r,\theta)\rho(r,\theta),$$

where $\rho(r,\theta)$ is the instantaneous radius of curvature, p and e are the momentum and charge of the particle and $B(r,\theta)$ is the magnitude of the magnetic field at that point. Substituting the expression for $\rho(r,\theta)$ in polar coordinates, the equation for the radial motion becomes:

$$\frac{d}{d\theta}\left(\frac{\dot{r}}{\sqrt{r^2+\dot{r}^2}}\right) = \frac{r}{\sqrt{r^2+\dot{r}^2}} - \frac{erB(r,\theta)}{p},$$

where the differentiation is with respect to θ and r is the radial distance to the particle. Let $r(\theta) = r_e(\theta)+x(\theta)$, where $r_e(\theta)$ is the radial distance to the E.O. and $x(\theta)$ is the radial displacement of a particle relative to this orbit. There exists a function $D(\theta)$ which defines $X(\theta)$ as follows:

$$x(\theta) \equiv D(\theta)\ X(\theta), \qquad (2.1)$$

such that with this transformation, the radial equation of motion for oscillations about the E.O. becomes:

$$\ddot{X}(\theta) + G(\theta)X(\theta) = K(X,\theta) + \delta K(X,\theta), \qquad (2.2)$$

where $K(X,\theta)$ represents all the non-linear terms arising from the main field, $\delta K(X,\theta)$ represents all terms arising from a small bump field and $G(\theta)$ is a periodic function characteristic of the linear oscillations.

According to Floquet's theorem[22], when $K(X,\theta)$ and $\delta K(X,\theta)$ are zero, a solution exists for Eq. (2.2) of the form :

$$X(\theta) = C(\theta) \exp [i\nu_r \phi(\theta)], \qquad (2.3)$$

where $\phi(\theta) = \theta + \psi(\theta)$. $C(\theta)$ and $\psi(\theta)$ are real periodic functions having the same periodicity as $G(\theta)$. Moreover, $C(\theta)$ and $\phi(\theta)$ satisfy the equations:

$$C^2\dot{\phi} = 1 \qquad (2.4)$$

and,

$$\ddot{C} + G(\theta)C = \nu_r^2 C^{-3}. \qquad (2.5)$$

Define $y(\phi)$ by:

$$X(\theta) \equiv C(\theta)y(\phi). \qquad (2.6)$$

With this transformation, Eq. (2.2) becomes:

$$d^2y(\phi)/d\phi^2 + \nu_r^2 y(\phi) = C^3[K(X,\theta) + \delta K(X,\theta)]$$

$$\equiv F(y,\phi) + \delta F(y,\phi), \qquad (2.7)$$

where $F(y,\phi)$ and $\delta F(y,\phi)$ are the forces associated with the main field and the bump field respectively. It is clear from this equation that the transformation from the variable $x(\theta)$ to the new variable $y(\phi)$ has the effect of converting the linear oscillations to simple harmonic motion; as a result, the non-linear force $F(y,\phi)$ and the perturbations produced by the field bump $\delta F(y,\phi)$ can now be treated as perturbations of a simple harmonic oscillator having frequency ν_r. Specific formulae for $D(\theta)$, $\psi(\theta)$, $C(\theta)$ and $G(\theta)$ will be given in section 5 below.

From the above results, $x(\theta)$ may be expressed as:

$$x(\theta) = D(\theta)C(\theta)\, y[\theta+\psi(\theta)]. \qquad (2.8)$$

Expanding this equation, the result is:

$$x(\theta)=D(\theta)C(\theta)y(\theta)+\psi(\theta)D(\theta)C(\theta)\ [dy(\theta)/d\theta]+....$$

Since $|\psi(\theta)| << 1$ and $|D(\theta)C(\theta) - 1| << 1$, then

$$x(\theta) = y(\theta) + [D(\theta)C(\theta) - 1]\, y(\theta) + \psi(\theta)\ [dy(\theta)/d\theta].$$

The quantities $[D(\theta)C(\theta)-1]$ and $\psi(\theta)$ contain mainly the harmonic of frequency three with harmonics 6, 9, etc.

being small and unimportant for this discussion; in addition, the harmonic of zero frequency in $[D(\theta)C(\theta)-1]$ is of second order ($\psi(\theta)$ has no zero harmonic by definition). Furthermore, since the second and fourth harmonics of $y(\phi)$ and $x(\theta)$ are usually small compared to the first harmonic, it is therefore possible to equate the first harmonic of $x(\theta)$ with the first harmonic of $y(\phi)$ to a good approximation as follows:

$$x_1(\theta) = y_1(\theta), \tag{2.8a}$$

where the subscript "one" designates the first-harmonic (or "quasi-first harmonic"). The fact of the near equivalence of the first harmonic of $y(\phi)$ and $x(\theta)$ allows a simple comparison of the theoretical and computer results to be made; that is, the theory is formulated in terms of the variable $y_1(\phi)$ while the computer results are in terms of $x(\theta)$; as a result of the above relation, it is then possible to make a direct comparison between the first harmonic of fixed point orbits in the two cases. It is possible of course, to exactly transform from $y(\phi)$ to $x(\theta)$ and vice versa through the above equations; however, the simplified theory to be presented here deals exclusively with the first harmonic content of $y(\phi)$ and Eq. (2.8a) provides the basis for checking the results

of this theory.

In the differential equation (2.7) for $y(\phi)$ the non-linear force $F(y,\phi)$ is a complicated function of $y(\phi)$ and its derivatives. Although the actual expression can be derived for $F(y,\phi)$ from the basic equation of motion [6], the present discussion will be restricted to a simple, semi-empirical expression for $F(y,\phi)$. This simplification seems justified by the fact that the present discussion deals only with the first harmonic content of the function $y(\phi)$. The present theory is therefore semi-empirical in nature and its principle advantage is its simplicity.

In the absence of the field bump, the differential equation for the first harmonic component, or the "quasi-first harmonic" component, of $y(\phi)$ in the non-linear case is assumed to be:

$$\ddot{y}(\phi) + \nu_r^2 y(\phi) = F(y,\phi) \equiv Ky^2\cos 3(\phi-\phi_o), \quad (2.9)$$

where K and ϕ_o are constants and the subscript "one" on $y(\phi)$ will no longer be needed. The constants K and ϕ_o, as will be seen later, specify completely the first harmonic component of the three unstable fixed point orbits associated with the main field. These constants could be determined from the theoretical formulae found elsewhere

[5,6]; however, we shall instead use the data from the Fixed Point Code for this purpose. The form of the semi-empirical non-linear force given above is the simplest one possible having the required properties. No cubic (frequency shifting) terms have been included in $F(y,\phi)$ assumed above since the quantitative theory of the fixed point orbits shows that such terms are canceled for a strictly isochronous field. As a result, the theory presented here will be applicable only in the isochronous portion of the magnetic field; that is, it will not be applicable near the magnet edge if the three outer stable fixed point orbits move in close to the three unstable fixed point orbits.

Consider now the effects of a field bump and the resultant perturbations $\delta F(y,\phi)$ which should be added to the right side of Eq. (2.9). Since ν_r is close to unity, a first harmonic perturbation force $\delta F_1(y,\phi)$ given by:

$$\delta F_1(y,\phi) = \delta\cos(\phi-\phi_1),$$

where δ and ϕ_1 are constants, acts as a resonant driving force and can lead to trouble even when δ is quite small. Such a perturbation arises not only from a field bump harmonic with frequency one, but also from those harmonics of frequency two and four. In addition, a second harmonic

gradient perturbation force $\delta F_2(y,\phi)$ given by:

$$\delta F_2(y,\phi) = \delta' y(\phi) \cos 2(\phi-\phi_2),$$

where δ' and ϕ_2 are constants, acts as an alternating-gradient force which tends to drive the oscillations into the 2/2 stop-band. Such a perturbation can arise not only from a field bump harmonic of frequency two, but also from those harmonics of frequency one and five. Introduction of these two perturbation forces into Eq. (2.9) gives the following differential equation for $y(\phi)$:

$$\ddot{y}(\phi) + \nu_r^2 y(\phi) = Ky^2 \cos 3(\phi-\phi_o) + \delta \cos(\phi-\phi_1) + \delta' y(\phi) \cos 2(\phi-\phi_2). \qquad (2.10)$$

It is this equation which forms the basis for the analysis to be given here. A field bump will in general produce perturbations of other frequencies and also of higher order in $y(\phi)$; however, for ν_r close to unity and relatively small field bumps the two perturbation terms given above will be the most important. Explicit formulae will be given in section 5 below for the parameters δ, δ', ϕ_1, and ϕ_2 as functions of the pertinent properties of the field bump.

A. Equations for Fixed Point Orbits: Since only the first harmonic of $y(\phi)$ is considered here, the equation for $y(\phi)$ for a fixed point orbit is:

$$y(\phi)=A\cos(\phi+\alpha-\phi_o)=(A/2)\exp[i(\phi+\alpha-\phi_o)]+c.c., \qquad (2.11)$$

where A and α are constants and ϕ_o is defined in Eq. (2.9). Substituting this expression for $y(\phi)$ into Eq. (2.10) and equating the coefficients of $e^{i\phi}$ (Harmonic Balance) gives:

$$\epsilon A e^{i\alpha} = (KA^2/8)e^{-2i\alpha}+(\delta/2)e^{i(\phi_o-\phi_1)} + (\delta' A/4)e^{-i\alpha}e^{2i(\phi_o-\phi_2)}, \qquad (2.12)$$

where $(\nu_r^2 - 1) \equiv 2\epsilon$ and where the equation has been multiplied through by a factor $e^{i\phi_o}$. Eq. (2.12) is the general equation for determining the constants A and α for the first harmonic of the fixed point orbits.

In the absence of a field bump, Eq. (2.12) reduces to:

$$\epsilon A e^{i3\alpha} = (K/8)A^2.$$

Since ϵ, A and K are positive, the acceptable solutions to this equation are: A=0 (E.O.); and for the three unstable fixed point orbits,

$$\alpha = 0, \text{ or } \pm 120^\circ$$

and,
$$A \equiv A_o = 8\epsilon/K, \qquad (2.13)$$

where A_o is the amplitude of the first harmonic of all three unstable fixed point orbits. Thus if $x_1(\theta)$ is the first harmonic component of an unstable fixed point orbit in the absence of a field bump, where:

$$x_1(\theta) = |x_1| \cos(\theta - \theta_1'),$$

then from the discussion connected with Eq. (2.8a) above, it follows that:

$$|x_1| = A_o$$

$$\theta_1' = \phi_o,\ \phi_o + 120°,\ \text{or}\ \phi_o - 120°.$$

As a result, the constants K and ϕ_o can be determined directly from the amplitude and phase of the first harmonic of one of the fixed point orbits in the absence of a field bump.

B. Approximate Phase Invariant: For a non-fixed point orbit, $y(\phi)$ is still given by Eq. (2.11) but A and α are considered as slowly varying functions of ϕ. The approximate differential equations for A and α are then given by:

$$\frac{dA^2}{d\phi} = -\frac{\partial H}{\partial \alpha}$$

and,

$$\frac{d\alpha}{d\phi} = \frac{\partial H}{\partial A^2},$$

where H is approximately given by:

$$H = \epsilon A^2 - (KA^3/12)\cos 3(\alpha) - \delta A \cos(\alpha-\phi_o+\phi_1)$$

$$- (\delta' A^2/4)\cos 2(\alpha-\phi_o+\phi_2). \qquad (2.14)$$

Using H it is possible to obtain a qualitative understanding of the phase plots; successive points in the phase plot should lie on a curve given by H equal to a constant. The phase plots obtained from computer results are in terms of (x, p_x) rather than the "quasi-first harmonic" $(y, \dot{y})$; therefore, the comparison between computer phase plots and the curves obtained from H above can only be qualitative.

Fig. 11 is a plot of H for various A and α values with δ and δ' equal to zero. The fixed points are located at $\alpha = 0$, or $\pm$ 120° at a distance A_o from the origin. The direction of the flow lines is obtained from $\dot{A}$ and $\dot{\alpha}$, and from H it is possible to determine whether a fixed point is stable or unstable. This figure should be compared with Figs. 14 and 15 of Chapter III.

2. One-Sector Perturbation.

The results obtained in this section are very similar to those obtained by L.J. Laslett and K.R. Symon [9] and L.J. Laslett and S.J. Wolfson [10]. Suppose $\delta' = 0$; then

Eq. (2.12) becomes:

$$\epsilon A e^{i\alpha} = (KA^2/8)e^{-2i\alpha+\delta/2}\, e^{i(\phi_o-\phi_1)}. \qquad (2.15)$$

In general Eq. (2.15) is difficult to solve for A and α. The present discussion will restrict itself entirely to the case of a symmetric perturbation where $\phi_1=\phi_o$ or $\phi_o\pm\pi$. When $\phi_1=\phi_o$, the situation is referred to as a "pure one-corner opening" of the stability triangle; when $\phi_1=\phi_o \pm \pi$, the situation is referred to as "pure two-corner opening" of the stability triangle, for reasons which will become apparent later. Actually, both cases will be covered simultaneously by setting $\phi_1 = \phi_o$ and considering δ as either positive or negative.

Set $\phi_1 = \phi_o$ in Eq. (2.15) and substitute for K the value obtained in Eq. (2.13). Upon equating the real and imaginary components of Eq. (2.15) the result is then:

$$(\sin\alpha)\left(1 + \frac{2A}{A_o}\cos\alpha\right) = 0 \qquad (2.15a)$$

$$\delta/2\epsilon \equiv \gamma = A\cos\alpha - \frac{A^2}{A_o}\cos 2\alpha. \qquad (2.15b)$$

From Eq. (2.15a), either $\sin\alpha = 0$ in which case $\alpha = 0$ or π; or $\cos\alpha = -A_o/2A$. The resultant values of A as a function of γ for each of these possible choices for α will be discussed in the succeeding paragraphs. With

$\phi_1 = \phi_o$ and $\delta' = 0$ Eq. (2.14) becomes:

$$H/\epsilon = A^2 - 2A^2/3A_o \cos 3\alpha - 2\gamma A \cos\alpha.$$

Figs. 12a and 12b show how the fixed points and invariant curves H change as a function of γ. With $\gamma > 0$, the curves illustrate the "pure one-corner opening" of the stable region; with $\gamma < 0$, the "pure two-corner opening" of the stable region is observed. If $\phi_1 \neq \phi_o$ or ϕ_o plus a multiple of 60°, then a mixture of the one and two-corner cases is generally observed.

Consider first the case of $\alpha = 0$ in Eq. (2.15b) which gives:

$$\gamma = A(1-A/A_o). \qquad (2.15c)$$

When $\gamma = 0$, $A = 0$ or $A = A_o$; $A = 0$ corresponds to the E.O. located at the origin in $(y,\dot{y})$ phase space space and $A = A_o$ corresponds to the unstable fixed point a distance A_o from the origin along the $\alpha = 0$ axis. As γ increases, the unstable fixed point and E.O. move toward each other along the $\alpha = 0$ axis. When $A=A_o/2$, $(\gamma=A_o/4)$, the two fixed points coincide and the stable region disappears; therefore, to have a stable region, γ must be less than $A_o/4$. For $\gamma < 0$, the fixed point along the $\alpha=0$ axis moves out along this axis away from the origin.

Consider next the case where $\alpha = \pi$ for which Eq. (2.15b) becomes:

$$\gamma = -A(1+A/A_o) \qquad (2.15d)$$

Since A and A_o are positive by definition, no fixed points exist along the $\alpha = \pi$ axis for $\gamma > 0$. When γ is zero, A = 0 represents the only valid solution which is the E.O. located at the origin. As $\gamma < 0$ decreases, the stable E.O. moves out along the $\alpha=\pi$ axis. It can be shown from the invariant H that when $A=A_o/2$, ($\gamma = -3A_o/4$) the displaced E.O. changes from a stable fixed point to an unstable fixed point.

Consider now the effect of the one-sector bump on the two unstable fixed points at $\alpha = \pm 120°$. In this case, $\cos\alpha = -A_o/2A$ and the resultant formula for γ is:

$$\gamma = -A_o(1-A^2/A_o^2). \qquad (2.15e)$$

When $\gamma = 0$, $A = A_o$ and $\alpha = \pm 120°$; this represents the two fixed points at $\alpha = \pm 120°$. For $\gamma > 0$, A is $> A_o$ and $-\cos\alpha < 1/2$. Therefore as γ increases the two unstable fixed points at $\alpha = \pm 120°$ move toward the $\alpha = \pm\pi/2$ axes with increasing A. If $\gamma<0$, A is $<A_o$ and $-\cos\alpha > 1/2$; therefore as $\gamma<0$ decreases the two unstable fixed points at $\alpha = \pm 120°$ move toward the $\alpha=\pi$ axis with decreasing A

(see Figs. 12a and 12b to see how fixed points move as a function of γ). However, cos α has a lower limit of -1 which occurs when $A = A_o/2$, ($\gamma = -3A_o/4$). It has previously been shown that when $\gamma = -3A_o/4$, the stable displaced E.O. moving out along the $\alpha=\pi$ axis, becomes unstable. It can be concluded that for negative γ, the E.O. moves out along the $\alpha= \pi$ axis and the two unstable fixed points at $\alpha \doteq \pm 120°$ move toward that axis. When $\gamma = -3A_o/4$ the three fixed points coincide and only one unstable fixed point remains; when this occurs, the stable region has disappeared. Therefore $\gamma= -3A_o/4$ is the critical value below which no stable region exists in the case of "pure two-corner opening". For γ less than this value, the one unstable fixed point continues to move out along the $\alpha = \pi$ axis.

It is now possible to sum up the results for the one-sector perturbation. As $\gamma > 0$ increases, the stable E.O. and the unstable fixed point along the $\alpha = 0$ axis move toward each other along that axis; at the same time, the two unstable fixed points at $\alpha = \pm 120°$ move toward the $\alpha = \pm \pi/2$ axis with increasing A. When γ equals the critical value γ_c given by:

$$\gamma_c = A_o/4,$$

for which,

$$A = A_o/2,$$

the stable displaced E.O. and the unstable fixed point

coincide and the stable region disappears.

As $\gamma < 0$ decreases, the unstable fixed point along the $\alpha = 0$ axis moves out along this axis; at the same time, the stable displaced E.O. moves out along the $\alpha = \pi$ axis and the two unstable fixed points at $\alpha = \pm 120°$ move toward that axis. When γ equals the critical value γ_c given by:

$$\gamma_c = -3A_o/4,$$

for which, $$A = A_o/2,$$

the displaced E.O. and the two unstable fixed points coincide on the $\alpha = \pi$ axis leaving only one unstable fixed point and no stable region; therefore as far as stability is concerned, the critical values for γ are $-3A_o/4$ and $A_o/4$ for two and one-corner opening respectively.

3. Two-Sector Gradient Perturbation.

For the case of the two-sector gradient perturbation, $\delta \doteq 0$ and Eq. (2.12) becomes:

$$\epsilon A e^{i\alpha} = (KA^2/8)e^{-2i\alpha} + (\delta' A/4)e^{-i\alpha}e^{2i(\phi_o - \phi_2)}. \quad (2.16)$$

Note that unlike the one-sector perturbation case discussed above, A=0 is always a solution; that is the E.O. is never

displaced; however, this fixed point changes from stable to unstable when $|\delta'| \geq 4\epsilon$ which corresponds to the 2/2 stop-band.

In general Eq. (2.16) is difficult to solve except when $\phi_2 = \phi_o$ or $\phi_o \pm \pi/2$. As in the case of the one-sector perturbation, the two cases correspond to the "pure one-corner opening" and "pure two-corner opening" of the stable triangular region. For cases other than these two, a mixture of one and two-corner opening is observed. In the present discussion, $\phi_2 = \phi_o$ and δ' is considered either positive or negative to cover both cases. Taking the real and imaginary components of Eq. (2.16) gives:

$$(\sin \alpha)\ (2 \cos \alpha + A/A_o) = 0 \qquad (2.16a)$$

$$\delta'/4\epsilon \equiv \gamma' = \cos 2\alpha - A/A_o \cos \alpha, \qquad (2.16b)$$

where $K = 8\epsilon/A_o$ from Eq. (2.13). These equations then specify the dependence of the parameters A and α on the strength of the perturbation.

The movement of the fixed points for a two-sector gradient perturbation is easier to visualize with the aid of a diagram. Therefore special attention should be paid while reading the following analysis, to Figs. 13a and 13b which indicate the movement of the fixed points

as a function of γ'. Again as in the case of the one-sector perturbation, the sequence of figures was obtained from the invariant H given by:

$$H/\epsilon = A^2 - \frac{2A^3}{3A_o} \cos 3\alpha - \delta' A^2 \cos 2\alpha.$$

From Eq. (2.16a), $\alpha = 0$ or π, or $\cos \alpha = -A/2A_o$. For $\alpha = 0$, Eq. (2.16b) gives:

$$\delta'/4\epsilon \equiv \gamma' = 1 - A/A_o \qquad (2.16c)$$

The above equation states that as $\gamma' > 0$ increases the E.O. remains fixed at the origin while the unstable fixed point along the $\alpha = 0$ axis moves in along this axis toward the E.O. at the origin. When $\gamma' = +1$, the two fixed points coincide at the origin leaving an unstable fixed point there; at this point, the stable region has disappeared. The effect has been to convert the E.O. from a stable to an unstable fixed point. The particular value $\gamma' = +1$ corresponds to that value at which the frequency of the radial oscillation about the E.O. reaches the stop-band value $\nu_r = 2/2$; it is clear then that the conversion of the E.O. from a stable to an unstable fixed point is due to this merging with one of the three unstable fixed point orbits. For $\alpha = 0$ and $\gamma' < 0$, the unstable fixed point along the $\alpha = 0$ axis will move out along this

axis away from the E.O. located at the origin.

Consider next the case where $\alpha = \pi$; in this case, Eq. (2.16b) becomes:

$$\gamma' = 1 + A/A_o. \qquad (2.16d)$$

From the above equation, since A is positive, γ' is never less than unity; for $\gamma' < +1$ no fixed points exist along the $\alpha = \pi$ axis. As γ' increases above unity, a stable fixed point moves out along the $\alpha = \pi$ axis leaving the unstable E.O. at the origin. When $+1 < \gamma' < +3$, the stable fixed point continues to move out along this axis. An analysis of the invariant H will show that when $\gamma' = +3$ and $A = 2A_o$, the stable fixed point becomes an unstable fixed point. For $\gamma' > +3$ and $A > 2A_o$ this unstable fixed point continues to move out along the $\alpha = \pi$ axis.

Consider next the case where $\cos \alpha = -A/2A_o$; in this case Eq. (2.16b) becomes:

$$\gamma' = (A/A_o)^2 - 1. \qquad (2.16e)$$

This equation represents the two unstable fixed points at $\alpha = \pm 120°$ and their motion as a function of γ'. When $\gamma' = 0$ (zero perturbation), $A = A_o$ and $\alpha = \pm 120°$. As $\gamma' > 0$ increases, $A > A_o$ increases and $-\cos \alpha > 1/2$. Therefore, as γ' increases the two unstable fixed points at

$\alpha = \pm 120°$ move toward the $\alpha = \pi$ axis with increasing A; however, cosα has a lower limit which occurs when $A = 2A_o$ and $\gamma' = +3$. It has previously been shown that when $\gamma' = +3$, $(A=2A_o)$, the stable fixed point becomes unstable. It can be concluded that when $\gamma' = +3$ the stable fixed point moving out along the $\alpha = \pi$ axis and the two unstable fixed points moving toward the $\alpha = \pi$ axis coincide on that axis and an unstable fixed point remains. When $\gamma' = +3$, the stable region has disappeared. For $\gamma' > +3$ the unstable fixed point continues to move out along the $\alpha = \pi$ axis. As $\gamma' < 0$ decreases, $-\cos\alpha < 1/2$, the two unstable fixed points at $\alpha = \pm 120°$ move toward the $\alpha = \pm \pi/2$ axis with decreasing A. When $\gamma' = -1$, the two unstable fixed points are at the origin where they merge with the E.O. leaving an unstable fixed point there.

It is now possible to sum up the results of a two-sector gradient perturbation. As γ' increases from 0 to +1, the E.O. stays fixed at the origin and the unstable fixed point along the $\alpha = 0$ axis moves toward the E.O. along that axis; when $\gamma' = +1$, the two fixed points coincide leaving an unstable E.O. at the origin and no stable region. At the same time, the two fixed points at $\alpha = \pm 120°$ move toward the $\alpha = \pi$ axis with increasing A. As γ' increases from +1 to +3, a stable fixed point emerges from

the origin leaving an unstable E.O. at the origin. For a particular $\gamma' = +2$, a closed triangular stable region bounded by the three unstable fixed points is again formed. For $\gamma' > +2$ but less than $+3$, there is then two-corner opening on the opposite side of this triangular region. When $\gamma' = +3$, the stable fixed point and the two unstable fixed points coincide on the $\alpha = \pi$ axis leaving an unstable fixed point and no stable region. For $\gamma' > +3$ this unstable fixed point continues to move out along the $\alpha = \pi$ axis. This sequence of events is illustrated in Fig. 13a.

Consider next the case where γ' is negative (two-corner opening). As γ' decreases from 0 to -1, the unstable fixed point along the $\alpha = 0$ axis moves out along this axis away from the origin. At the same time, the two unstable fixed points at $\alpha = \pm 120°$ move in toward the $\alpha = \pm \pi/2$ axes with decreasing A. When $\gamma' = -1$, the two unstable fixed points originally at $\alpha = \pm 120°$ and the stable E.O. coincide at the origin leaving an unstable fixed point and no stable region.

As was noted previously, Figs. 13a and 13b are plots showing the movement of the fixed points as a function of γ'; the one and two-corner opening effect of the stable triangle is again illustrated. When $\gamma' = \pm 1$, an unstable

E.O. is situated at the origin in $(y,\dot{y})$ phase space. It is for this value of γ' that the two-sector gradient perturbation has driven the linear oscillations into the 2/2 stop-band. As far as stability is concerned, the critical value of γ' is then:

$$\gamma' = \pm 1.$$

4. Simple Criterion for Stability.

In the previous sections of this chapter, the effects of a field bump have been analyzed in terms of the behavior of the fixed point orbits and the characteristics of the phase space diagrams. The problem of stability or instability produced by a field bump can however be attacked from another point of view. The field bump produces a shift in the position of the "equilibrium orbit" and a change in the linear oscillation frequency about this orbit. If ν_r^* is the frequency of the linear oscillations about the displaced E.O., then a simple criterion for stability is that ν_r^* be real. Moreover, when ν_r^* becomes imaginary (stop-band), the stability region vanishes. The present section considers then a semi-quantitative calculation of ν_r^*. The principle advantage of the results obtained here over those obtained in the

previous sections is that no restriction is made on the values ϕ_1 and ϕ_2 in obtaining these results.

The discussion begins with the differential equation for $y(\phi)$ given by Eq. (2.10). A particular periodic solution of this differential equation is $y_e(\phi)$ which represents the equation for the displaced equilibrium orbit, such that $y_e(\phi)$ is zero in the absence of a bump field. The variable $\eta(\phi)$ is defined by:

$$y(\phi) = y_e(\phi) + \eta(\phi),$$

so that $\eta(\phi)$ is then the coordinate describing the motion about the displaced equilibrium orbit. The equation for the linear oscillations about the displaced E.O. is therefore obtained by inserting the above definition into the differential equation for $y(\phi)$ and maintaining only the linear terms in $\eta(\phi)$; the resultant equation for $\eta(\phi)$ is then:

$$\ddot{\eta}(\phi) + \nu_r^2\eta(\phi) = \eta(\phi)[\delta' \cos 2(\phi-\phi_2) + 2Ky_e(\phi) \cos 3(\phi-\phi_o)].$$

The right-hand side of this equation is an alternating-gradient force predominantly of frequency two, and since ν_r is close to one, the effect of this force is to drive the oscillation frequency ν_r^* into the 2/2 stop-band.

The first problem to be dealt with is the evaluation of $y_e(\phi)$. It is assumed here that δ and δ' are sufficiently small such that a perturbation expansion of $y_e(\phi)$ is possible in powers of δ and δ'. Actually, only the first order effect of the field bump will be considered here. The resultant equation for $y(\phi)$ is then:

$$y_e(\phi) \cong \delta/2\epsilon \cos(\phi-\phi_1),$$

where $2\epsilon = (\nu_r^2 - 1) \cong 2(\nu_r - 1)$.

When this $y_e(\phi)$ is inserted into the differential equation above for $\eta(\phi)$ the result is:

$$\ddot{\eta} + \nu_r^2\eta = [\delta' \cos 2(\phi-\phi_2) + K(\delta/2\epsilon) \cos(2\phi-3\phi_o+\phi_1)]\eta,$$

where a term of frequency four has been discarded since its effect is negligible. This differential equation is rewritten in the following form:

$$\ddot{\eta} + \nu_r^2\eta = [\Delta\cos 2(\phi-\phi_2')]\eta,$$

where ϕ_2' is irrelevant to the discussion and Δ is given by:

$$\Delta^2 = (\delta')^2 + (4\delta/A_o)^2 + 2\delta'(4\delta/A_o) \cos(3\phi_o-\phi_1-2\phi_2), \quad (2.17)$$

where the substitution $K = 8\epsilon/A_o$ has been made in accordance with the results of Eq. (2.13). Since ν_r^* and ν_r

are both close to unity, an appropriate equation for the value of ν_r^* is then:

$$(\nu_r^*-1)^2 = (\nu_r-1)^2 - |\Delta/4|^2,$$

which is correct to second order in Δ. Since the above calculation gives Δ correct to first order in δ and δ', this result is then correct to second order in both δ and δ'. According to this equation, ν_r^* will be real and a stability region will exist when $|\Delta| < 4\epsilon$; moreover, ν_r^* will be imaginary (in the stop-band) and no stability region will exist when $|\Delta| > 4\epsilon$. Inserting the above value for Δ^2, the simple criterion for stability is then given by:

$$(\delta')^2 + (4\delta/A_o)^2 + 2\delta'(4\delta/A_o)\cos(3\phi_o-\phi_1-2\phi_2) < (4\epsilon)^2, \quad (2.18)$$

and naturally, the more strongly this inequality holds, the larger the available stability region will be.

If $\delta' = 0$, the above inequality reduces to simply:

$$|\delta/2\epsilon| \equiv |\gamma| < 1/2\ A_o. \quad (2.18a)$$

In section 2 above it was shown that conditions for stability with one-corner opening and two-corner opening are respectively:

$$|\gamma| \leqq 1/4\ A_o,$$

and

$$|\gamma| \leqq 3/4\ A_o,$$

so that the results given by Eq. (2.18a) above is just the average of these two extreme situations. Now if $\delta = 0$, then the condition for stability given by Eq. (2.18) is:

$$|\delta'/4\epsilon| \equiv |\gamma'| < 1, \qquad (2.18b)$$

which agrees with the results obtained in section 3 above for both one and two-corner openings.

The above condition (2.18) for stability shows that when both a one-sector and two-sector gradient perturbation are present, their effects add "vectorially". Thus if both perturbations are so phased as to produce one-corner opening at the same corner ($\phi_1 = \phi_o$, $\phi_2 = \phi_o$), or two-corner opening of the same two corners ($\phi_1 = \phi_o + \pi$, $\phi_2 = \phi_o + \pi/2$), then their individual effects reinforce each other such that the stability condition (2.18) becomes:

$$\delta' + (4\delta/A_o) < 4\epsilon. \qquad (2.18c)$$

On the other hand, if one of these perturbations is phased to produce one-corner opening at a specific corner while the other is phased to produce two-corner

opening of the opposite two corners, then their individual effects tend to cancel each other such that the stability condition becomes:

$$|\delta' - 4\delta/A_o| < 4\epsilon. \qquad (2.18d)$$

5. Evaluation of Perturbation Parameters for a Given Bump Field.

The theory presented above contains certain parameters (δ, δ', ϕ_1, ϕ_2) characterizing the effect of the field bump. In the present section, a reasonably accurate procedure will be given for evaluating these parameters in terms of the properties of the field bump. Unlike the case of the non-linear force $F(y,\phi)$, for which a semi-empirical representation was employed, the force $\delta F(y,\phi)$ in Eq. (2.7) associated with the field bump will be evaluated in a realistic fashion.

Assume that $b(r,\theta)$ is the magnetic field associated with the field bump; the expression for $\delta K(r,\theta)$ is then:

$$\delta K(r,\theta) = -(eR/p)\, rb(r,\theta), \qquad (2.19)$$

where R is the mean radius of the E.O. and p is the momentum of the particle; and $p \cong eRB_o(R)$.

Introducing the variable $x(\theta)$ through the defining equation:

$$r(\theta) = r_e(\theta) + x(\theta),$$

where $r_e(\theta)$ is the equation for the E.O., then the equation for δK in terms of $x(\theta)$, expanded to first order in this variable, is:

$$\delta K(x,\theta) = -\left[\frac{rb(r,\theta)}{B_o(r)}\right]_e - x\left[\frac{1}{B_o}\ \frac{\partial}{\partial r}\ rb(r,\theta)\right]_e, \quad (2.19a)$$

where the subscript "e" implies that the quantity in the bracket is to be evaluated at $r = r_e$ (the E.O.).

The equation for the E.O. is of the following form:

$$r_e(\theta) = R[1 + \xi(\theta)],$$

where $\xi(\theta)$ is the periodic function, having zero average, which specifies deviation of this orbit from a circle of radius R. The expression for $\delta K(x,\theta)$ is now expanded to first order in $\xi(\theta)$ with the following result:

$$\delta K(x,\theta) = -R[\beta(R,\theta) + \xi(\theta)\ \beta'(R,\theta)]$$

$$- x[\beta'(R,\theta) + \xi(\theta)\beta''(R,\theta)],$$

where the dimensionless quantities β, β', and β'' are defined by the following equations:

$$\beta(R,\theta) = b(R,\theta)/B_o(R)$$

$$\beta'(R,\theta) = \frac{1}{B_o(R)}\ \frac{\partial}{\partial R}\ [rb(r,\theta)$$

$$\beta''(R,\theta) = \frac{R}{B_o(R)} \frac{\partial^2}{\partial R^2} [rb(r,\theta)].$$

The next step is to transform from the variable $x(\theta)$ to the variable $X(\theta)$ using Eq. (2.1), which is:

$$x(\theta) = D(\theta)X(\theta),$$

where, $$D(\theta) \cong 1 + 1/2\ \xi(\theta),$$

which is correct to the 1st order in the quantity $\xi(\theta)$.

The resultant expression for $\delta K(x,\theta)$ is then:

$$\delta K(x,\theta) = -R[\beta + \xi\beta'] - X(\theta)\ [\beta' + \xi(\beta'' + 1/2\beta')],$$

which is then correct to first order in $\xi(\theta)$.

The next step is to carry out the transformation from the variables (X,θ) to the variables y and ϕ through the defining equations:

$$X(\theta) = C(\theta)\ y(\phi)$$

and, $$\delta F(y,\phi) = C^3[\delta K(X,\theta)],$$

where the functions $C(\theta)$ and ϕ are defined through Eqs. (2.4) and (2.5). The quantity $\delta F(y,\phi)$ is then the force term due to the bump field which must be inserted on the right-hand side of the differential equation (2.7).

The functions $w(\theta)$ and $\phi(\theta)$ are defined as follows:

$$C(\theta) = 1 + w(\theta); \qquad \phi(\theta) = \theta + \psi(\theta), \tag{2.20}$$

and as will be shown later, the magnitude of $w(\theta)$ and $\psi(\theta)$ are small compared to unity. Using these relations, the resultant expression for $\delta F(y,\phi)$ is then given by:

$$\delta F(y,\phi) = -\mathbb{R}[\beta - \psi(d\beta/d\theta) + 3w\beta + \xi\beta']$$

$$- y[\beta' - \psi(d\beta'/d\theta) + 4w\beta' + \xi(\beta'' + 1/2\beta')],$$

where this expression has been evaluated correct to first order only in the quantities ψ, w and ξ. Note that all quantities in this experssion, which were formerly functions of θ are now functions of the new variable ϕ.

In order to cast the form of $\delta F(y,\phi)$ given above into an expression more suitable to calculations, it is necessary to develop suitable expressions for the functions $\xi(\theta)$, $w(\theta)$ and $\psi(\theta)$. Assume that the main magnetic field has the form:

$$B(r,\theta) = B_0(r) + B_1(r) \cos 3(\theta - \zeta_1(r)),$$

as discussed in Chapter I; this is actually not a very restrictive assumption since the higher harmonics in the magnetic field play an insignificant role in these phenomena. The equation for $\xi(\theta)$ can then be written:

$$\xi(\theta) = \xi_1 \cos 3(\theta - \zeta_1), \qquad (2.21)$$

where $\zeta_1 = \zeta_1(R)$ and ξ_1 is given by:

$$\xi_1 \cong f/(8-p^2), \tag{2.22}$$

where $f = B_1(R)/B_o(R)$ and p is the momentum in mc units.

To evaluate $w(\theta)$ and $\psi(\theta)$, it is necessary to have an expression for $G(\theta)$ appearing in Eq. (2.5); actually, only the oscillatory (zero-average) part of this function is needed here. If $G(\theta)$ is defined as $G(\theta) = G_o + g(\theta)$ where $g(\theta)$ averages to zero, then the value of $g(\theta)$ correct to first-order in the flutter is given by:

$$g(\theta) = [(R/B_o)(dB_1/dR)+(3/2)f+(3/2)\xi_1(1+3p^2+2p^4)]\cos 3(\theta-\zeta_1)$$

$$+ 3f(R\delta\zeta_1/dR) \sin 3(\theta-\zeta_1), \tag{2.23}$$

where all functions of r are evaluated at R. Let g_1 and λ be defined by the equation:

$$g(\theta) = g_1 \sin 3(\theta-\lambda), \tag{2.24}$$

where g_1 and λ may then be calculated from the above equation for $g(\theta)$.

The differential equations for $w(\theta)$ and $\psi(\theta)$ follow from those of $C(\theta)$ and ϕ given in Eqs. (2.4) and (2.5); when these are evaluated correct to first order in the flutter field, the result is:

$$\ddot{w} + 4\nu_r^2 w = -g(\theta)$$

$$\dot{\psi} = -2w(\theta).$$

Solutions of these equations are then:

$$w(\theta) = w_1 \sin 3(\theta-\lambda)$$

$$\psi(\theta) = (2/3) w_1 \cos 3(\theta-\lambda),$$

where, $$w_1 = g_1/(9-4\nu_r^2). \qquad (2.25)$$

Consider now the representation of the field bump in a Fourier series as follows:

$$b(r,\theta) = \Sigma b_n(r) \cos n(\theta-\theta_n), \qquad (2.26)$$

where $b_n(r)$ is the amplitude of the nth harmonic and θ_n is its phase. In the present discussion, θ_n is treated as a constant; that is, the bump is considered to have negligible "spiral". If it should be desirable to consider bumps having considerable spiral, then the subsequent analysis should be modified accordingly.

The bump force $\delta F(y,\phi)$ is likewise resolved into components as follows:

$$\delta F(y,\phi) = \Sigma \delta F_n(y,\phi), \qquad (2.27)$$

where δF_n is the perturbation produced by the nth harmonic

of the bump field. The following set of parameters are now defined in connection with Eq. (2.27) above which characterize the pertinent properties of the bump field:

$$\beta_n = b_n(R)/B_o(R)$$

$$\beta'_n = \frac{1}{B_o(R)} \frac{\partial}{\partial R} [rb_n(r)]$$

$$\beta''_n = \frac{R}{B_o(R)} \frac{\partial^2}{\partial R^2} [rb_n(r)].$$

With these definitions, the expression for δF_n becomes:

$$\begin{aligned}
\delta F_n(y,\phi) = -R[&\beta_n \cos n(\phi-\theta_n) + (2n/3)w_1\beta'_n \sin n(\phi-\theta_n)\cos 3(\phi-\lambda) \\
&+ 3w_1\beta_n \cos n(\phi-\theta_n) \sin 3(\phi-\lambda) \\
&+ \xi_1\beta'_n \cos n(\phi-\theta_n) \cos 3(\phi-\zeta_1)] \\
&- y(\phi)[\beta'_n \cos n(\phi-\theta_n) \\
&+ (2/3)w_1\beta'_n \sin n(\phi-\theta_n) \cos 3(\phi-\lambda) \\
&+ 4w_1\beta'_n \cos n(\phi-\theta_n) \sin 3(\phi-\lambda) \\
&+ \xi_1(\beta''_n + 1/2\beta'_n) \cos n(\phi-\theta_n) \cos 3(\theta-\zeta_1)],
\end{aligned}$$

where the quantities w_1, ξ_1, λ, and ζ_1 have been defined above in the Eqs. (2.25), (2.22), (2.24) and (2.21). It

is clear from this formula, that a one-sector perturbation of the form considered in the previous sections can arise not only from the n=1 component of the bump field but also from n=2 and n=4 components as a result of the coupling of these harmonics with the three-sector structure of the Floquet functions and the E.O. In addition, it is clear that a two-sector gradient perturbation can arise not only from the n=2 component of the bump field but also from the n=1 and n=5 components. Note that higher harmonics in the bump field can give rise to such perturbations only through interference with the 6, 9,... frequency components of the E.O. and alternating-gradient motion.

For the n=1 component of the field bump, the following expression for $\delta F_1(y,\phi)$ is obtained:

$$\delta F_1(y,\phi) = -R\beta_1 \cos(\phi-\theta_1)-[y(5/3)w_1\beta_1' \sin(2\phi-3\lambda+\theta_1)$$

$$+1/2\xi_1(\beta_1'' + 1/2\beta_1') \cos(2\phi-3\zeta_1+\theta_1)],$$

where all terms not having the desired periodicity have been dropped.

In the same way the expressions for $\delta F_2(y,\phi)$, $\delta F_4(y,\phi)$ and $\delta F_5(y,\phi)$ are:

$$\delta F_2(y,\phi) = -R[(5/6)w_1\beta_2 \sin(\phi-3\lambda+2\theta_2)$$
$$+ 1/2\xi_1\beta_2' \cos(\phi-3\zeta_1+2\theta_2)]$$
$$- y[\beta_2' \cos 2(\phi-\theta_2)]$$

$$\delta F_4(y,\phi) = -R[(-1/6)w_1\beta_4 \sin(\phi-4\theta_4+3\lambda)$$
$$+ 1/2\xi_1\beta_4' \cos(\phi-4\theta_4+3\zeta_1)]$$

$$\delta F_5(y,\phi) = y[(1/3)w_1\beta_5' \sin(2\phi-5\theta_5+3\lambda)$$
$$- 1/2\xi_1(\beta_5''+1/2\beta_5') \cos(2\phi-5\theta_5+3\zeta_1)].$$

In the theory presented in the previous sections, $\delta F(y,\phi)$ was represented as follows:

$$\delta F(y,\phi) = \delta\cos(\phi-\phi_1) + \delta' y \cos 2(\phi-\phi_2).$$

The parameters δ, ϕ_1, δ', and ϕ_2 can now be directly correlated with the bump field characteristics as evaluated above. For convenience, table 2-1 and table 2-2 are given showing the contribution of each harmonic in the bump field to these parameters. If the bump field contains more than one harmonic, then the entries in a given column should be added algebraically to get the net result in each case.

It is evident from the results in tables 2-1 and

2-2 that a one-sector field bump (n=1) will produce not only a one-sector perturbation but also a two-sector gradient perturbation; moreover, this is true even if $b_1(r)$ is constant, that is a flat bump. In like manner, a two-sector bump (n=2) produces not only a two-sector gradient perturbation but also a one-sector perturbation; moreover, this is true even for a pure two-sector gradient bump where $b_2(R) \equiv 0$, $db_2/dR \neq 0$. However, as will be seen later, for a flat one-sector bump, the resultant two-sector gradient perturbation is negligibly small; likewise, for a two-sector gradient field bump the resultant one-sector perturbation is smaller, though not negligible.

TABLE 2-1: Correlation between the bump field and imperfection parameters for the one-sector perturbation.

n	$\delta \cos \phi_1$	$\delta \sin \phi_1$
1	$-R\beta_1 \cos \theta_1$	$-R\beta_1 \sin \theta_1$
2	$-\frac{5}{6}Rw_1\beta_2 \sin(2\theta_2-3\lambda)-\frac{1}{2}R\xi_1\beta_2' \cos(3\zeta_1-2\theta_2)$	$-\frac{5}{6}Rw_1\beta_2 \cos(2\theta_2-3\lambda)-\frac{1}{2}R\xi_1\beta_2' \sin(3\zeta_1-2\theta_2)$
4	$\frac{1}{6}Rw_1\beta_4 \sin(3\lambda-4\theta_4)-\frac{1}{2}R\xi_1\beta_4' \cos(4\theta_4-3\zeta_1)$	$\frac{1}{6}Rw_1\beta_4 \cos(3\lambda-4\theta_4)-\frac{1}{2}R\xi_1\beta_4' \sin(4\theta_4-3\zeta_1)$

TABLE 2-2: Correlation between the bump field and imperfection parameters for the two-sector gradient perturbation.

n	$\delta' \cos 2\phi_2$	$\delta' \sin 2\phi_2$
2	$-\beta_2' \cos 2\theta_2$	$-\beta_2' \sin 2\theta_2$
1	$-\frac{5}{3}w_1\beta_1' \sin(\theta_1-3\lambda)-\frac{1}{2}\xi_1(\beta_1''+\frac{1}{2}\beta_1')\cos(3\zeta_1-\theta_1)$	$-\frac{5}{3}w_1\beta_1' \cos(\theta_1-3\lambda)-\frac{1}{2}\xi_1(\beta_1''+\frac{1}{2}\beta_1')\sin(3\zeta_1-\theta_1)$
5	$\frac{1}{3}w_1\beta_5' \sin(3\lambda-5\theta_5)-\frac{1}{2}\xi_1(\beta_5''+\frac{1}{2}\beta_5') \cos(5\theta_5-3\zeta_1)$	$\frac{1}{3}w_1\beta_5' \cos(3\lambda-5\theta_5)-\frac{1}{2}\xi_1(\beta_5''+\frac{1}{2}\beta_5')\sin(5\theta_5-3\zeta_1)$

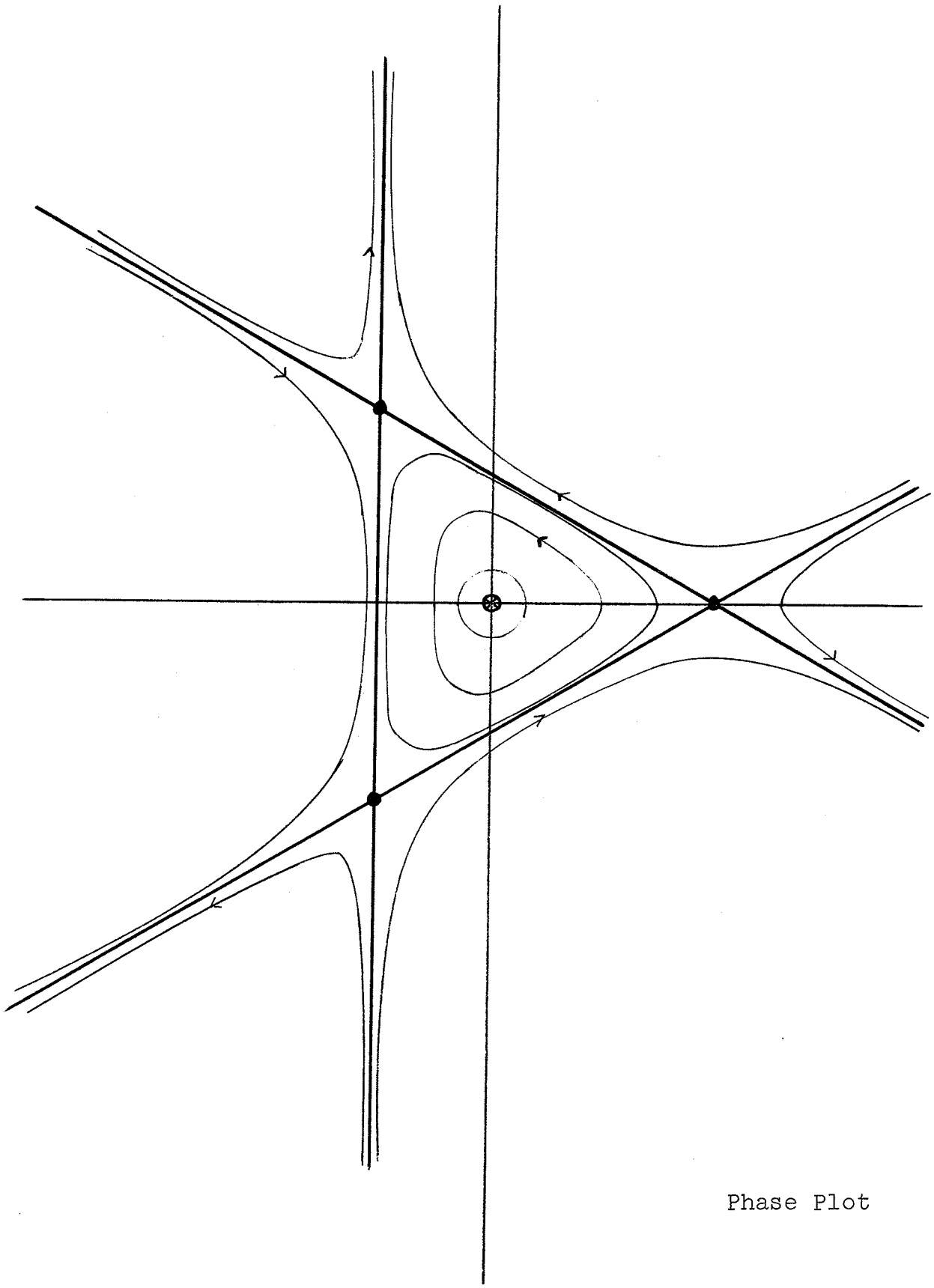

Figure 11: Qualitative curves obtained from Phase Invariant (H) where δ and δ' are equal to zero.

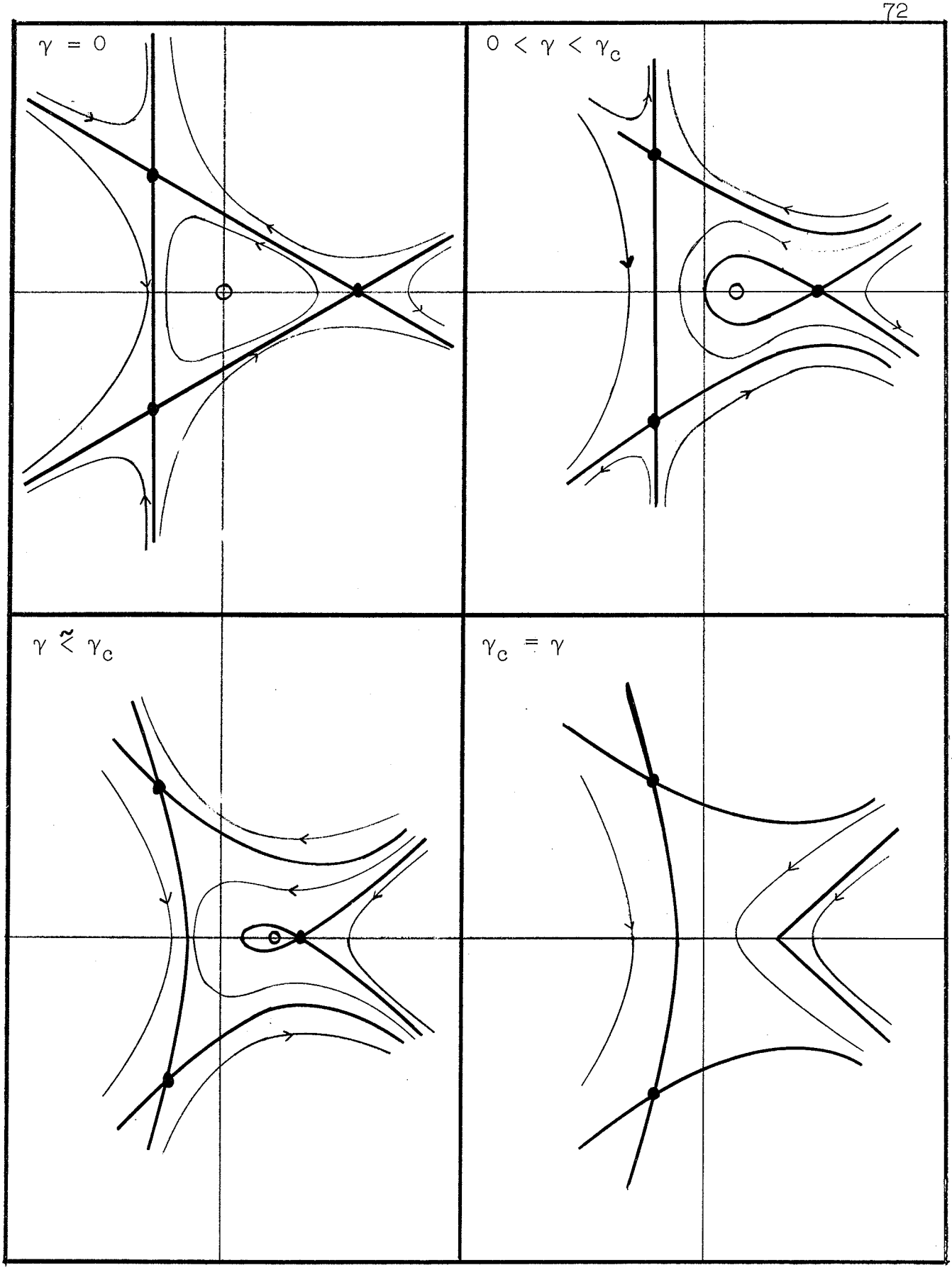

Figure 12a: Qualitative evolution of three-sector phase plots with increasing one-sector perturbation: $\phi_1 = \phi_o$.

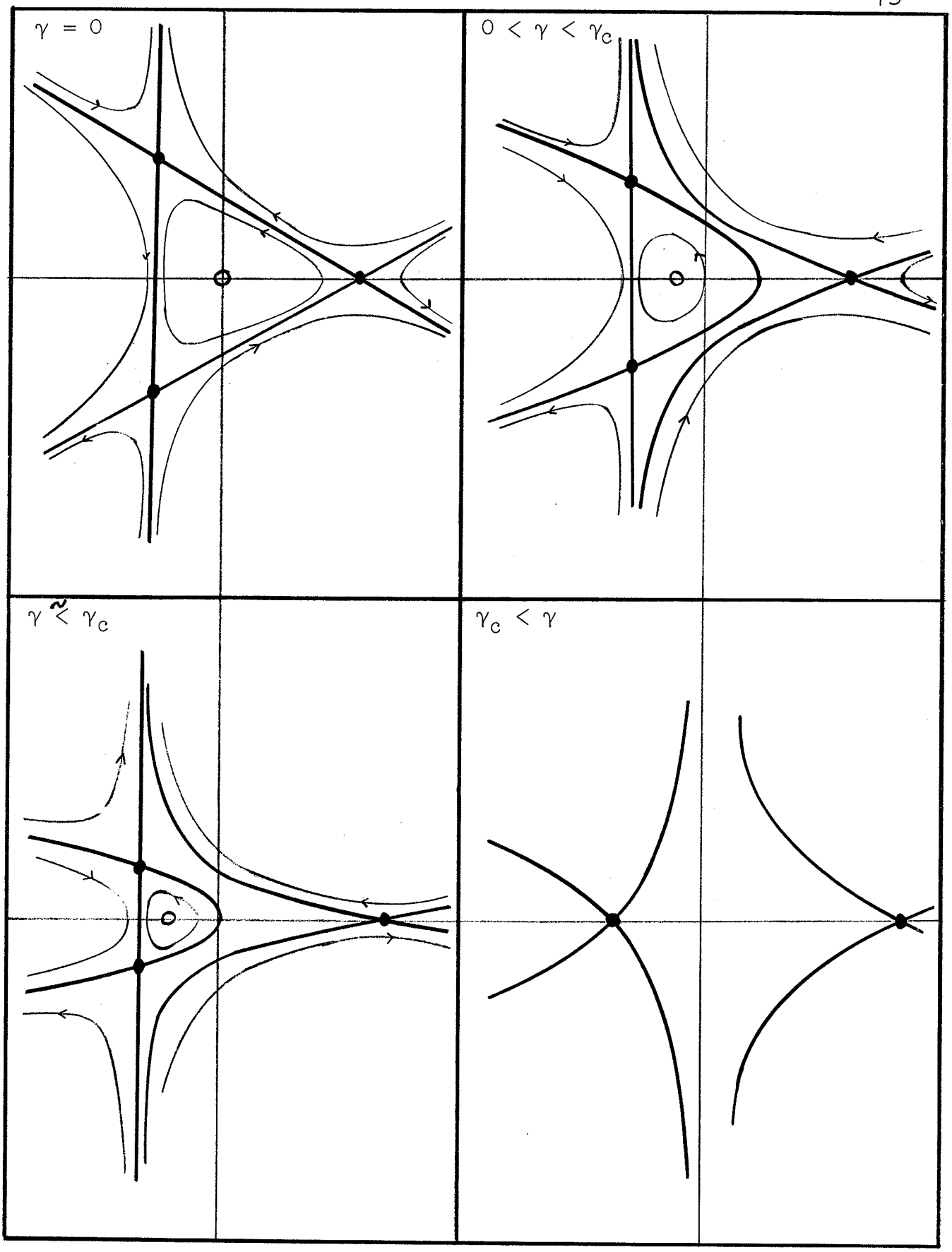

Figure 12b: Qualitative evolution of three-sector phase plots with increasing one-sector perturbation: $\phi_1=\phi_o + \pi$.

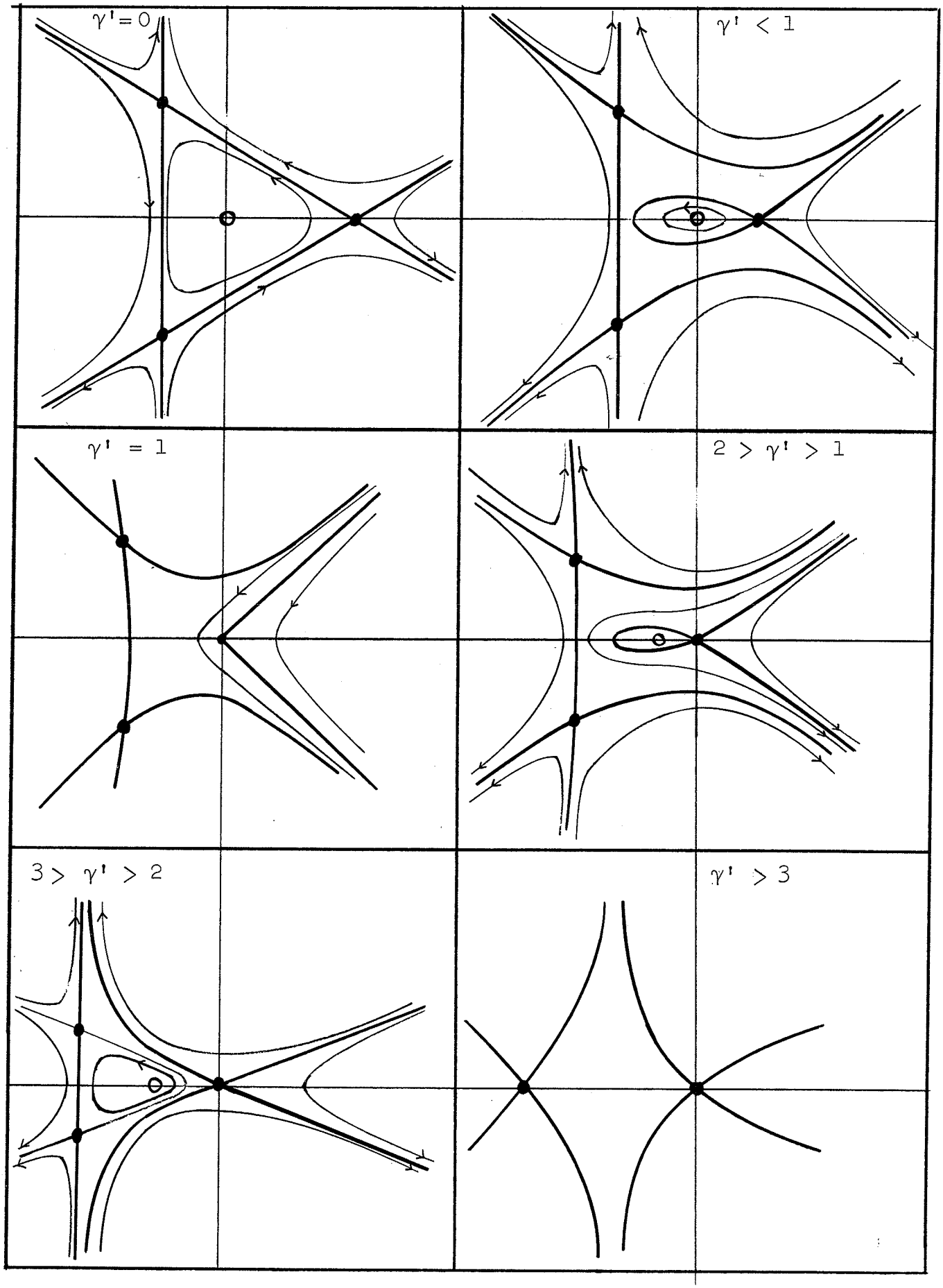

Figure 13a: Qualitative evolution of three-sector phase plots with increasing two-sector gradient perturbation: $\phi_2 = \phi_0$.

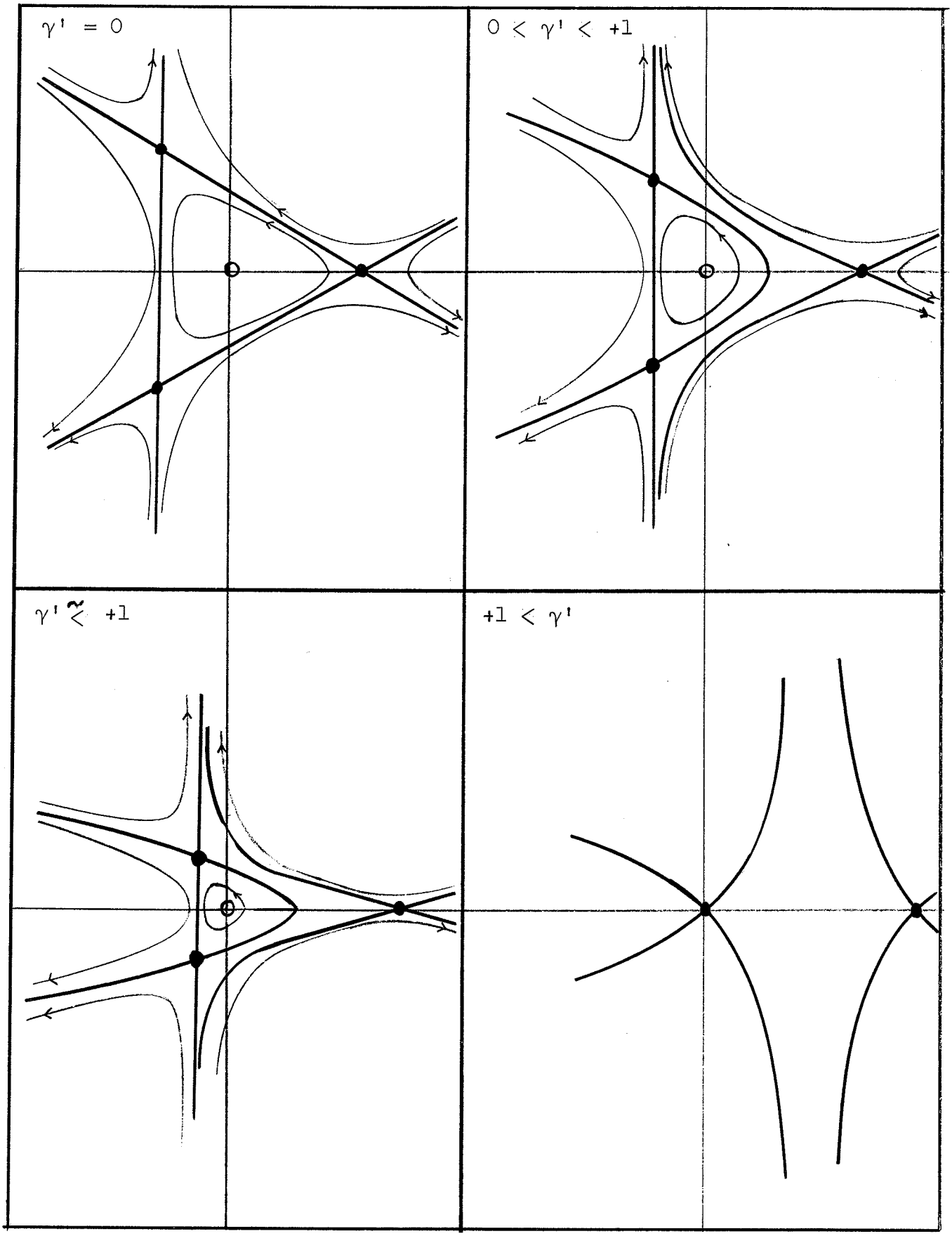

Figure 13b: Qualitative evolution of three-sector phase plots with increasing two-sector gradient perturbation: $\phi_2 = \phi_o + \pi/2$.

CHAPTER III

COMPARISON OF THEORY WITH COMPUTER RESULTS

In the following sections, a comparison will be made between the theoretical predictions of Chapter II and the computer results obtained from computer programs to see how closely the theory predicts the actual behavior of the fixed points as a function of the bump strength. In addition, the essential features of the static (no energy gain) phase plots to be introduced in the following sections will be examined and the conditions under which instability arises for a given bump field will be analyzed with the aid of the theory. Moreover, the relative stability of the two fields under investigation in this report, namely B26.29A and B26A1, will become apparent.

Recall that the theory of the previous chapter assumed the equations of motion could be expanded in a Taylor series in powers of $x(\theta)$. With the assumption that the fixed point orbits remain close to the equilibrium orbit, the higher powers of $x(\theta)$ were neglected. At energies to be considered in this report, the amplitude of the first harmonic of a fixed point orbit in the case of B26.29A is approximately 40% of the mean radius

of the E.O.; in the case of B26A1, however, the amplitude of the first harmonic is approximately 15% of the mean radius of the E.O. It is clear that the theory cannot be expected to hold as well for field B26.29A; as a result, the direct detailed comparison will be given in section 1-C between the theory and the computer results only for B26A1. However, in all other sections of this chapter, the theory has been applied to both fields and with few exceptions, seems to work about equally well for both fields.

The computer studies undertaken in this report consisted of making phase plots of results obtained from the General Orbit Code and finding fixed points with the Fixed Point Code. Given initial (r, p_r) coordinates for the particle, the General Orbit Code integrates the equations of motion and prints out the (r, p_r) of the particle along with other information once per revolution at a specified θ value. In the phase plots to be presented, the (r, p_r) of the particle was printed once per revolution at $\theta=0$. The phase plots are plots of the (r, p_r) values as obtained from the General Orbit Code with successive phase space points joined by a smooth curve. The Fixed Point Code (see Chapter I, section 5) prints out the (r, p_r) of the fixed point at $\theta=0$ and also

other data about the fixed point orbit. The fixed points found by the Fixed Point Code are accurate to 10^{-7} or 10^{-8}. All of the computer results for B26.29A are at 18.97 Mev while the results for B26A1 are at 20 Mev. These two energies were chosen because: 1. the stability region of the two fields is near its maximum at these energies; 2. the orbits are far enough from the edge field so that the field in this region is isochronous; and 3. the stable fixed points are substantially further out than the unstable fixed points. As a result of this choice, the critical values of the field bumps investigated in this report therefore represent approximately the maximum strength tolerable for the whole machine.

In the preceding chapter, it was pointed out that the bump field could be represented by Eq. (2.26); in the following sections, θ_n will be set equal to a constant. Two types of bump fields will be considered in this report: 1. a flat bump where $b_n(r)$ is constant over the radius of the machine with individual attention given to the n=1, 2, and 4 case; and 2. a two-sector gradient bump with $b_2(r)$ given by:

$$b_2(r) = a(r-R), \qquad (3.1)$$

where a is a constant and R the mean radius of the E.O. The only reason for restricting the investigation to these very simple kinds of field bumps is to simplify the analysis.

1. Orbit Properties in the Absence of a Field Bump.

Before proceeding any further, certain information pertinent to the following discussion will be presented. Figs. 14 and 15 are the (r, p_r) static phase plots for the unbumped fields B26.29A and B26A1 at 18.97 Mev and 20 Mev respectively. The three unstable fixed points and the E.O. are all indicated. In order to identify these fixed points uniquely for future reference, the three unstable fixed points will be designated as U1, U2 and U3 and the E.O. located near the center of the stable triangular region will be designated simply as E.O. from here on. Note that in Figs. 14 and 15, the same scale is used for both fields; this will be the procedure followed throughout this report. The unstable fixed point U1 was tracked by the General Orbit Code for one revolution and a Fourier analysis was made of the fixed point orbit. In table 3-1 is the amplitude and phase of the zero, first, second, third and fourth harmonic of U1 as obtained from the Fourier analysis of this orbit for fields

B26.29A and B26A1; where the equation for the orbit is assumed to be:

$$x(\theta) = \sum_{n=o} |x_n| \cos n(\theta - \theta'_n).$$

The amplitude, $|x_n|$, of the fixed point orbit of U2 and U3 is the same as the amplitude of U1; the phase, θ'_n, of U2 and U3 with respect to the phase of U1 is 120° less for U2 and 120° greater for U3. In the previous chapter, it was assumed that the first harmonic of the fixed point orbit was the dominant term in the Fourier series (Chapter II, section 1). The following data indicates that this assumption was correct.

TABLE 3-1: Amplitude and phase of the zero, first, second, third and fourth harmonic of the fixed point orbit for U1.

B26.29A	U1	
	x_n	θ'_n
$x_o(\theta)$	.01043	
$x_1(\theta)$	.08256	170.2°
$x_2(\theta)$	.00683	-56.5°
$x_3(\theta)$	.00222	117.0°
$x_4(\theta)$	.00299	42.7°

B26A1	U1	
	x_n	θ'_n
$x_o(\theta)$	.00113	
$x_1(\theta)$	.02842	167.5°
$x_2(\theta)$	.00323	41.4°
$x_3(\theta)$	.00041	-12.4°
$x_4(\theta)$	.00076	16.9°

In the previous chapter, the solution of a fixed point orbit (with or without a field bump) was assumed to be:

$$y_1(\phi) = A \cos (\phi+\alpha-\phi_o).$$

On the other hand, the first harmonic component of the displacement $x(\theta)$ of the fixed point orbit relative to the E.O. position (in the absence of a field bump) is given by:

$$x_1(\theta) = |x_1| \cos (\theta-\theta_1'), \qquad (3.2)$$

where x_1 and θ_1' are obtained from the Fourier analysis of the fixed point orbit and for the case of the unbumped fields are given above. Since it is assumed $y_1(\theta) \cong x_1(\theta)$ in accord with the discussion of the previous chapter,

$$\theta_1' = \phi_o - \alpha \qquad (3.2a)$$

$$A = |x_1|. \qquad (3.2b)$$

If U1 is specified as being along the α=0 axis, ϕ_o=170.2° in the case of B26.29A and ϕ_o=167.5° for B26A1. For B26A1, U2 is then located at 47.5° and U3 at 287.5° corresponding to $\alpha = \pm$ 120°. If on the other hand, it is specified that U2 is located along the α=0 axis, ϕ_o=47.5°. Similarly if U3 is on the α=0 axis,

$\phi_o = 287.5°$

With the data given above, it is possible to specify ϕ_1 so as to obtain "pure one-corner opening" or "pure two-corner opening" of the stable triangle for B26A1. In the case of the one-sector perturbation, if $\phi_1 = \theta_1' = 167.5°$, "pure one-corner opening" of the stable triangle is obtained at U1. If on the other hand, $\phi_1 = \theta_1' + \pi = 347.5°$, "pure two-corner opening" of the stable triangle is obtained at U2 and U3. To obtain "pure one-corner opening" at U2, $\phi_1 = 47.5°$; to obtain "pure one-corner opening" at U3, $\phi_1 = 287.5°$. If $\phi_1 = 47.5° + \pi = 227.5°$, "pure two-corner opening" of the triangle is obtained at U1 and U3; if $\phi_1 = 287.5° - \pi = 107.5°$, "pure two-corner opening" is obtained at U1 and U2. To go from "pure one-corner opening" to "pure two-corner opening" or vice versa, the location of ϕ_1 need only be rotated by 60°. Note that if ϕ_1 has a value intermediate between any of the six specified values of ϕ_1 an appropriate mixture of one and two-corner opening is obtained.

A similar analysis may be carried out for the case of a two-sector gradient perturbation for field B26A1. If $\phi_2 = \theta_1' = 167.5°$ (or 347.5°), "pure one-corner opening" is obtained at U1; for $\phi_2 = \theta_1' \pm 90° = 77.5°$ or 257.5°,

"pure two-corner opening" is obtained at U2 and U3. To observe "pure one-corner opening" at U2, ϕ_2 = 47.5° or 227.5°; to observe "pure one-corner opening" at U3, ϕ_2 = 287.5° or 107.5°. If ϕ_2 = 137.5° or 317.5°, "pure two-corner opening" is obtained at U1 and U3; for "pure two-corner opening" at U1 and U2, ϕ_2 = 17.5° or 197.5°. If ϕ_2 has a value other than the twelve specified above, an appropriate mixture of one and two-corner opening is obtained. For the two-sector gradient perturbation, the location of ϕ_2 need only be rotated by 30° to go from "pure one-corner opening" to "pure two-corner opening" or vice versa. The same procedure may be applied to field B26.29A to determine when "pure one or two-corner opening" or a mixture of one and two-corner opening occurs for a specific value of ϕ_1 or ϕ_2. The results obtained for the one-sector perturbation and two-sector gradient perturbation are summed up in the following tables for fields B26A1 and B26.29A; furthermore, for a given field bump, the values of ϕ_1 and ϕ_2 can be obtained from the formulae in tables 2-1 and 2-2. In the following table, if ϕ_2 is replaced by $\phi_2 + \pi$, the same result is obtained.

TABLE 3-2: Specification of ϕ_1 and ϕ_2 to obtain "pure one-corner opening" or "pure two-corner opening" of the stable triangle for fields B26A1 and B26.29A.

B26A1	ONE-SECTOR PERTURBATION		TWO-SECTOR GRADIENT PERTURBATION
ϕ_1	Open Corner(s)	ϕ_2	Open Corner(s)
47.5°	U2	17.5°	U1 and U2
107.5°	U1 and U2	47.5°	U2
167.5°	U1	77.5°	U2 and U3
227.5°	U1 and U3	107.5°	U3
287.5°	U3	137.5°	U1 and U3
347.5°	U3 and U2	167.5°	U1
B26.29A	ONE-SECTOR PERTURBATION		TWO-SECTOR GRADIENT PERTURBATION
ϕ_1	Open Corner(s)	ϕ_2	Open Corner(s)
50.2°	U2	20.2°	U1 and U2
110.2°	U1 and U2	50.2°	U2
170.2°	U1	80.2°	U2 and U3
230.2°	U1 and U3	110.2°	U3
290.2°	U3	140.2°	U3 and U1
350.2°	U2 and U3	170.2°	U1

To explain the motion of the fixed points and the qualitative features of the static phase plots, a number

of parameters introduced in the previous chapter will have to be evaluated, namely ξ, w_1, 3λ and ζ_1. The parameters ξ_1, w_1, 3λ and ζ_1 may be calculated for the two fields from Eqs. (2.16), (2.18), (2.19) and (2.15a) or; the parameters ξ_1 and ζ_1 may be obtained from the Fourier analysis of the E.O. Below is a comparison of ξ_1 and ζ_1 as determined from the formulae and as determined from the Fourier analysis of the E.O. The data shows the similarity of the two results.

B26.29A		
	FOURIER ANALYSIS	FORMULAE
ξ_1	+.0506	+.0511
ζ_1	6.7°	6.7°

B26A1		
	FOURIER ANALYSIS	FORMULAE
ξ_1	+.0239	+.0240
ζ_1	68.6°	68.7°

Below are the values of ξ_1, ζ_1, w_1 and 3λ obtained from the Fourier analysis of the E.O. and Eqs. (2.25) and (2.24). The values of R and ν_r were obtained from the E.O. Code; the value of $A_o = |x_1|$ was obtained from table 3-1 and the value of ϕ_o was obtained for U1 from table 3-1.

TABLE 3-3: Numerical representation of certain parameters necessary to discuss the phase plots.

	B26.29A	B26A1
Energy (Mev)	18.97	20.00
R(Mean Radius)	.1969	.2029
ξ_1	+.0506	+.0239
ζ_1	6.7°	68.6°
w_1	+.183	+.165
3λ	269.1°	178.6°
ν_r	1.0552	1.0383
A_o	.0826	.0284
ϕ_o	170.2°	167.5°
B_o	1.0079	1.0187

2. Flat One-Sector Bump Field.

A. General Results: The flat one-sector bump field $b(r,\theta)$ is given by:

$$b(r,\theta) = b_1 \cos(\theta-\theta_1),$$

where b_1 and θ_1 are constant over the radius of the machine.

From the formulae of tables 2-1, 2-2 and the results presented at the end of the previous section, the following

results are obtained for fields B26.29A and B26A1.

TABLE 3-4: Relations between perturbation parameters and the bump field for the flat one-sector bump for B26.29A.

B26.29A	n=1
$\delta\cos\phi_1$	$-.1954\ b_1 \cos\theta_1$
$\delta\sin\phi_1$	$-.1954\ b_1 \sin\theta_1$
$\delta'\cos 2\phi_2$	$-.303\ b_1 \sin(\theta_1-269.1°)-(.0127)\ b_1 \cos(20.1°-\theta_1)$
$\delta'\sin 2\phi_2$	$-.303\ b_1 \cos(\theta_1-269.1°)-(.0127)\ b_1 \sin(20.1°-\theta_1)$

TABLE 3-5: Relations between perturbation parameters and the bump field for the flat one-sector bump for B26A1.

B26A1	n=1
$\delta\cos\phi_1$	$-.1992\ b_1 \cos\theta_1$
$\delta\sin\phi_1$	$-.1992\ b_1 \sin\theta_1$
$\delta'\cos 2\phi_2$	$-(.270)\ b_1 \sin(\theta_1-178.6°)-(.00589)b_1\cos(205.8°-\theta_1)$
$\delta'\sin 2\phi_2$	$-(.270)\ b_1 \cos(\theta_1-178.6°)-(.00589)b_1\sin(205.8°-\theta_1)$

From the above tables, the second term of $\delta'\cos 2\phi_2$ and $\delta'\sin 2\phi_2$ is small in comparison with the first term and may be neglected. The quantity $|\delta'/(4\ \delta/A_o)|$ gives an estimate of the relative effect on stability of the two-

sector gradient perturbation in comparison to the one-sector perturbation according to Eq. (2.18) in the previous chapter. Below is the evaluation of this quantity for the two fields.

n=1	B26.29A	B26A1
$\lvert\delta'/(4\ \delta/A_o)\rvert$	.032	.010

It may be concluded that in comparison to the one-sector perturbation effect, the two-sector gradient perturbation effect is small and can be neglected. Since δ is positive by definition, the formulae of tables 2-1 and 2-2 give:

$$\delta = R\,|b_1|/B_o \tag{3.3}$$

$$\phi_1 = \theta \pm 180°,\ b_1 > 0;$$

$$\phi_1 = \theta_1,\ b_1 < 0. \tag{3.4}$$

From Eq. (2.18c), the stability condition gives the critical value of δ for "pure one-corner opening" as:

$$\delta_c/A_o = \epsilon/2. \tag{3.5}$$

For "pure two-corner opening", the critical value is three times as great and is given as:

$$\delta_c/A_o = 3\epsilon/2. \tag{3.6}$$

If the field bump is phased so that a mixture of one and two-corner opening is obtained, the critical value of δ will lie between these two limits. Combining Eqs. (3.3) and (3.5) gives the critical value of b_1 for which the stable region disappears in the case of "pure one-corner opening" as:

$$(b_1)_c = \epsilon A_o B_o / 2R. \tag{3.7}$$

Below are the critical values of b_1 for both fields for both one and two-corner opening.

One-corner Opening:

B26.29A: $(b_1)_c = +.0117 = 159$ gauss

B26A1: $(b_1)_c = +.0027 = 38.8$ gauss

Two-corner Opening:

B26.29A: $(b_1)_c = +.0351 = 478$ gauss

B26A1: $(b_1)_c = +.0081 = 116$ gauss.

It is evident from Eq. (3.7) that the critical bump strength is much greater for B26.29A than for B26A1 because the value of A_o is substantially higher for B26.29A. This result will be generally true over the entire machine since the stability limits for the weak-spiral field B26.29A are much greater than those for the moderate-spiral field B26A1.

B. Discussion of the Phase Plots: The field bumps to be investigated in this section have been specialized to the case where $\theta_1 = 0$ and $b_1 > 0$. Since δ is positive by definition, the following results are obtained from the formulae of tables 3-4 and 3-5 for the case where $\theta_1 = 0$ and $b_1 > 0$.

$$\text{B26.29A, B26A1:} \phi_1 = 180° \tag{3.8}$$

$$\text{B26A1: } \delta = .1992 b_1 \tag{3.9a}$$

$$\text{B26.29A:} \delta = .1954 b_1 . \tag{3.9b}$$

It was stated in the previous section that if $\phi_1 = 167.5°$, "pure one-corner opening" is obtained at U1 for field B26A1. Since $\phi_1 = 180°$ when $\theta_1 = 0$ and $b_1 > 0$, a mixture of one and two-corner opening is expected at U1 and U3 (see table 3-2) with the one-corner opening at U1 dominating over the two-corner opening at U1 and U3. Figs. 16a, 16b and 16c are phase plots for B26A1 with $\theta_1 = 0$ and $b_1 = +.001$, $+.002$ and $+.004$ respectively. On all of the phase plots to be presented in this chapter, the new location of the four fixed points will be designated by "circles" (0) and the position of the four fixed points before any bump field was added will be designated by "x's". Figs. 16a, 16b and 16c show that as b_1 increases,

the two fixed points U1 and E0 move toward each other. As evidenced by Figs. 16b and 16c, the two fixed points U1 and E0 coincide and the stable region disappears at a value of $+002 < b_1 < +.004$. According to Eq. (3.7), the critical value of b_1 which corresponds to the disappearance of the stable region for "pure one-corner opening" is given by:

$$(b_1)_c = \epsilon A_o B_o / 2R = +.0027 = 38.8 \text{ gauss.}$$

Since the case being considered here is not "pure one-corner opening", the critical value of b_1 for which the stable region disappears should be somewhat greater than $b_1 = +.0027$ but substantially less than three times this value (i.e. $b_1 = +.0081$). Using the results of Figs. 14, 16a and 16b, a semi-quantitative extrapolation based on the theory of Chapter II gives the value of $b_1 = +.0031$ as the critical value for which the stable region should disappear in this case which is in agreement with the results obtained above.

At the same time as U1 and E0 move toward each other, the two fixed points U2 and U3 move away from the initial position of E0 and qualitatively move toward the $\alpha = \pm 90°$ axes as measured from the axis joining the initial positions of U1 and E0. A comparison of these

results with Fig. 12a shows the qualitative similarity between the computer results and theoretical predictions; that is, the theory predicted that for "pure one-corner opening" U1 and E0 would move toward each other along the $\alpha = 0$ axis and at the same time, the two fixed points at $\alpha = \pm 120°$ move toward the $\alpha = \pm 90°$ axes. These same general features are observed in Figs. 16a, 16b and 16c. Since Figs. 16a, 16b and 16c represent a mixture of one and two-corner opening at U1 and U3, qualitatively the fixed point U3 experiences a force tending to move U3 out toward the $\alpha = -90°$ axis and a weaker force tending to move U3 toward E0; therefore, it is expected and observed that U2 moves out toward the $\alpha = +90°$ axis faster than U3 moves out toward the $\alpha = -90°$ axis.

With the addition of the bump field, the stable region is determined by U1 and E0. As evidenced in Figs. 16a, 16b and 16c, as b_1 increases, U1 and E0 move toward each other and the stable region becomes smaller until it disappears for some critical value of b_1. In Figs. 16a, 16b and 16c, the curves labeled (a) are indicative of the nearly "pure one-corner opening" at U1; the curve labeled (b) shows the presence of the small "two-corner opening" at U1 and U3.

Consider next the effects of the field bump on the field B26.29A. Figs. 17a and 17b are phase plots for B26.29A with $b_1 = +.004$ and $+.02$ respectively. From the figures, the stable region disappears for some b_1 between these values. According to Eq. (3.5), the critical value of b_1 for "pure one-corner opening" is given by:

$$(b_1)_c = \epsilon A_o B_o / 2R = + .0117 = 159 \text{ gauss.}$$

For "pure two-corner opening", the critical bump strength is three times this value (i.e. $b_1 = +.0351$). A semi-quantitative linear interpolation from Figs. 15 and 17a gives $b_1 = +.013$ as the critical value for which the stable region of B26.29A will disappear assuming "pure one-corner opening". It is seen that this is in agreement with the result obtained from Eq. (3.5).

Since ϕ_1 is again 180° and since $\phi_1 = 170.2°$ corresponds here to "pure one-corner opening" at U1 for field B26.29A, the fixed points of B26.29A undergo almost the same relative displacement as the fixed points of B26A1. As a result, the discussion given above for B26A1 serves equally well to explain the behavior of the fixed points for B26.29A. Again the curves labeled ⓐ indicate the one-corner opening effect at U1 and curves labeled ⓑ indicate the small two-corner opening effect at U1 and U3.

C. Detailed Comparison of Computer Results with the Theory: As was mentioned previously, a direct comparison of the computer results and the theoretical predictions will be made only for field B26A1. In section 2 of Chapter II, formulae were obtained governing the motion of the fixed points for a one-sector perturbation for the "pure one-corner opening" and "pure two-corner opening" situations. In the present section, the results will be presented of computer studies aimed at checking in detail the accuracy of these formulae.

From tables 3-4 and 3-5, if $\theta_1 = -12.5°$, $\phi_1 = 167.5°$ $= \phi_o$. According to the theory, when $\phi_1 = \phi_o$, "pure one-corner opening" is obtained at U1 when γ is positive and "pure two-corner opening" is obtained at U2 and U3 when γ is negative where $\gamma \equiv \delta/2\epsilon$. To check the theory of Chapter II, the flat one-sector bump field given by:

$$b(r,\theta) = b_1 \cos(\theta+12.5°),$$

was used in a new set of orbit computations. With this choice, "pure one-corner opening" should be observed at U1 when b_1 is positive, and "pure two-corner opening" should be observed at U2 and U3 when b_1 is negative.

For each value of b_1 the Fixed Point Code was used to find all four of the fixed points for this field at

θ=0. Each of the fixed points was then run through the General Orbit Code for one revolution to obtain the fixed point orbit at all 48θ values; a Fourier analysis was then made of each fixed point orbit. From the Fourier Analysis Code [23], the amplitude $|x_1|$ and the phase θ_1' of the first harmonic, as defined in Eq. (3.2a) and (3.2b) were obtained for each fixed point. Recall that at the beginning of this chapter it was pointed out the A = $|x_1|$ and $\alpha = \phi_1 - \theta_1'$ where A and α are the parameters specifying the fixed point orbit as defined in the theory of Chapter II. In table 3-6 the resultant values of the amplitude A and the phase α are given for all of the fixed points for each value of b_1. In addition, the entry in parenthesis in table 3-6 was obtained from the theoretical formulae of Chapter II to give some idea of the difference between the theoretical predictions and the computer results at this value of b_1 where the greatest difference occurs. According to the theory, with b_1 positive and $\phi_1 = 167.5°$ "pure one-corner opening" is obtained at U1; moreover, both E0 and U1 should have $\alpha = 0$ in this case. The theory also predicts that the amplitude of U2 and U3 will be equal and that U2 and U3 will have α equal in magnitude but opposite in sign for a given b_1; furthermore, as $b_1 > 0$ increases, the value of α for U2 and U3 should

TABLE 3-6: Values of A and α for E0, U1, U2, and U3 for various bump strengths.

	E0		U1		U2		U3	
b_1	A	α	A	α	A	α	A	α
+.0026	.01108	-.1°	.01735	-.1°	.03163	116.4°	.03175	-116.3°
+.0020	.00691	-.1°	.02154	-.1°	.03091	117.1°	.03101	-117.0°
+.0014	.00433	-.1°	.02410	0°	.03018	117.9°	.03026	-117.9°
+.0010	.00293	-.1°	.02550	0°	.02969	118.5°	.02974	-118.4°
+.0060	.00168	-.1°	.02675	0°	.02918	119.1°	.02922	-119.0°
0	0	-	.02842	0°	.02842	120.0°	.02842	-120.0°
-.0040	.00834	180.3°	.03674	+.2°	.02285	129.5°	.02245	-130.0°
-.0060	.01161	181.4°	.04001	+.3°	.01963	138.7°	.01880	-140.2°
-.0070	.01316	183.7°	.04155	+.3°	.01789	146.3°	.01663	-150.3°
(-.0070)	(.01260)	(180.0°)	(.04080)	(0°)	(.01705)	(146.5°)	(.01705)	(-146.5°)
-.0080			.04296	+.4°	.01620	159.0°		

go from $\pm$ 120° to $\pm$ 90° respectively. Table 3-6 shows that these results to a good approximation are indeed obtained for positive b_1.

If b_1 is negative, "pure two-corner opening" should be obtained at U2 and U3; moreover, U1 should still have $\alpha = 0$ but E0 should now have $\alpha = 180°$. Again the magnitude of A should be the same for U2 and U3 and the value of α for U2 and U3 should be equal in magnitude and opposite in sign; this time however, α should go from $\pm$ 120°to $\pm$ 180° as $b_1 < 0$ decreases.

The computer results of table 3-6 agree very well with the theoretical predictions for positive b_1 where fairly weak field bumps were used. In the case of negative b_1, the agreement is not quite as good especially for values of b_1 near the stability limit. It will be shown later that the variation between the theoretical predictions and computer results is due to a shift from "pure two-corner opening" for large negative field bumps.

In table 3-6 the values of A and α are given only for U1 and U2 for $b_1 = -.0080$. According to Eq. (3.6), this value of b_1 is very close to the stability limit and the three fixed points U2, U3 and E0 are very close together. Two attempts were made to find the other two fixed points at this value of b_1 but in each instance,

the Fixed Point Code found only U1 and U2. It is possible but not probable, for reasons to be given below, that the two fixed points U3 and E0 still exist. To resolve the problem of the existance or non-existance of U3 and E0 would require an excessive amount of computer time and since it was believed that U3 and E0 no longer existed for this value of b_1, no further attempt was made to resolve the problem.

In the following pages, reference will be made to the quantity γ introduced in Chapter II, section 2. From Eq. (3.3), it is possible to evaluate the quantity γ in terms of the bump strength. Eq. (3.3) gives the following result for γ:

$$\gamma \equiv \delta/2\epsilon = Rb_1/2B_o(\nu_r-1).$$

Along with this quantity γ, reference will also be made to a number of formulae derived in Chapter II. For convenience, the equations which will be referred to in the following discussion will be listed again along with the fixed points which corresponds to each equation.

$$b_1 > 0;$$

$$\text{U1, E0: } \alpha=0;\ \gamma = A(1-A/A_o) \qquad (3.10)$$

U2, U3: $\cos \alpha = -A_o/2A$, $(A>A_o)$;

$$\gamma = -A_o(1 - A^2/A_o^2) \tag{3.11}$$

$$b_1 < 0;$$

U1: $\alpha = 0$; $\gamma = A(1 - A/A_o)$ (3.12)

E0: $\alpha = \pi$; $\gamma = -A(1 + A/A_o)$ (3.13)

U2, U3: $\cos \alpha = - A_o/2A$, $(A < A_o)$;

$$\gamma = -A_o(1-A^2/A_o^2) \tag{3.14}$$

Fig. 18 is a plot of γ versus A; Fig. 19 is a plot of γ versus α. The solid lines in each figure represent plots of the theoretical equations above. The fixed point which belongs with a certain section of the curve is indicated on the figure and the direction in which the fixed point is moving as a function of the bump strength is also shown by an arrow. The points on the figures represent the computer results obtained from table 3-6. Even though no phase plots were obtained for these cases, a comparison of the theory of the previous chapter with table 3-6 and Figs. 18 and 19 gives reasonable proof that "pure one-corner opening" was obtained at U1 for positive b_1 and nearly "pure two-corner opening" was obtained at U2 and U3 for negative b_1.

Figs. 18 and 19 indicate that some of the computer points do not fall exactly on the theoretical curves for $b_1 < 0$; moreover, the more negative b_1, the more pronounced the difference between the theoretical curves and the computer results becomes. It is evident from Figs. 18 and 19 that for values of b_1 near the stability limit there is a shift from "pure two-corner opening" at U2 and U3 to a mixture of two-corner opening at U2 and U3 and one-corner opening at U3. It should be emphasized however that the deviation from "pure two-corner opening" is very small. According to the theory, for "pure two-corner opening" E0, U2 and U3 should meet on the $\alpha = 180°$ axis simultaneously when $b_1 = -.0081$. Figs. 18 and 19 and the results of table 3-6 indicate that E0 and U3 merge first leaving only one fixed point U2 which will presumably move out toward the $\alpha = 180°$ axis. In Fig. 18, the dashed line joins the computer results of table 3-6 for negative values of b_1; from the figure, it can be assumed that E0 and U3 merge at a value of b_1 somewhat greater than -.0081; since "pure two-corner opening" is the extreme magnitude of b_1 for destruction of the stable region, it is therefore expected that U3 and E0 will meet for some value of b_1 less than this critical value.

Since the theory of Chapter II is only semi-quanti-

tative, perfect agreement between the theory and computer results is not expected. Furthermore, it was previously pointed out that the flat one-sector field bump gives rise to a two-sector gradient perturbation which is about 1% in effect of the one-sector perturbation for field B26A1. Since $\delta' \neq 0$, it is expected that neglecting the two-sector gradient perturbation will have some effect on the theoretical curves.

3. Flat Two and Four-Sector Bump Field.

A. General Considerations: The next two bump fields investigated in this report were the flat two-sector bump field and flat four-sector bump field given by:

$$b(\bar{r},\theta) = b_n \cos n(\theta-\theta_n), \qquad (3.15)$$

where $n = 2$ or 4, θ_n is a constant and b_n is constant over the radius of the machine. From the formulae of tables 2-1, 2-2 and the results of table 3-3, it is possible to calculate the parameters δ, δ', ϕ_1 and ϕ_2 in terms of the two constants b_n and θ_n for the flat two and four-sector bump field. In the tables immediately below, the parameters δ, δ', ϕ_1 and ϕ_2 have been evaluated in terms of these two constants for the n=2 and the n=4 case for both fields under investigation in this report.

TABLE 3-7: Evaluation of perturbation parameters in terms of the bump strength and phase angle for fields B26.29A and B26A1 for the two-sector flat bump.

n=2	B26.29A	B26A1
δ	$(.0345)b_2$	$(.0286)b_2$
ϕ_1	$182.1°-2\theta_2$	$84.3°-2\theta_2$
δ'	$b_2/1.0079$	$b_2/1.0187$
ϕ_2	$90° + \theta_2$	$90° + \theta_2$

TABLE 3-8: Evaluation of perturbation parameters in terms of the bump strength and phase angle for fields B26.29A and B26A1 for the four-sector flat bump.

n=4	B26.29A	B26A1
δ	$(.0109)b_4$	$(.00692)b_4$
ϕ_1	$4\theta_4+171.4°$	$4\theta_4+289.3°$

Note that δ is independent of θ_n for both fields.

a) General Considerations For The Two-Sector Flat Bump Field: According to the theory of Chapter II, section 4, the quantity $|\delta'/(4\delta/A_o)|$ gives an estimate of the relative effect on stability of the two-sector gradient perturbation in comparison to the one-sector perturbation. Immediately below, the quantity $|\delta'/(4\delta/A_o)|$

has been evaluated for fields B26.29A and B26A1 using the flat two-sector bump field parameters given above.

TABLE 3-9: Evaluation of the quantity $|\delta'/(4\delta/A_o)|$ for fields B26.29A and B26A1 for the two-sector flat bump.

n=2	B26.29A	B26A1
$\|\delta'/(4\delta/A_o)\|$	.594	.244

Unlike the n=1 case discussed in the previous section, the relative effect of the two-sector gradient perturbation on stability is no longer negligible in comparison to the one-sector perturbation; as a result, when discussing the phase plots for n=2, the effect on stability of the two-sector gradient perturbation cannot be neglected. The detailed theory given in Chapter II governing the motion of the fixed points as a function of the bump strength was limited to the cases where either δ or δ' were identically equal to zero. As shown above, the two-sector flat bump introduces into the equations of motion both a one-sector perturbation and a two-sector gradient perturbation neither of which is negligible in comparison to the other; as a result, the detailed theory on the motion of the fixed points given in sections 2 and 3 in the previous chapter is not quantitatively applicable

here.

It was shown in Chapter II, section 4, that when both a one-sector perturbation and two-sector gradient perturbation are present the simple criterion for stability is given by:

$$\Delta^2 \equiv (\delta')^2+(4\delta/A_o)^2 + 2\delta'(4\delta/A_o)\cos(3\phi_o-\phi_1-2\phi_2)<(4\epsilon)^2. \quad (3.16)$$

It must be remembered however, that the above equation gives only an approximate value for the critical bump strength.

If the results of table 3-7 are substituted into Eq. (3.16), it turns out that the function Δ as defined in section 4, Chapter II is independent of θ_2. Below is the evaluation of Δ in terms of b_2 for fields B26.29A and B26A1.

$$\text{B26.29A:} \quad \Delta = (.974)\, b_2 \quad (3.17)$$

$$\text{B26A1} \quad : \quad \Delta = (3.66)\, b_2. \quad (3.18)$$

The critical value of b_2 may then be found by setting $\Delta = 4\epsilon$. If this is done, the critical value of b_2 for fields B26.29A and B26A1 turns out to be:

$$\text{B26.29A:} \ (b_2)_c = + .227 = 3100 \text{ gauss}$$

$$\text{B26A1} \ : \ (b_2)_c = + .0419 = 571 \text{ gauss}.$$

A comparison of the critical values for the flat two-sector field bump with those determined in the previous section for the flat one-sector field bump shows the critical values for the flat two-sector bump to be 15 or 20 times greater than the critical values for the flat one-sector bump.

b) General Considerations for the Flat Four-Sector Field Bump: The flat four-sector bump field introduces only a one-sector perturbation into the equations of motion; as a result, a quantitative comparison can be made between the theory of Chapter II, section 2 and the computer results. As in the case of the flat one-sector field bump, Eq. (3.5) gives the critical value of b_4 for "pure one-corner opening" and Eq. (3.6) may be used to determine the critical value of b_4 for "pure two-corner opening". Using the results in table 3-8, the critical value of b_4 obtained for "pure one-corner opening" for fields B26.29A and B26A1 is given by:

$$\text{B26.29A: } (b_4)_c = .209 = 2850 \text{ gauss}$$
$$\text{B26A1 : } (b_4)_c = .0788 = 1070 \text{ gauss.}$$

The critical value of b_4 for "pure two-corner opening" is three times the critical value for "pure one-corner opening". For a mixture of one and two-corner opening, the critical value of b_4 lies somewhere between these

two extreme values. A comparison of the critical values for the flat four-sector bump with those of the flat one-sector bump indicates that the critical value for b_4 is 18 times larger than $(b_1)_c$ for field B26.29A and 27 times larger for field B26A1.

B. Discussion of the Phase Plots:

a) Flat Two-Sector Bump Field: All the phase plots to be presented in this section are for a flat two-sector bump field which have been specialized to the case where $\theta_2 = 0$. Substitution of this value of θ_2 into the formulae of table 3-7 gives the following results for B26.29A and B26A1.

n=2	B26.29A	B26A1
ϕ_1	182.1°	84.3°
ϕ_2	90°	90°

The effect on the fixed points of each perturbation will be presented as if the other perturbation were not present and the net effect of the flat two-sector bump field will be determined from the phase plots. In the following phase plots, the new location of the four fixed points for the field being used will be designated by "circles" (0) and the position of the four fixed points before any bump field was added will be designated by "x's".

According to table 3-2, if $\phi_1 = 83.4°$ for field B26A1, a mixture of one and two-corner opening should be observed with the two-corner opening U1 and U2 dominating over the one-corner opening at U2. This would be the situation if the two-sector perturbation were not present. According to this same table, with $\phi_2 = 90°$, a mixture of two-corner opening at U2 and U3 and one-corner opening at U3 would be observed for field B26A1 were the one-sector perturbation not present. Figs. 20a and 20b are static phase plots for field B26A1 with $b_2 = +.004$ and $+.020$ respectively. From the two figures, the effect of the flat two-sector bump field appears to be nearly "pure one-corner opening" at U2 which is not inconsistent with the considerations immediately above. The figures indicate that as b_2 increases, E0 and U2 move toward each other and the stable region which is now determined by E0 and U2 is reduced in size; at the same time, U3 remains almost stationary and U1 moves away from E0. When $b_2 = +.020$ the stable region is almost non-existent indicating that a further increase in b_2 would result in the disappearance of the stable region. In Figs. 20a and 20b, the curves labeled ⓐ indicate the one-corner opening at U2; none of the curves shown indicate any two-corner opening.

According to Eq. (3.16), the critical value of b_2 which will cause the stable region of B26A1 to disappear is:

$$(b_2)_c = +.0419 = 571 \text{ gauss};$$

this value is almost twice as large as the value obtained from the phase plots. If the two-sector gradient perturbation is neglected, which is not too unrealistic for B26A1 (see table 3-9), the critical value of b_2 according to Eqs. (3.5) and (3.6) lies between +.0190 and +.0571. It is evident from Figs. 20a and 20b that the stable region disappears when b_2 is slightly larger than +.020 which is a little larger than the critical value for "pure one-corner opening" obtained from Eq. (3.4). The critical value of b_2 calculated from Eq. (3.16) is approximately twice as large as it should be. Since the two perturbations produce nearly "pure one-corner opening" at U2, it is expected that the critical value of b_2 will be less than the critical value determined from Eq. (3.16).

Consider next the case of B26.29A; for this field, $\phi_1 = 182.1°$ and $\phi_2 = 90°$ as obtained from table 3-7. According to table 3-2, if $\phi_1 = 182.1°$ nearly "pure one-corner opening" would be observed at U1 along with a small amount of two-corner opening at U1 and U3 if the two-sector gradient perturbation were not present; with

$\phi_2 = 90°$, a mixture of two-corner opening at U2 and U3 and one-corner opening at U3 should be observed if the one-sector perturbation were not present. Figs. 21a and 21b are static phase plots for B26.29A with $b_2 = +.020$ and $+.100$ respectively. The two figures indicate that the flat two-sector bump field produces nearly "pure one-corner opening" at U3 along with some two-corner opening at U2 and U3; this result is not apparently consistent with the values given above in the notion of the vector addition of the two effects. In Figs. 21a and 21b, the curves labeled (a) indicate the one-corner opening at U3 and the curves labeled (b) indicate the small amount of two-corner opening at U2 and U3. As b_2 increases, E0 and U3 move toward each other and the stable region shrinks; at the same time, U1 moves away from E0 and U2 moves toward E0. From these figures, it is estimated that for some value of b_2 slightly greater than $+.100$ the stable region disappears. According to Eq. (3.16), the critical value of b_2 which will cause the stable region to disappear is:

$$(b_2)_c = +.227 = 3100 \text{ gauss},$$

which is again about twice the actual value observed. From the data of table 3-9, it is clear that both per-

turbations must play a significant role in determining stability and therefore it is not realistic to compute the critical bump strength assuming one or the other is negligible; as noted above, since the result of the two perturbations is nearly "pure one-corner opening" it is expected that the critical bump strength will be less than the critical value determined from Eq. (3.16).

b) Flat Four-Sector Bump Field: As in the n=1 and n=2 cases, the phase plots to be presented for the flat four-sector bump field have been specialized to the case where $\theta_4 = 0$. Substitution of this value of θ_4 into table 3-8 gives the following results for B26.29A and B26A1.

n=4	B26.29A	B26A1
δ	$(.0109)b_4$	$(.00692)b_4$
ϕ_1	171.4°	289.3°

Consider first the case of B26A1; since ϕ_1=289.3° and from table 3-2, ϕ_o for U3 is 287.5°, it is expected that nearly "pure one-corner opening" should be observed at U3. Fig. 22 is a static phase plot for B26A1 with $b_4 = +.040$. The figure clearly shows that nearly "pure one-corner opening" is indeed obtained at U3. In Fig. 22, the curves labeled ⓐ indicate the one-corner opening

at U3. As b_4 increases, U3 and E0 move toward each other very nearly along the axis which joins the initial position of U3 and E0. At the same time, U1 and U2 move away from the initial position of E0 with U2 moving somewhat faster than U1. As b_4 increases, E0 and U3 move toward each other and the stable region shrinks. According to Eq. (3.5), for the case of "pure one-corner opening", the stable region will disappear when $b_4 = +.0788$. It is possible to determine an approximate critical value of b_4 from Fig. 22 and Eq. (2.15b). Using the displacement of U3 from its initial position in Eq. (2.15b) gives the extrapolated critical value of b_4 as +.08 which agrees quite well with the critical value of b_4 determined from the theory.

Consider next the field B26.29A; Figs. 23a and 23b are static phase plots for B26.29A with $b_4 = +.10$ and +.30 respectively. It was pointed out in the table above that $\phi_1 \doteq 171.4°$ for field B26.29A. According to table 3-2, if $\phi_1 = 170.2°$, "pure one-corner opening" is obtained at U1. It is therefore expected that nearly "pure one-corner opening" will be observed at U1 with a very small amount of two-corner opening at U1 and U3. Figs. 23a and 23b show that this is indeed the observed effect. In Figs. 23a and 23b, the curves labeled ⓐ indicate the

predominant one-corner opening at U1 and the curves labeled ⓑ indicate the small two-corner opening at U1 and U3. It is seen that as b_4 increases, U1 and E0 move toward each other along the axis joining the initial position of U1 and E0. As b_4 increases, U2 and U3 move away from E0 toward the $\alpha = \pm 90°$ as measured from the axis joining the initial position of U1 and E0; moreover, the relative displacement of U2 and U3 from their initial positions in the unbumped field is nearly equal as expected from the theory in Chapter II for "pure one-corner opening".

According to Eq. (3.5), the stable region should disappear when $b_4 = +.209$. By extrapolation from the results shown in Fig. 23a, an approximate critical value of b_4 may be obtained. Using the displacement of E0 from its initial position in the unbumped field in Eq. (2.15b) gives an approximate critical value of b_4 as +.20 which is in good agreement with the critical value of b_4 determined from the theory.

4. Two-Sector Gradient Bump Field.

A. General Considerations: In this section, the effect on stability of a two-sector gradient bump field will be investigated. In keeping with the definition

given at the beginning of this chapter, the two-sector gradient bump field is given by:

$$b(r,\theta) = a(r-R) \cos 2(\theta-\theta_2), \qquad (3.19)$$

where "a" and θ_2 are constants and R is the mean radius of the equilibrium orbit. The values of a are in c.u. and a conversion factor is provided by the equation:

$$a = 1 \text{ c.u.} = 150.4 \text{ gauss/inch.}$$

The value of R is given in table 3-3 for fields B26.29A and B26A1. From the formulae in tables 2-1 and 2-2 and the results in table 3-3, the parameters δ, δ', ϕ_1 and ϕ_2 may be determined directly in terms of the two constants a and θ_2. Assuming that δ and δ' are positive, the following results are obtained for positive and negative a for fields B26.29A and B26A1.

TABLE 3-10: Evaluation of the perturbation parameters for fields B26.29A and B26A1 for the two-sector gradient perturbation.

n=2	B26.29A	B26A1
δ	$(.000981)\lvert a\rvert$	$(.000485)\lvert a\rvert$
ϕ_1	$200.1°-2\theta_2$, $a > 0$; $20.1° - 2\theta_2$, $a < 0$	$25.8° - 2\theta_2$, $a > 0$; $205.8° - 2\theta_2$, $a < 0$
δ	$.1954\lvert a\rvert$	$.1992\lvert a\rvert$
ϕ_2	$90°+\theta_2$, $a > 0$; θ_2, $a < 0$	$90°+\theta_2$, $a > 0$; θ_2, $a < 0$

Note that δ is independent of θ_2.

According to the theory of Chapter II, section 4, the quantity $|\delta'/(4\delta/A_o)|$ gives an estimate of the relative effect on stability of the two-sector gradient perturbation in comparison to the one-sector perturbation. In the table below, the quantity $|\delta'/(4\delta/A_o)|$ has been evaluated using the results of table 3-10 for fields B26.29A and B26A1.

TABLE 3-11: Evaluation of $|\delta'/(4\delta/A_o)|$ for fields B26.29A and B26A1 for the two-sector gradient bump field.

n=2	B26.29A	B26A1
$\lvert\delta'/(4\delta/A_o)\rvert$	4.11	2.92

Note that the quantity $|\delta'/(4\delta/A_o)|$ is independent of a. It is evident from the above table that the two-sector gradient perturbation is the main factor determining stability; however, the effect on stability of the one-sector perturbation is not negligible.

According to Chapter II, section 4, when both a one-sector perturbation and two-sector gradient perturbation are present, the simple approximate criterion for stability is given by Eq. (3.16) which may be used to determine an approximate value for the critical bump strength. If the results of table 3-10 are substituted into this equation, it turns out that the quantity Δ is independent of θ_2. Below is the evaluation of Δ in terms of a for fields B26.29A and B26A1.

$$\text{B26.29A:} \quad \Delta = (.168)|a|$$
$$\text{B26A1} \quad : \quad \Delta = (.240)|a|.$$

From Eq. (3.16), a critical value of a may be found by setting $\Delta_c = 4\epsilon$; then, the critical value of a for the two fields considered in this report is found to be:

$$\text{B26.29A:} \quad (a)_c = +1.31 \tag{3.20}$$
$$\text{B26A1:} \quad (a)_c = +.644. \tag{3.21}$$

It should be emphasized that the critical value of a

obtained from Eq. (3.16) is only an approximation. An alternative method may be used to determine an approximate critical value of a; assuming that the one-sector perturbation is negligible, the critical value of a may be obtained directly from Eq. (2.18b). Using the results of table 3-10 and Eq. (2.18b), the critical value of a for the two fields is then given by:

$$\text{B26.29A:} \quad |a|_c = +\ 1.13 \tag{3.22}$$

$$\text{B26A1:} \quad |a|_c = +\ .769. \tag{3.23}$$

The two critical values of a determined from Eqs. (3.16) and (2.18b) differ by less than 10% for B26.29A, and for B26A1 the two values differ by less than 20%. Note that these critical values of a when expressed in gauss/inch represent fairly sizeable field gradients.

B. Discussion of the Phase Plots:

a) Phase Plots for B26A1 with $\theta_2 = 0$: The phase plots to be presented first in this section have been specialized to the case where $\theta_2 = 0$ and the constant a is either positive or negative. Consider first the case where a is positive; from table 3-10, when $\theta_2 = 0$, $\phi_1 = 25.8°$ and $\phi_2 = 90°$. According to table 3-2, if $\phi_1 = 25.8°$ for B26A1 a mixture of two-corner opening at U2 and U3 and one-corner opening at U2 would be observed

if the two-sector gradient perturbation were not present; moreover, the one-corner opening at U2 dominates over the two-corner opening at U2 and U3. If $\phi_2 = 90°$ for B26A1, a mixture of two-corner opening at U2 and U3 and one-corner opening at U3 would be observed with the two-corner opening slightly more dominant if the one-sector perturbation is neglected. It should be kept in mind that the two-sector gradient perturbation has approximately three times the effect on stability as the one-sector perturbation; as a result, the phase plots should tend to bring out the features due to the two-sector gradient perturbation more strongly than the features due to the one-sector perturbation. Figs. 24a, 24b, and 24c are static phase plots for B26A1 with a = +.10, + .30, and +.60 respectively and $\theta_2 = 0$. In the phase plots, the new positions of the four fixed points in the bumped field are indicated by "circles" (0) and the initial positions of the four fixed points in the unbumped field are indicated by "x's". Figs. 24a, 24b and 24c show that the effect of the two-sector gradient field bump is nearly "pure two-corner opening" at U2 and U3 along with a small amount of one-corner opening at U2 which is not inconsistent with the expected results given above. In the figures, the curves labeled (b) indicate

the predominant two-corner opening at U2 and U3 and the curve labeled (a) in Fig. 24c indicates the one-corner opening at U2. As a increases, U2 and U3 move toward E0 and U1 moves away from E0. In the case being considered here, the three fixed points E0, U2 and U3 determine the stable region; as a result, as a increases the stable region is reduced in size. From Figs. 24b and 24c, it is evident that for some value of a greater than +.30 but less than +.60, E0 and U2 coincide and the stable region disappears. From the spacing of successive points on the curve labeled (a) in Fig. 24c it is safe to say that the stable region disappeared for some value of a very close to +.60.

According to Eq. (3.21), the critical value of a for which the stable region will disappear is +.644. It is possible to obtain an approximate critical value of a by extrapolation directly from Figs. 24a and 24b if the one-sector perturbation is neglected. It is assumed that the amplitude A of the first harmonic of U3 is equal to the relative displacement of U3 from E0 in the bumped field and that the distance from E0 to U3 in the unbumped field is A_o. Thus it is possible to determine the amplitude A of U3 in terms of A_o at the two values of a in Figs. 24a and 24b. If A is plotted against $\gamma' \equiv \delta'/4\epsilon$

for a = +.10 and a = +.30 and a parabolic curve is passed through these points, (assuming Eq. (2.16e) is valid), then the approximate critical value of a is found to be:

$$|a|_c = +.60.$$

This computer value of a is in fairly good agreement with the theoritical critical values given in Eqs. (3.21) and (3.23).

Consider next the case where a is negative and $\theta_2 = 0$. From table 3-10, $\phi_1 = 205.8°$ and $\phi_2 = 0°$. According to table 3-2, if $\phi_1 = 205.8°$ for B26A1, a mixture of one-corner opening at U1 and two-corner opening at U1 and U3 would be observed with the two-corner opening the dominant feature. This would be the observed effect if the two-sector gradient perturbation were not present; since the two-sector gradient perturbation has approximately three times the effect on stability as the one-sector perturbation, it is expected that the features due to the two-sector gradient perturbation will be more pronounced. With $\phi_2 = 0°$, a mixture of one-corner opening at U1 and two-corner opening at U1 and U2 would be observed if the one-sector perturbation were absent. Figs. 24d and 24e are static phase plots for B26A1 with a = -.30 and -.60 respectively and $\theta_2 = 0$. The figures indicate

that a mixture of one-corner opening at U1 and two-corner opening at U1 and U2 is obtained which agrees with the results immediately above; moreover, the one-corner opening is the dominant effect. In Figs. 24d and 24e, the curves labeled ⓐ indicate the one-corner opening at U1 and the curves labeled ⓑ indicate the two-corner opening at U1 and U2. It is seen from Figs. 24d and 24e that as $|a|$ increases, U1 and E0 move toward each other and U2 and U3 move away from E0 with U3 moving somewhat faster than U2. For some value of $-60 < a < -.30$, U1 and E0 coincide and the stable region disappears. In the case being discussed, it is possible to calculate an approximate critical value of a directly from Fig. 24d. Assume that the amplitude A of the first harmonic of U1 in the bumped field is equal to the relative displacement of U1 from E0. Assume further that a linear relation holds between A and $\gamma' \equiv \delta'/4\epsilon$ as predicted by Eq. (2.16c) for "pure one-corner opening"; this is not an unrealistic approach if the one-sector perturbation is small and nearly "pure one-corner opening" is obtained which is nearly the case here. With these assumptions, the approximate critical value of a is then found to be:

$$|a|_c \cong +.60,$$

which is in agreement with the theoretical critical values given in Eqs. (3.21) and (3.23) above. From Fig. 24e, the piling of the points in the region where E0 and U1 would be expected to lie indicates by itself that E0 and U1 will coincide for some value of $|a| \cong +.60$.

According to the theory of Chapter II, section 3, if $\delta = 0$, E0 should remain fixed; it is evident from Figs. 24a, 24b, and 24d that this is not the case here. Consequently there must be some one-sector perturbation present; however, since the displacement of E0 is small compared to that of the fixed points this one-sector perturbation must be small in comparison to the two-sector gradient perturbation in agreement with the results immediately above.

In the case of a "pure" two-sector gradient perturbation with "pure one-corner opening" at U1, E0 and U1 will coincide at the critical bump strength leaving an unstable fixed point at the initial position of E0; moreover, as depicted in Fig. 13a, if the bump strength is increased beyond this value then a new stable fixed point should emerge from E0 and move toward U2 and U3. Since the bump being considered in this case does not produce a "pure" two-sector gradient perturbation, no attempt was made to pursue this result further; however, another

reference will be made to this phenomenon later.

b) Phase Plot for B26.29A with $\theta_2 = 0$: Consider now the field B26.29A with a positive and $\theta_2 = 0$. From table 3-2, if $\theta_2 = 0$, $\phi_1 = 200.1°$ and $\phi_2 = 90°$. According to table 3-2, if $\phi_1 = 200.1°$ for B26.29A a mixture of one-corner opening at U1 and two-corner opening at U1 and U3 would be observed in the absence of the two-sector gradient perturbation. According to this same table, if the one-sector perturbation were not present and $\phi_2 = 90°$, a mixture of two-corner opening at U2 and U3 and one-corner opening at U3 would be observed with the two-corner opening dominant. It is expected that the features of the two-sector gradient perturbation will be more pronounced than the features of the one-sector perturbation because the two-sector gradient perturbation has roughly four times the effect of the one-sector perturbation on stability as noted in table 3-11.

Fig. 25 is a static phase plot for B26.29A with $a = +.30$ and $\theta_2 = 0$. The figure shows the result of the two-sector gradient bump to be nearly "pure one-corner opening" at U3 and what is believed to be two-corner opening at U2 and U3 which is consistent with the results immediately above. The curve labeled (a) in Fig. 25 indicates the one-corner opening at U3. Although no

curves are shown in Fig. 25 which indicate two-corner opening at U2 and U3, it is highly probable that some two-corner opening exists. This conclusion is drawn from the position of the fixed points U1 and U2 relative to the curve labeled ⓐ in Fig. 25. As a increases, U3 moves toward E0 and the stable region is reduced in size; at the same time, E0 remains almost stationary, U1 moves away from E0, and U2 moves away from its initial position but its relative displacement from E0 remains unchanged.

From Eqs. (3.20) and (3.22), the calculated critical value of a is +1.31 and +1.13 which are about four times greater than the strength of the field bump used in Fig. 25. Comparing the stable region of Figs. 24b, 24d and 25 which all have $|a| = +.30$, it is evident that it will take a much larger value of a to destroy the stable region of B26.29A than the stable region of B26A1.

c) Phase Plots For B26A1 for Other θ_2 Values: Fig. 26 is a static phase plot for B26A1 with a = -.30 and $\theta_2 = -12.5°$. Substitution of $\theta_2 = -12.5°$ into the defining equation for ϕ_1 and ϕ_2 in table 3-10 for negative a gives the values of ϕ_1 and ϕ_2 as:

$$\phi_1 = 230.8°$$

$$\phi_2 = 347.5°.$$

curves are shown in Fig. 25 which indicate two-corner opening at U2 and U3, it is highly probable that some two-corner opening exists. This conclusion is drawn from the position of the fixed points U1 and U2 relative to the curve labeled ⓐ in Fig. 25. As a increases, U3 moves toward E0 and the stable region is reduced in size; at the same time, E0 remains almost stationary, U1 moves away from E0, and U2 moves away from its initial position but its relative displacement from E0 remains unchanged.

From Eqs. (3.20) and (3.22), the calculated critical value of a is +1.31 and +1.13 which are about four times greater than the strength of the field bump used in Fig. 25. Comparing the stable region of Figs. 24b, 24d and 25 which all have $|a| = +.30$, it is evident that it will take a much larger value of a to destroy the stable region of B26.29A than the stable region of B26A1.

c) Phase Plots For B26A1 for Other θ_2 Values: Fig. 26 is a static phase plot for B26A1 with a = -.30 and $\theta_2 = -12.5°$. Substitution of $\theta_2 = -12.5°$ into the defining equation for ϕ_1 and ϕ_2 in table 3-10 for negative a gives the values of ϕ_1 and ϕ_2 as:

$$\phi_1 = 230.8°$$

$$\phi_2 = 347.5°.$$

This value of θ_2 was chosen in an attempt to illustrate the "pure one-corner opening" at U1; according to the theory of Chapter II, section 3, "pure one-corner opening" should be obtained at U1 when $\phi_2 = 347.5°$, a value obtained for ϕ_2 when $a < 0$ and $\theta_2 = -12.5°$ according to table 3-10. From table 3-2, if $\phi_1 = 230.8°$ and the two-sector gradient perturbation is not present, a mixture of two-corner opening at U1 and U3 and one-corner opening at U3 would be observed with the two-corner opening at U1 and U3 the dominant feature; however, the one-sector perturbation is much smaller in effect than the two-sector gradient perturbation as noted previously. Fig. 26 shows the effect of the two-sector gradient field bump to be a dominance of one-corner opening at U1 with some two-corner opening at U1 and U3 which is consistent with the forgoing results. In the figure, the one-corner opening at U1 is illustrated by the curve labeled ⓐ and the two-corner opening at U1 and U3 is illustrated by the curve labeled ⓑ. Comparing Fig. 24d with Fig. 26, indicates that for a change in θ_2 of 12.5° a shift from two-corner opening at U1 and U2 to two-corner opening at U1 and U3 occurs; however, the dominant feature is still one-corner opening at U1 which is consistent with the expected results.

One more phase plot will be presented where a = -.30 and θ_2 = -16.5°. Note that the only difference between this case and the previous case is a shift of 4° in θ_2. As it turns out, this small shift in θ_2 has a marked effect on the phase plot. Substituting θ_2 = -16.5° into the formulae for ϕ_1 and ϕ_2 in table 3-10 gives ϕ_1 and ϕ_2 as:

$$\phi_1 = 238.8°$$

$$\phi_2 = 343.5°;$$

that is, ϕ_1 is shifted by 8° and ϕ_2 is shifted by 4° from the corresponding values for the case immediately above. From table 3-2, if ϕ_2 = 343.5° nearly "pure one-corner opening" is obtained at U1 with a very small amount of two-corner opening at U1 and U3. From this same table, if ϕ_1 = 238.8° for B26A1 a mixture of predominately two-corner opening at U1 and U3 and slight one-corner opening at U3 would be observed in the absence of the two-sector gradient perturbation; recall again however, that the two-sector gradient perturbation is the dominant effect here. These conclusions are practically the same as those above where θ_2 = 12.5°. Fig. 27 is a phase plot for B26A1 with a = -.30 and θ_2 = -12.5°. From the figure it is evident that a mixture of one-corner opening

at U1 and two-corner opening at U1 and U3 is obtained with the one-corner opening the dominant feature. This result is consistent with the discussion above.

A comparison of Figs. 26 and 27 brings out the marked difference between the phase plots brought about by a shift of only 4° in θ_2. In Fig. 26, only four fixed points exist with the stable region centered about E0; however, in Fig. 27, six fixed points exist; four unstable fixed points and two stable fixed points; moreover, two stable regions now exist centered around the two stable fixed points. The most probable explanation for the two extra fixed points is that E0 has split into two stable fixed points and one unstable fixed point although no further investigation has been carried out to verify this hypothesis. This explanation seems reasonable in view of the fixed point evolution depicted in Fig. 13a; furthermore, the figure "8" nature of the flow lines near the center is of the type associated with a 2/2 resonance with a substantial frequency shifting term in the equation of motion. For convenience, the two stable fixed points shall be designated as E01 and E02 where E01 is closest to the original E0 and the unstable fixed point midway between the two stable fixed points shall be designated UE. The three remaining unstable fixed points shall still be designated as U1, U2 and U3 as

indicated in Fig. 27. It is expected as $|a|$ increases, first U1 and EO1 will coincide and vanish leaving UE, EO2, U3 and U2 and then later U3 and EO2 will coincide and vanish leaving the two unstable fixed points U2 and UE as the only remaining fixed points. This result is consistent with the one-corner opening case for a two-sector gradient perturbation depicted in Fig. 13a.

To obtain a "pure" two-sector gradient perturbation, a mixed field bump must be constructed to nullify the effect of the one-sector perturbation. One such mixed field bump is given by:

$$b(r,\theta) = a[r-r_e(\theta)] \cos 2(\theta-\theta_2), \qquad (3.24)$$

where the quantities in this equation have been defined previously. Since this field bump is identically equal to zero along the E.O., no displacement of this orbit can result. Preliminary investigations with this type of field bump indicate that EO remains fixed. It is hoped that in the near future the investigation will be completed and a direct comparison made between the computer results and the detailed theory of Chapter II, section 3 as was done for the one-sector perturbation in section 2 of this chapter.

APPENDIX

Extension of Theory to a Four-Sector Geometry.

For a four-sector cyclotron it is the $\nu_r = 4/4$ non-linear resonance which imposes stability limits on the radial motion in the absence of a bump field, and the discussion of Chapter II must be modified accordingly. In this note a quite brief description is given of the results obtained when the theory of Chapter II is applied to a four-sector geometry; all "sections" referred to here are those of Chapter II.

The transformation from $x(\theta)$ to $y(\phi)$ in section (1) is quite general and applies equally well to a four-sector geometry. The near equivalence of the n=1 component of $x(\theta)$ with the n=1 component of $y(\phi)$, as discussed for Eq. (2.8), is again valid since the n=3 and n=5 components of these functions are relatively small.

The differential equation for the first harmonic (or "quasi-first harmonic") component of $y(\phi)$ in the absence of a field bump now has the form:

$$\ddot{y} + \nu_r^2 y = Ky^3 \cos 4(\phi-\phi_o), \qquad (A.1)$$

where K and ϕ_o are constants, and the non-linear driving

force is again semi-empirical in form. The form of the perturbation forces arising from the bump field, $\delta F(y,\phi)$, is exactly the same here as in Eq. (2.10).

Extending the discussion of the fixed point orbits given in section (1A), the form of $y(\phi)$ here is again given by Eq. (2.11). The general equation for A and α is, instead of Eq. (2.12), now given by:

$$Ae^{i\alpha} = (A^3/A_o^2)e^{-i3\alpha} + \gamma \exp i(\phi_o-\phi_1)$$
$$+\gamma' Ae^{-i\alpha} \exp 2i(\phi_o-\phi_2), \qquad (A.2)$$

where $\gamma = \delta/2\epsilon$, $\gamma' = \delta'/4\epsilon$ as before, but here:

$$A_o^2 = (16\epsilon)/K. \qquad (A.3)$$

In the absence of a field bump ($\gamma = \gamma' = 0$), there are now four unstable fixed points all having $A=A_o$, but with $\alpha = 0, \pm 90°, 180°$.

Following the discussion of section (1B), the approximate phase invariant $H(\alpha, A^2)$ is now given by:

$$H/\epsilon = A^2 - 1/2(A^4/A_o^2)\cos 4\alpha$$
$$-2\gamma A\cos(\alpha+\phi_1-\phi_o)$$
$$-\gamma' A^2 \cos2(\alpha+\phi_2-\phi_o) \qquad (A.4)$$

Following the discussion of section (2) for the

one-sector perturbation case ($\gamma' = 0$), there are two symmetric situations, namely: $\phi_1 = \phi_o$ plus an integral multiple of 90°, for which "one-corner opening" occurs; and $\phi_1 = \phi_o$ plus an odd-integral multiple of 45°, for which "two-corner opening" occurs. In the first-mentioned situation (see Fig. 28), one of the fixed points and E.O. move directly toward each other and merge at $A = A_o/\sqrt{3}$; the critical value of γ is then:

$$\gamma_{c1} = (2\sqrt{3}/9)A_o. \qquad (A.5)$$

Accompanying the one-corner opening in this situation, there is also two-corner opening at the two fixed points initially $\pm$ 90° from the one which disappears. In the other symmetric situation, (see Fig. 28), there is two-corner opening at two adjacent fixed points; these two fixed points move inward and toward each other, while the E.O. moves outward to meet them. These three fixed points merge at $A = A_o/\sqrt{3}$ for a value of γ given by:

$$\gamma_c = (4\sqrt{3}/9)\ A_o, \qquad (A.6)$$

leaving one unstable fixed point as a result of the merger, and no stable region. For any value of ϕ_1 intermediate between the eight special values given above, the

critical value of γ will lie between the two values of (A.5) and (A.6).

Consider next the two-sector gradient perturbation acting by itself ($\gamma = 0$) corresponding to the discussion of section (3); here again the critical value of γ' is effectively $\gamma'_c = 1$, at which value the E.O. becomes unstable. For the four-sector main field case, however, the behavior of the fixed points and phase invariants is quite different.

The simplest case to analyse is when $\phi_2 = \phi_o$ plus an integral multiple of 90°; this case corresponds to a "double" one-corner opening (see Fig. 29). As γ' increases two of the opposite fixed points (say, the $\alpha = 0$ and $\alpha = 180°$) move toward the E.O. and define the shrinking stability region between them; when $\gamma' = 1$, they merge with E.O. leaving an unstable fixed point there. The other two fixed points ($\alpha = \pm 90°$) are disconnected and move outward without changing their α values.

The other situation which is amenable to analysis is when $\phi_2 = \phi_o$ plus an odd integral multiple of 45°, (see Fig. 29). Consider first that the α values are shifted by 45° so that the fixed points are initially at $\alpha = \pm 45°, \pm 135°$. As γ' increases the two fixed

points $\alpha \doteq 45°$ and $\alpha = -45°$ move toward $\alpha = 0$, while those at $\alpha = +135°$ and $\alpha = -135°$ move toward 180°, all maintaining $A = A_o$. For $\gamma' > 1$ the E.O. splits into an unstable E.O. plus two stable fixed points which move outward along the $\alpha = 0$ and 180° directions, respectively. When $\gamma' = \sqrt{2}$, two triangular closed "stability" regions are formed on each side of E.O.; for $\gamma' > \sqrt{2}$ each triangle undergoes two-corner opening; when $\gamma' = 2$, each stable fixed point merges with its companion pair of unstable fixed points leaving just one unstable fixed point in each case at $A = A_o$ on the $\alpha = 0$ and 180° axes; for $\gamma' > 2$, these latter points move out away from E.O.

The derivation of the simple stability criterion given in section (4) can be readily extended to the four-sector case. The criterion is again, $|\Delta| \leqq 4\epsilon$, where now:

$$\Delta^2 = (\delta')^2 + (3\delta^2/\epsilon A_o^2)^2$$

$$+2\delta'(3\delta^2/\epsilon A_o^2) \cos (4\phi_o - 2\phi_1 - 2\phi_2), \qquad (A.7)$$

to lowest (non-vanishing) order in δ and δ'. Note that in contrast to the three sector case, the effect of δ' adds vectorially with the "squared" effect of δ.

The results given in section (5) for calculating

the perturbation parameters in terms of the physical characteristics of a given bump field can be extended without difficulty to the four-sector case. It is clear that a one-sector perturbation can arise here not only from the bump field harmonic n=1, but also n=3 and n=5, to a lesser extent. Likewise, a two-sector gradient perturbation arises mainly from the harmonic n=2, but also much more weakly from n=6. For this perturbation the n=2 harmonic contributes both directly and also indirectly through coupling with the four-sector field.

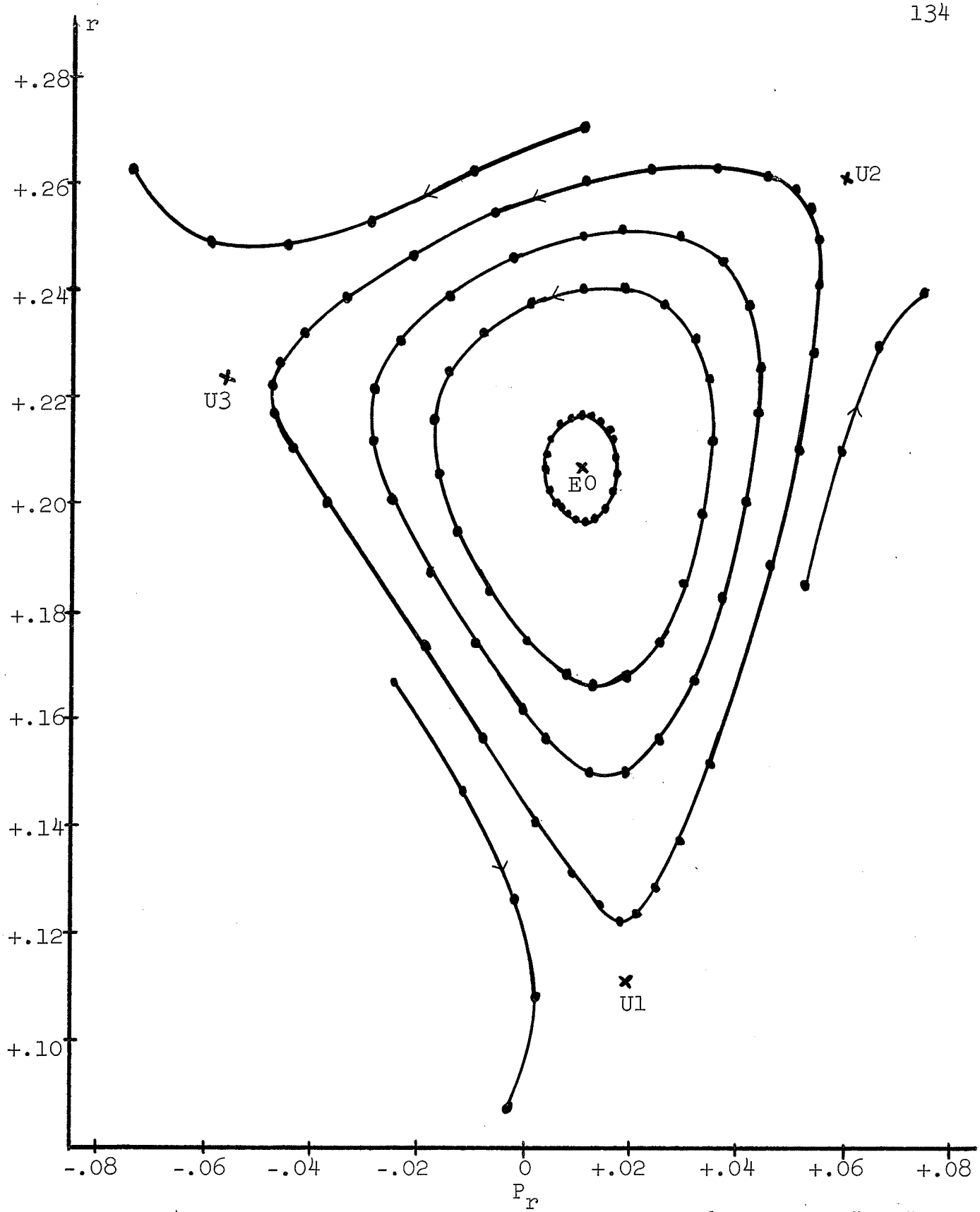

Figure 14: Phase plot for the unbumped field B26.29A; the "x's" represent the three unstable fixed points (U1,U2,U3) and the stable equilibrium orbit (E0).

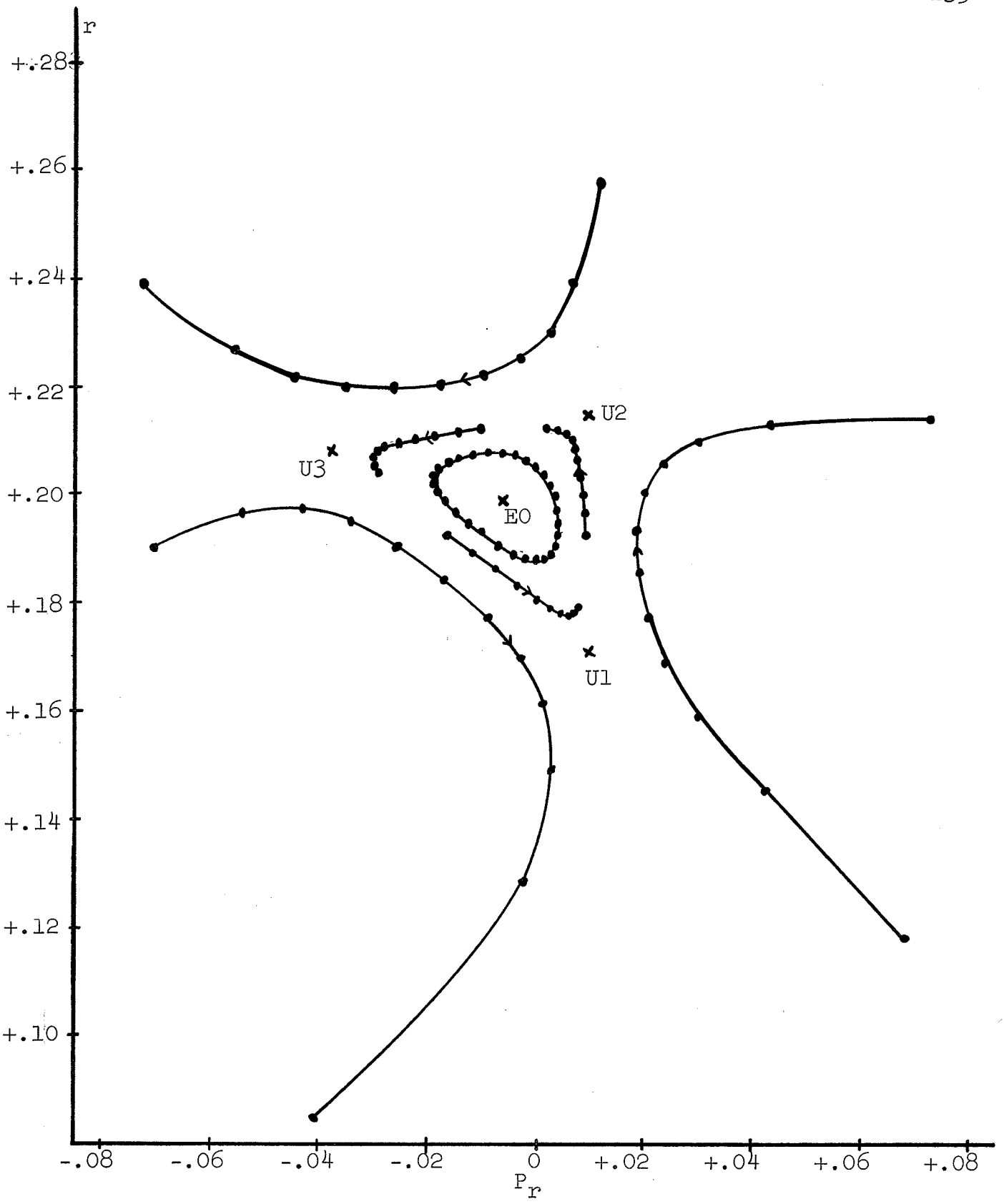

Figure 15: Phase Plot for the unbumped field B26A1; the "x's" represent the three unstable fixed points (U1,U2,U3) and the stable equilibrium orbit (E0).

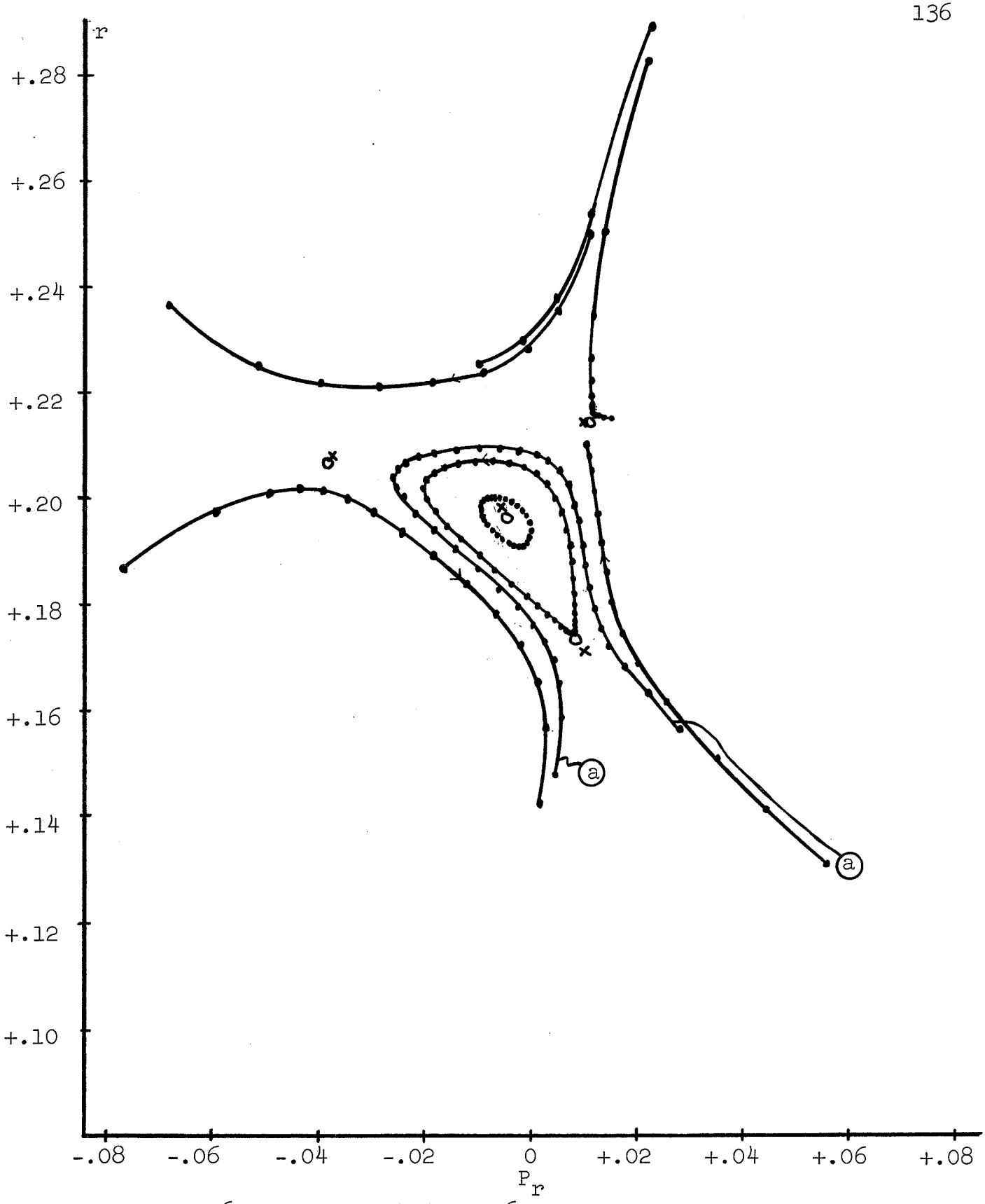

Figure 16a: Phase plot for B26A1 with: $b_1 = +.001$, $\theta_1 = 0$.

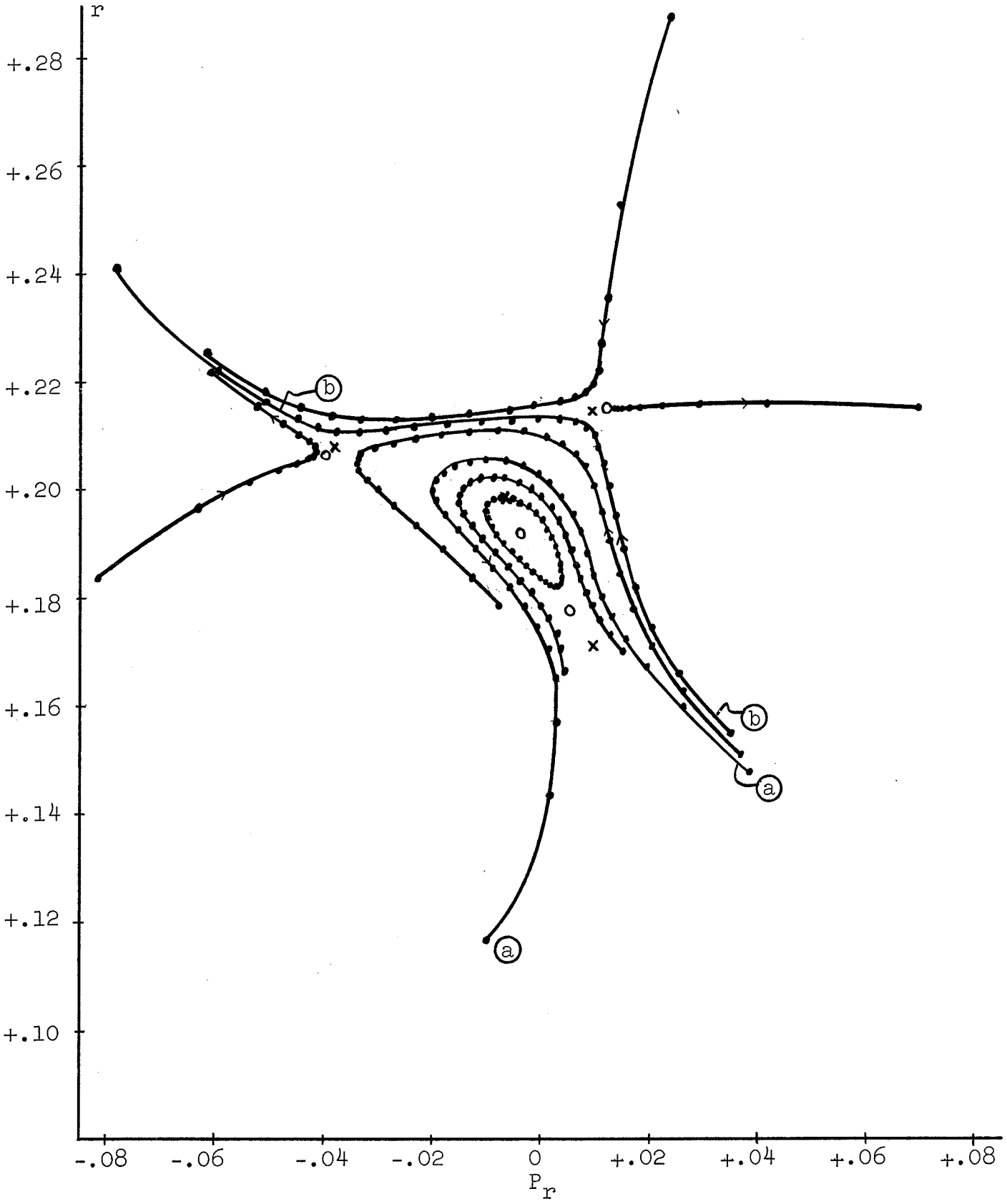

Figure 16b: Phase plot for B26A1 with: $b_1 = +.002$, $\theta_1 = 0$.

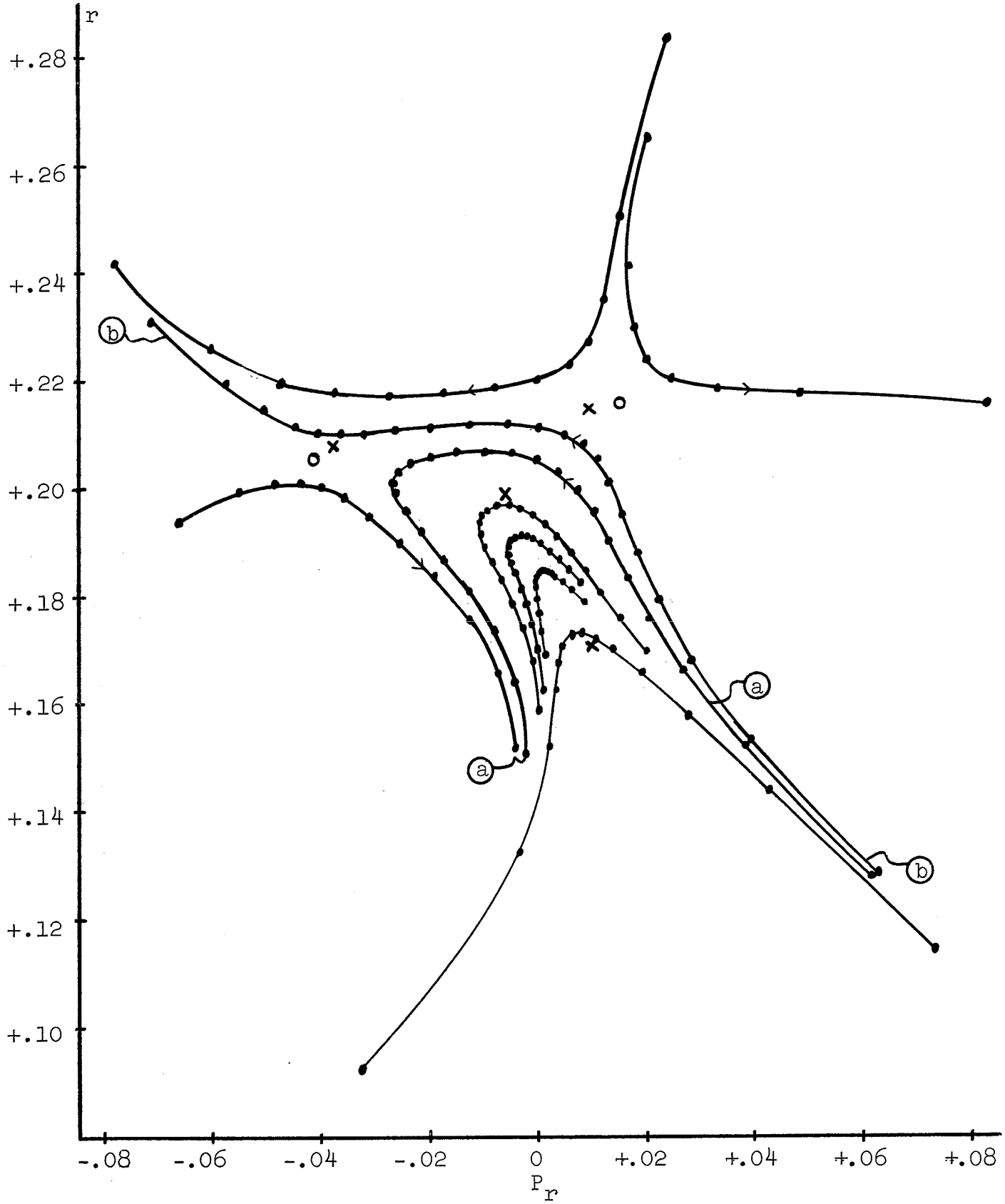

Figure 16c: Phase plot for B26A1 with: $b_1 = +.004$, $\theta_1 = 0$.

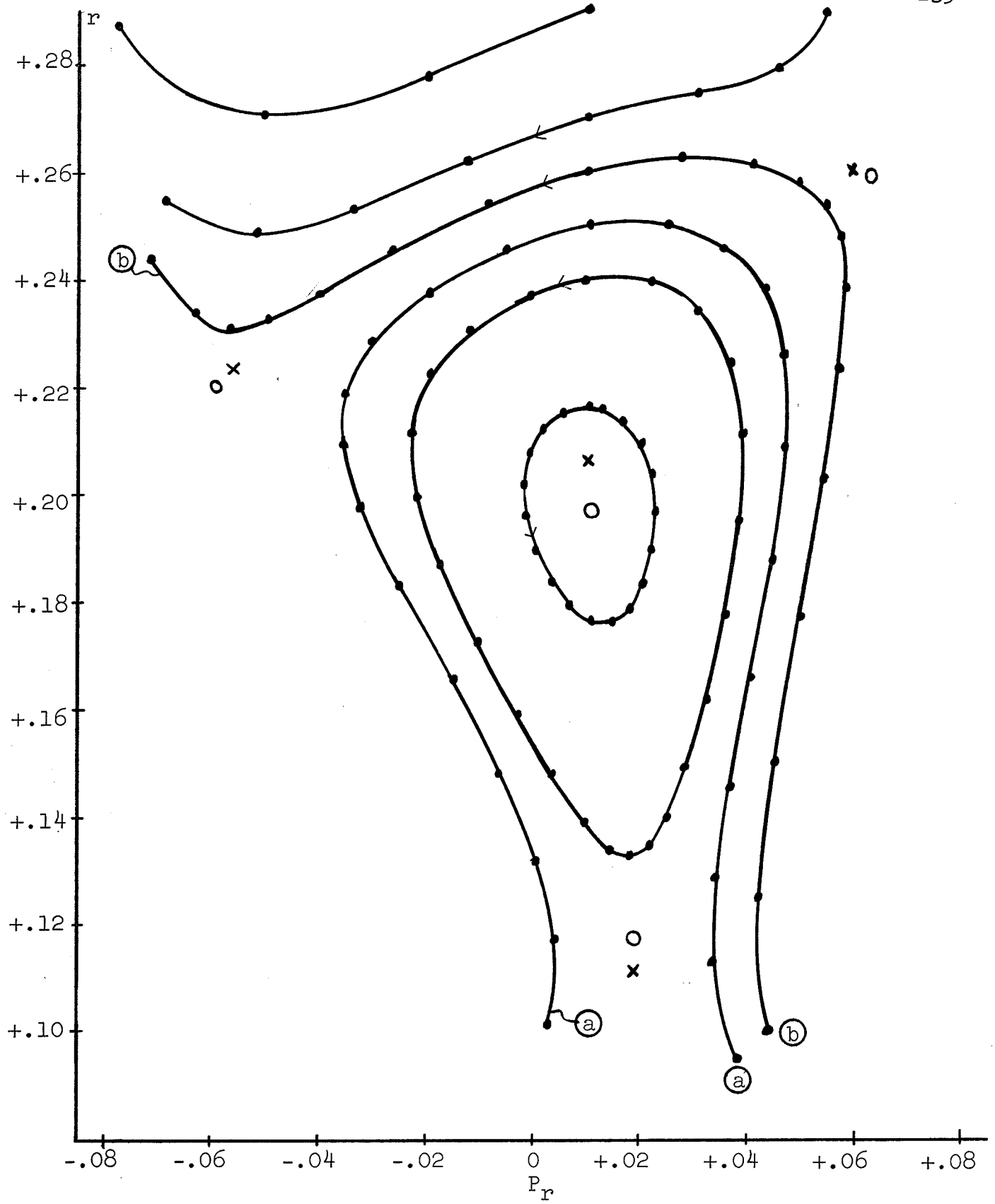

Figure 17a: Phase plot for B26.29A with: $b_1 = +.004$, $\theta_1 = 0$.

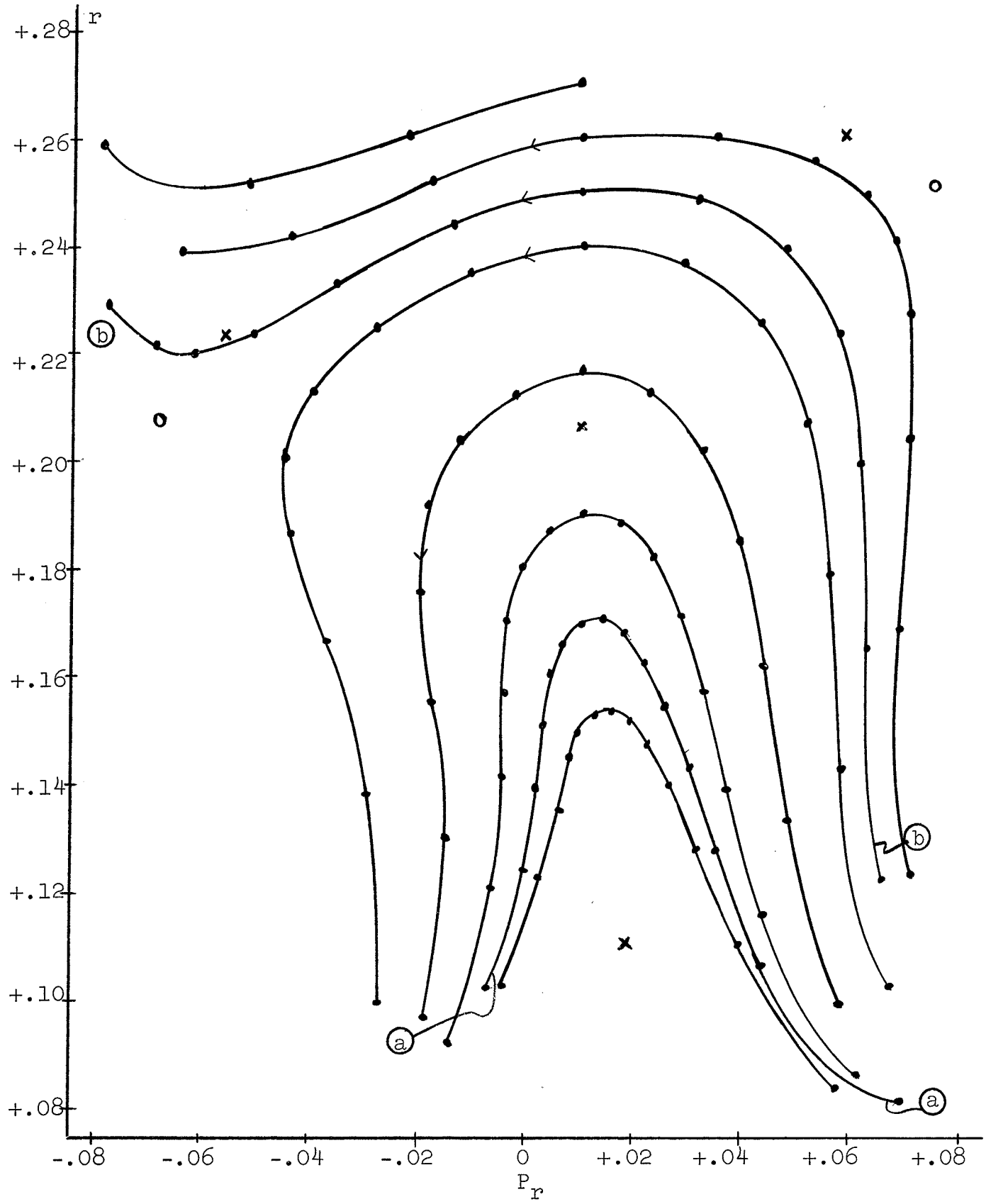

Figure 17b: Phase plot for B26.29A with: $b_1 = +.02$, $\theta_1 = 0$.

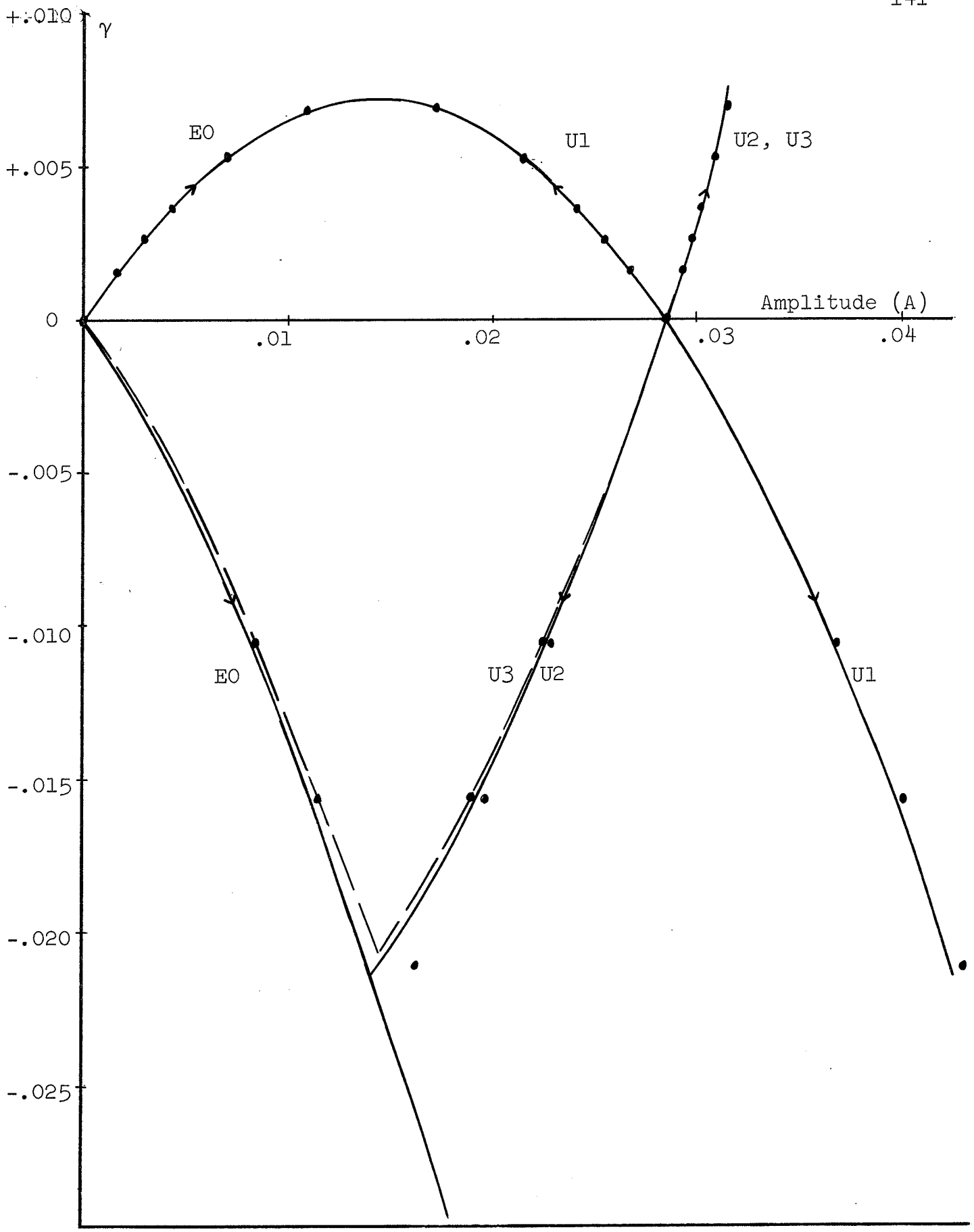

Figure 18: Amplitude (A) as a function of bump strength; solid lines represent theoretical curves; dots represent computer results.

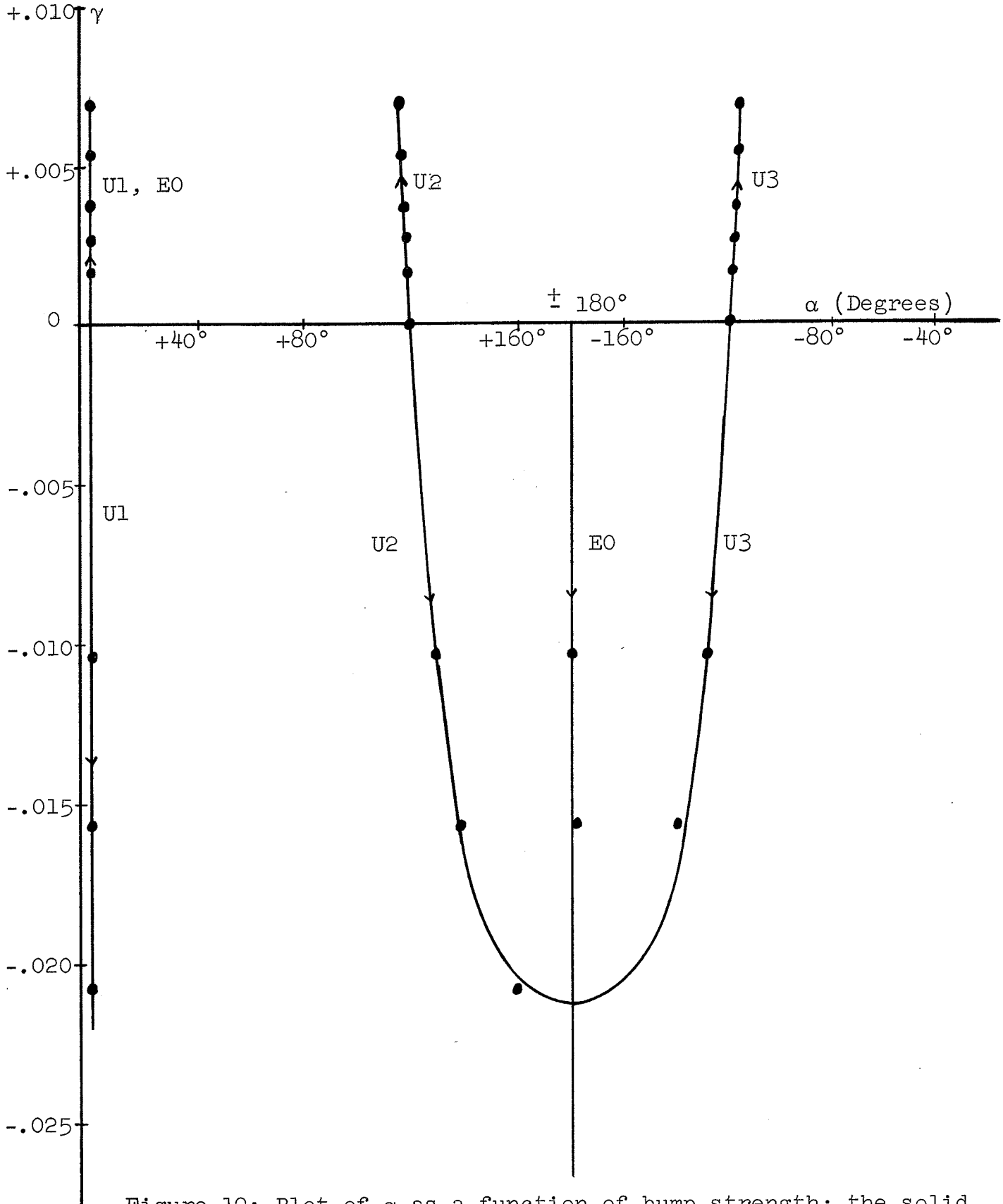

Figure 19: Plot of α as a function of bump strength; the solid lines represent the theoretical curves; the dots represent the computer results.

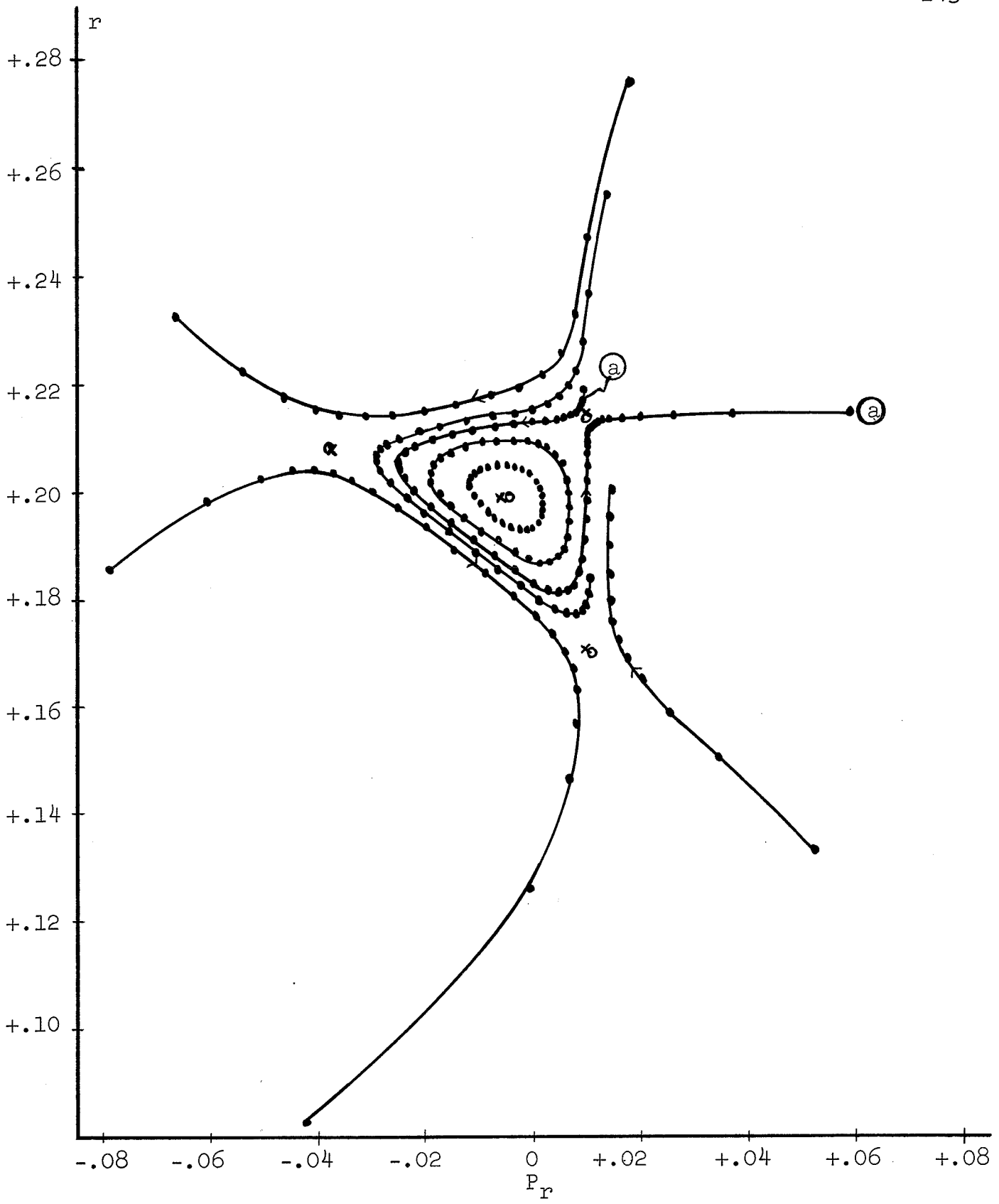

Figure 20a: Phase plot for B26A1 with: $b_2 = +.004$, $\theta_2 = 0.$

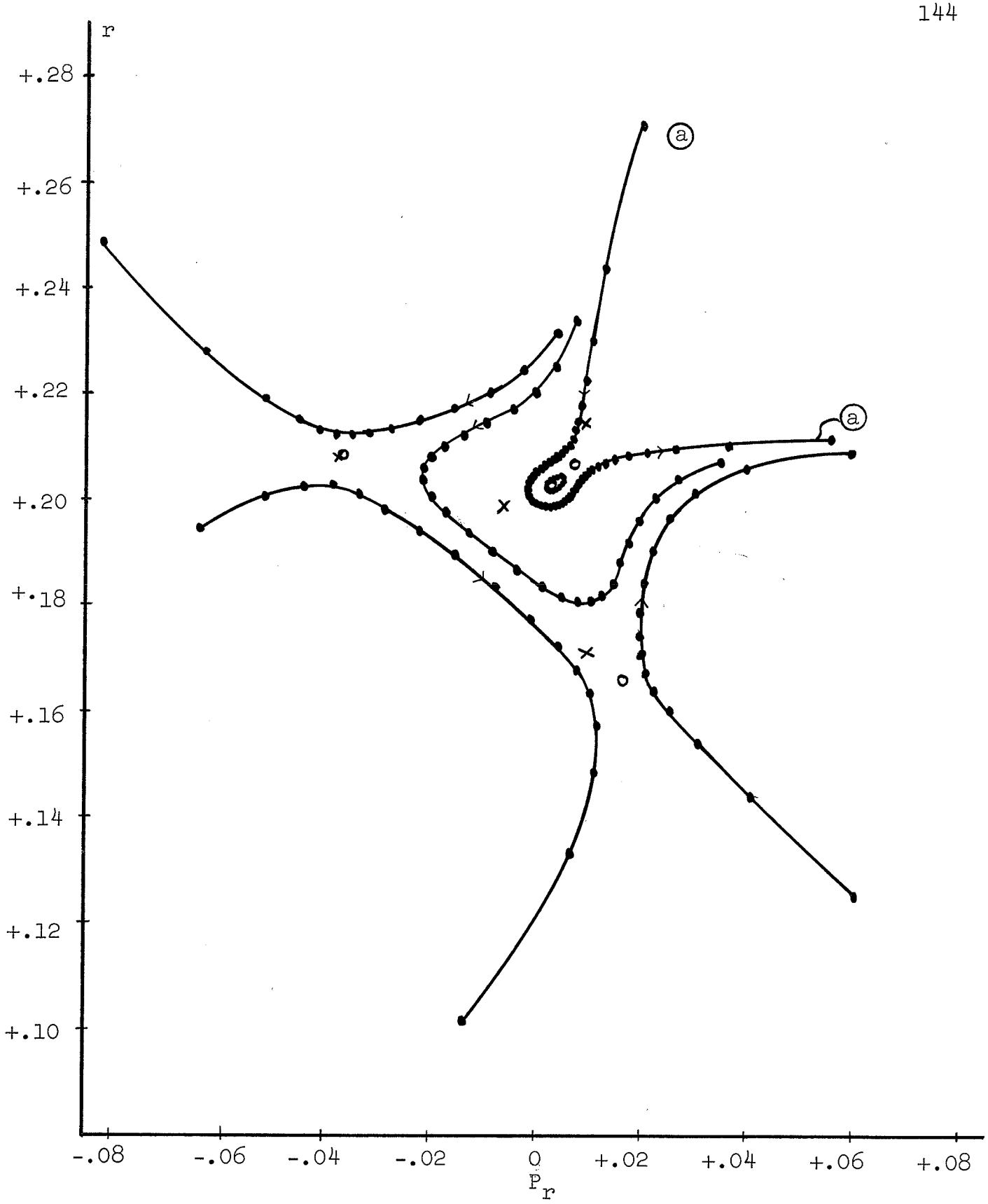

Figure 20b: Phase Plot for B26A1 with: $b_2 = +.020$, $\theta_2 = 0.$

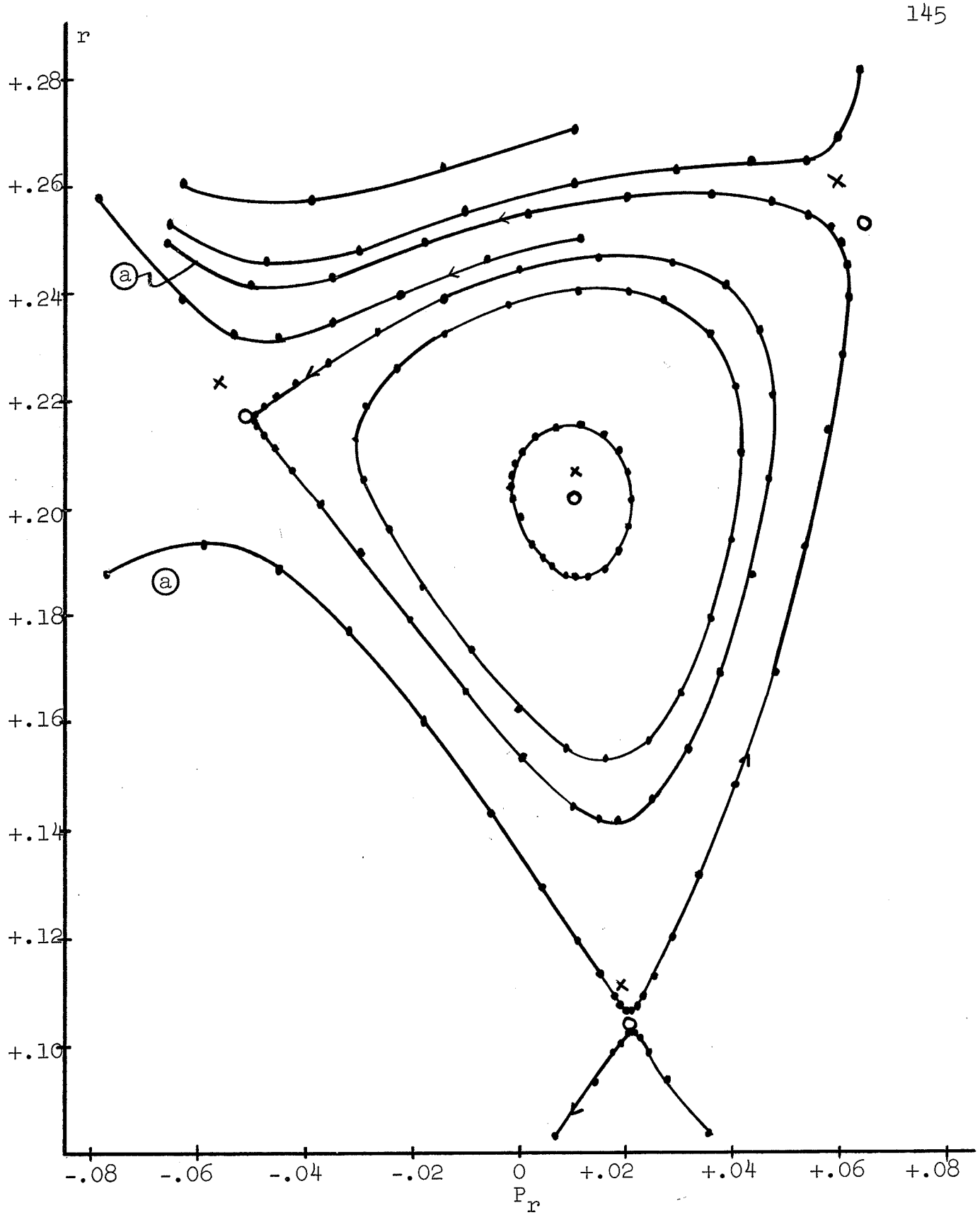

Figure 21a: Phase Plot for B26.29A with: $b_2 = +.020$, $\theta_2 = 0.$

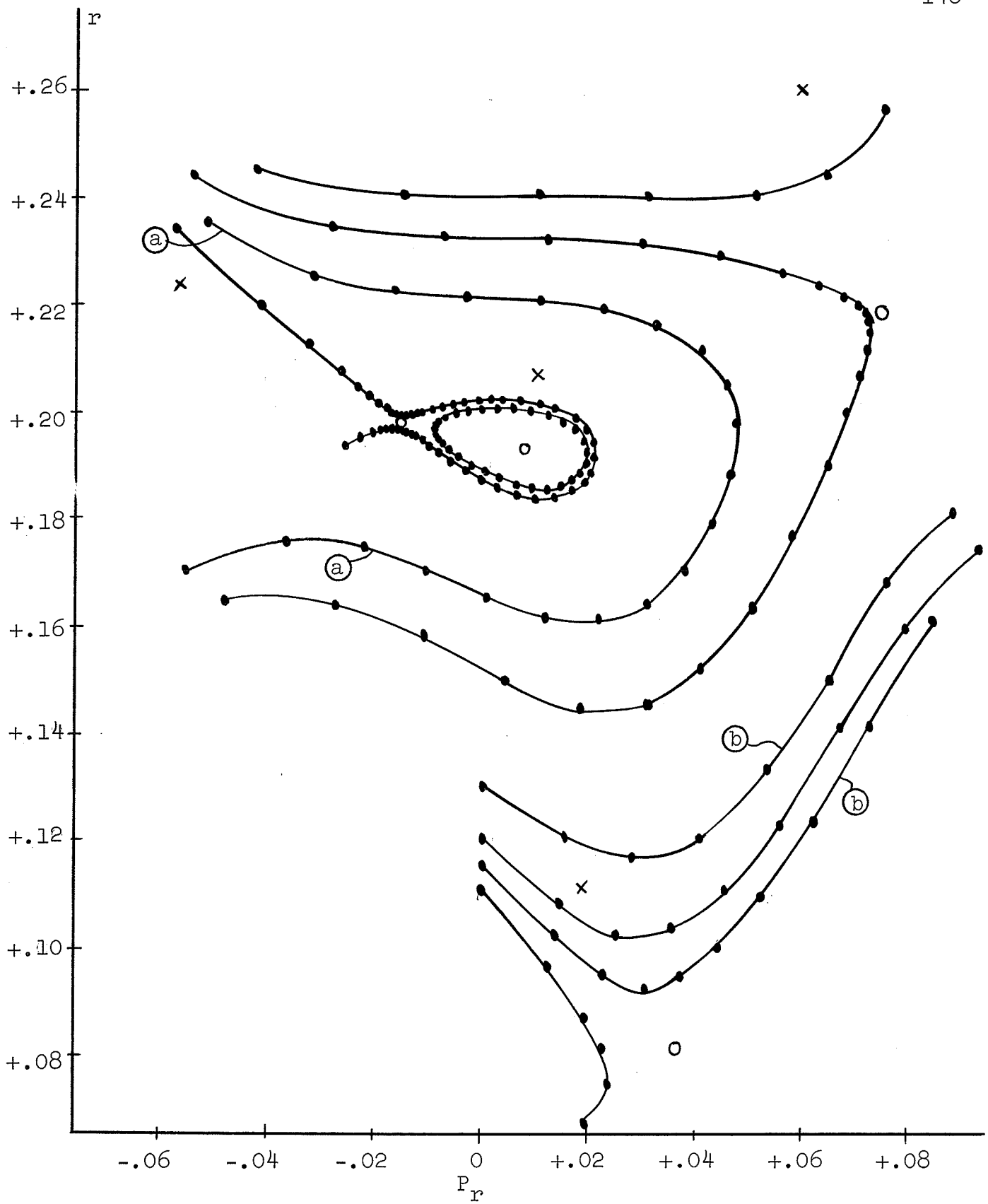

Figure 21b: Phase plot for B26.29A with: $b_2 = +.100$, $\theta_2 = 0.$

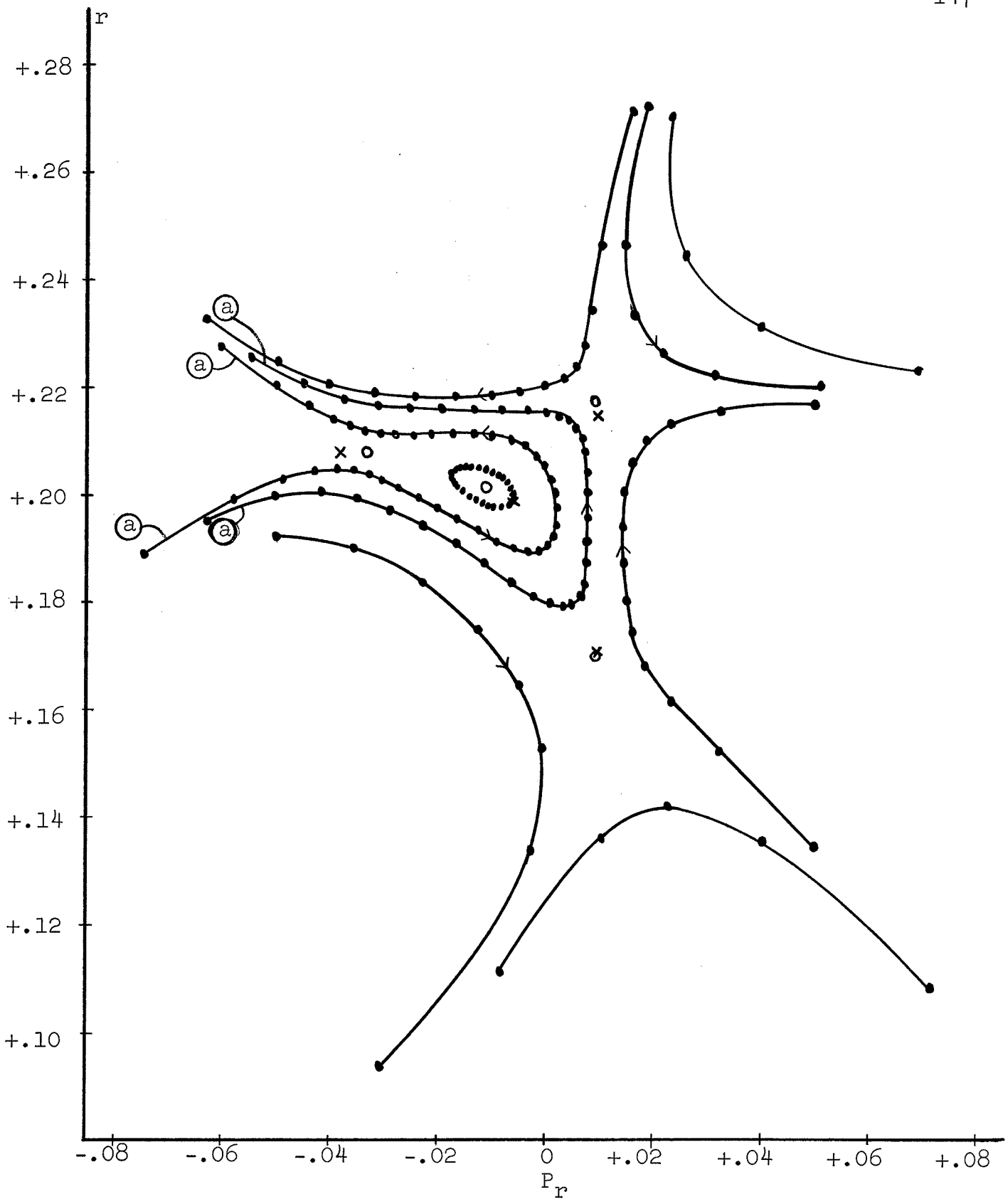

Figure 22: Phase plot for B26A1 with: $b_4 = +.040$, $\theta_4 = 0$.

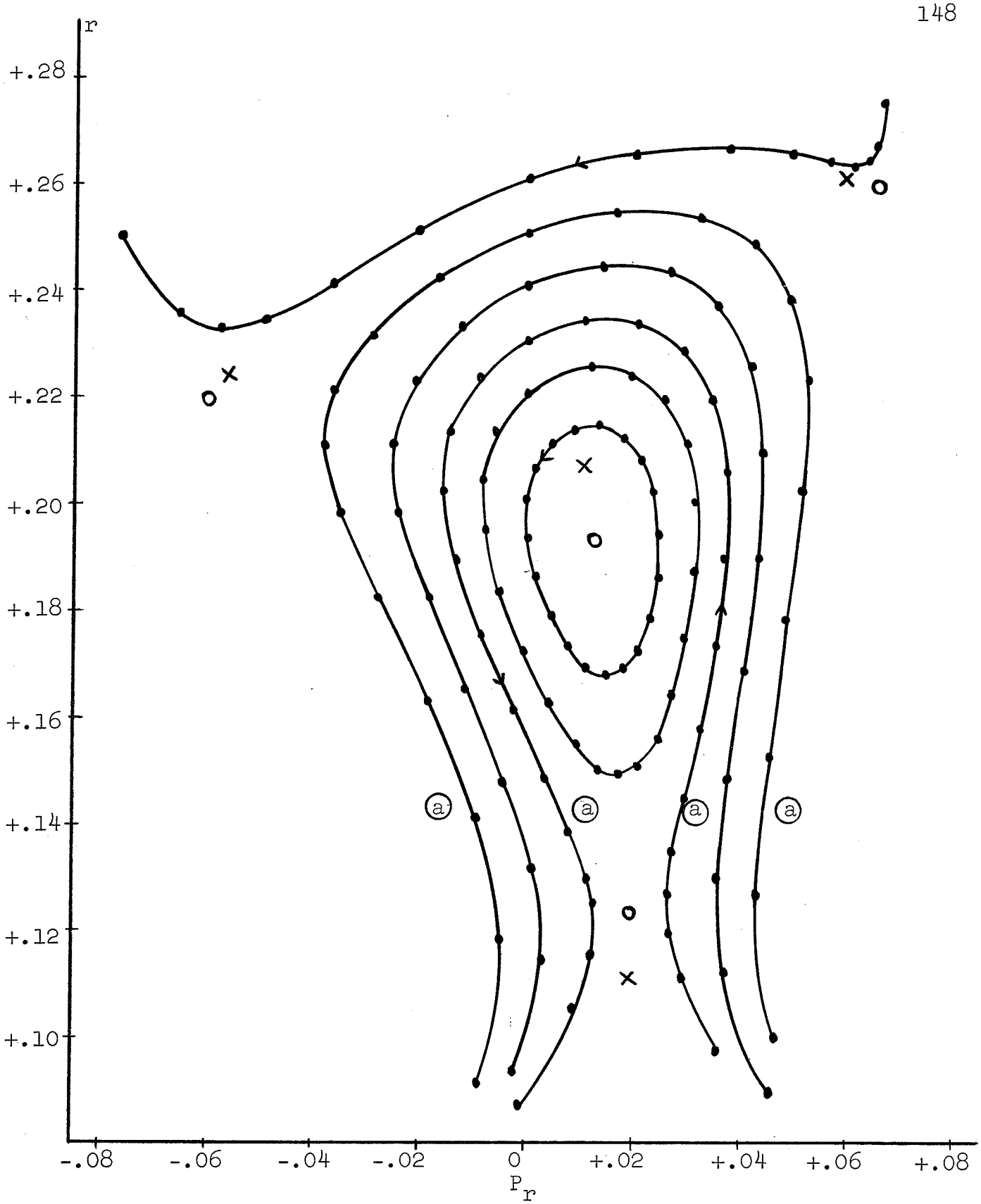

Figure 23a: Phase plot for B26.29A with: $b_4 = +.100$, $\theta_4 = 0$.

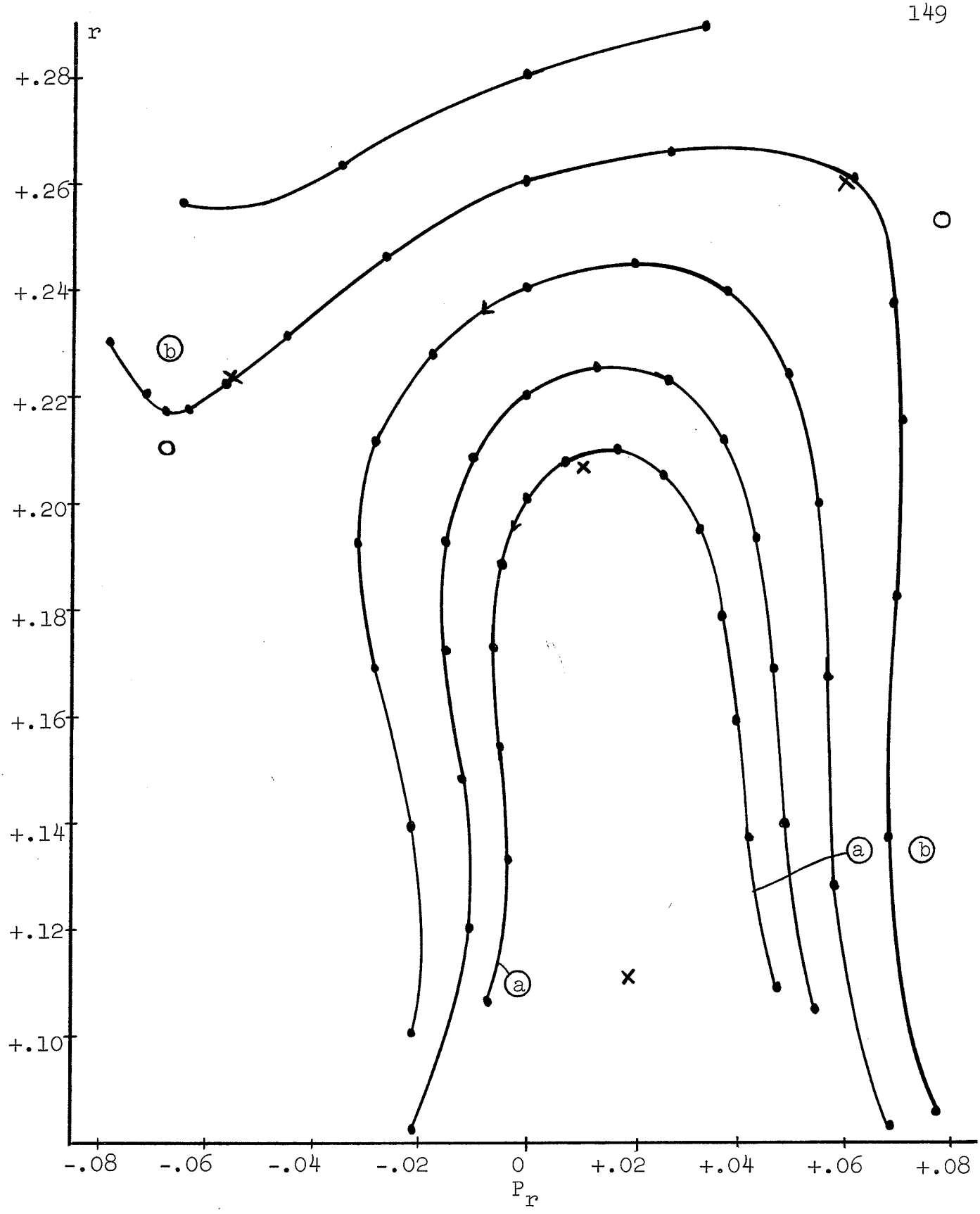

Figure 23b: Phase plot for B26.29A with: $b_4 = +.300$, $\theta_4 = 0$.

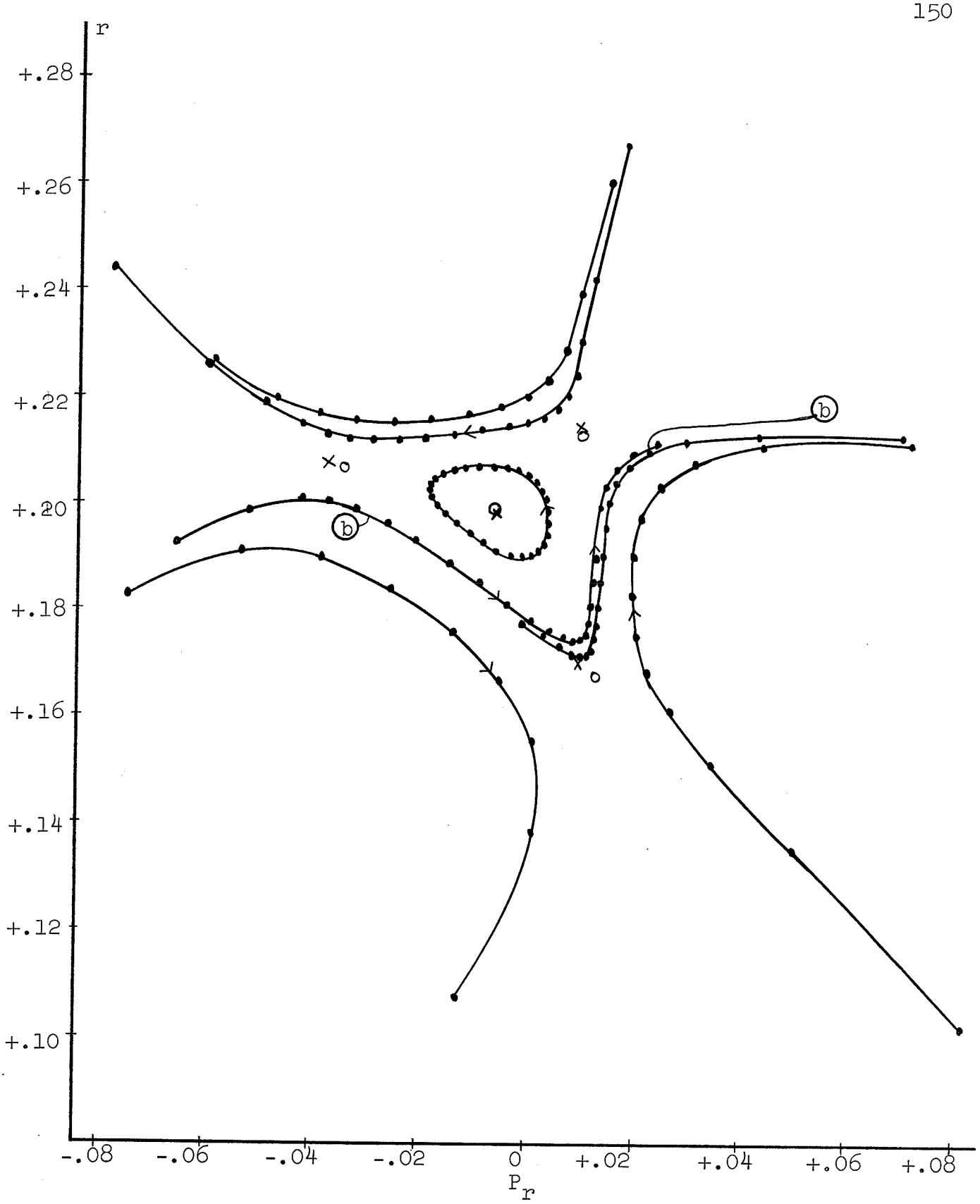

Figure 24a: Phase plot for B26A1 with: a = +.10, θ_2 = 0.

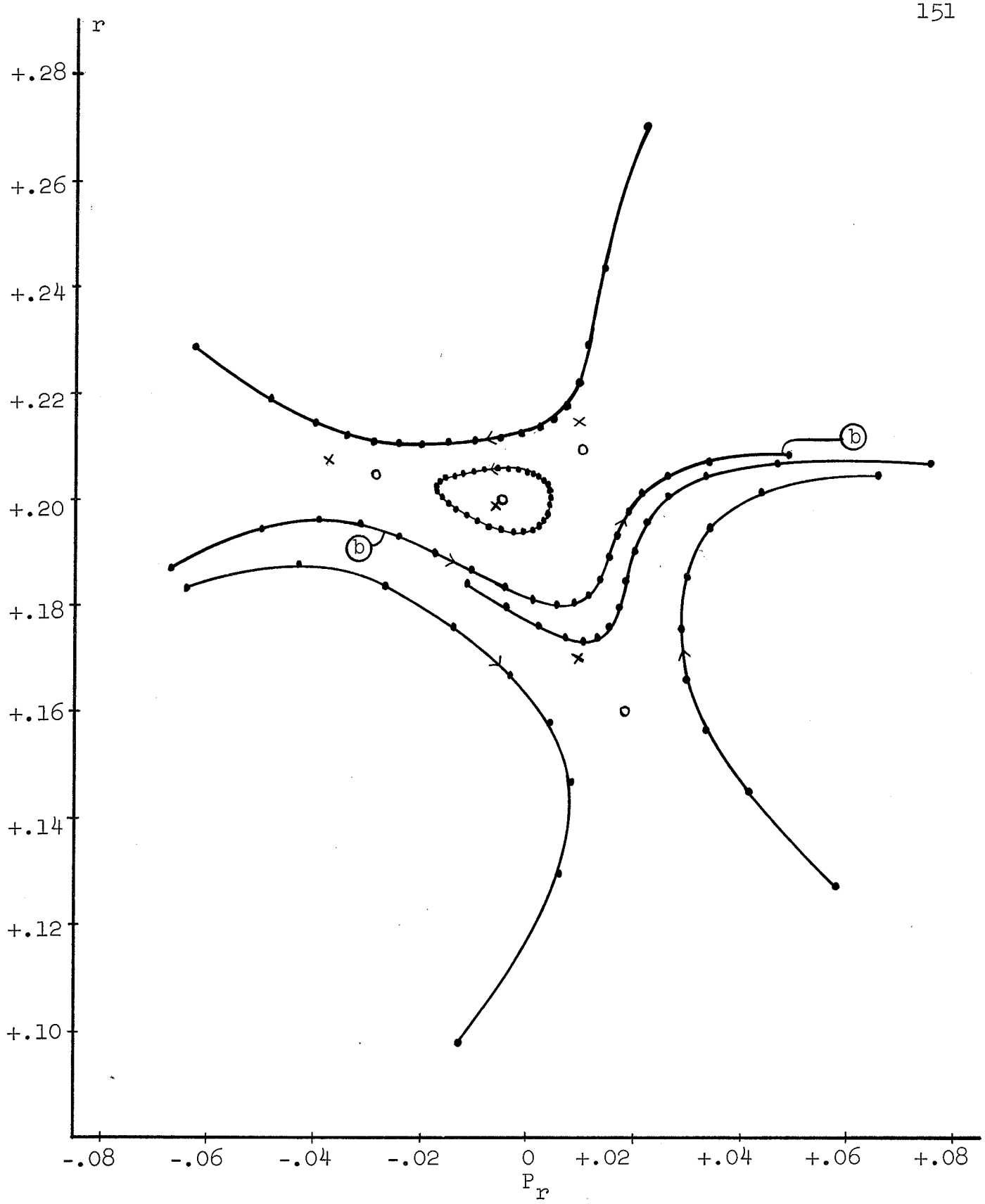

Figure 24b: Phase plot for B26A1 with: a = +.30, θ_2 = 0.

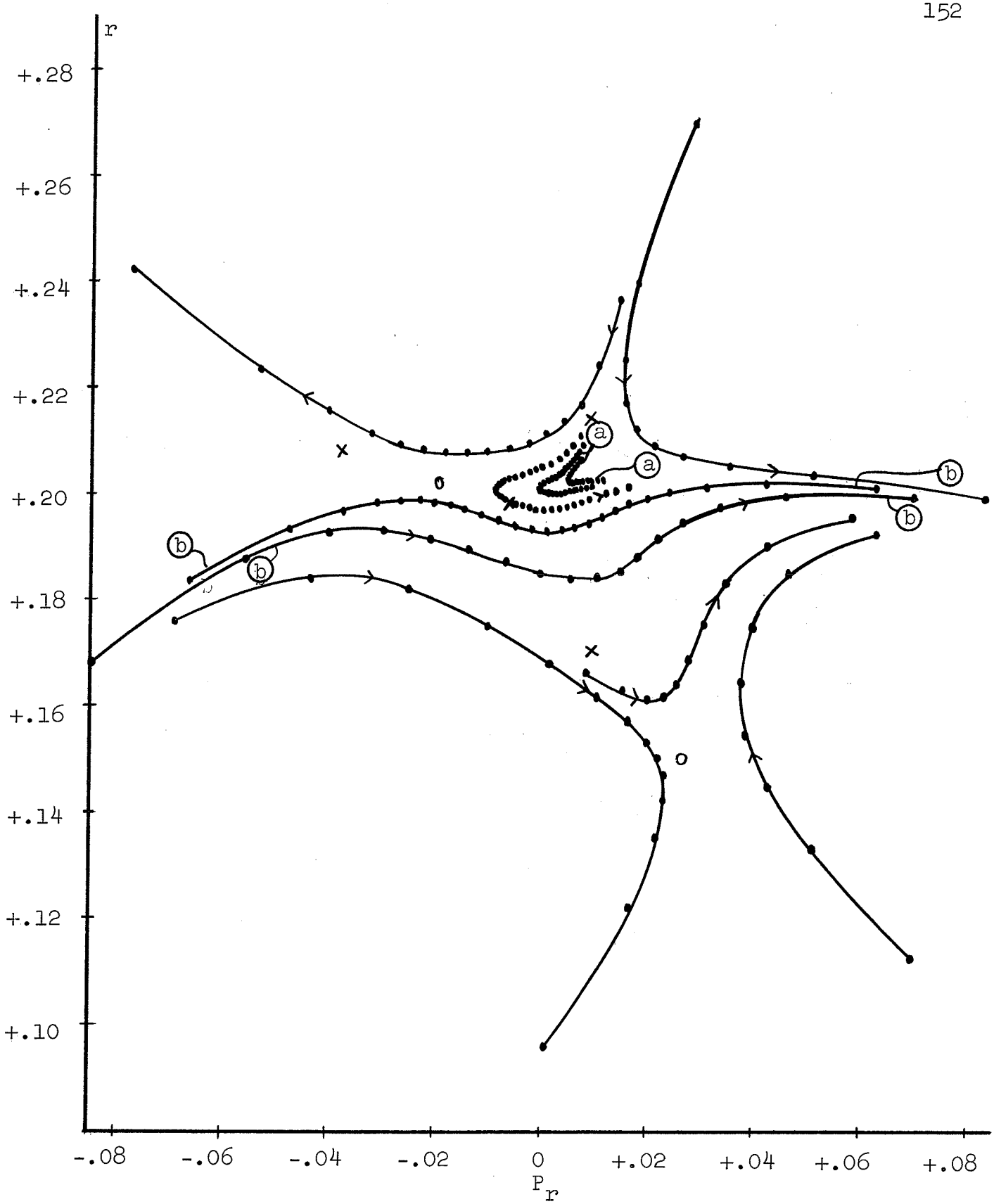

Figure 24c: Phase plot for B26A1 with: a = +.60, θ_2 = 0.

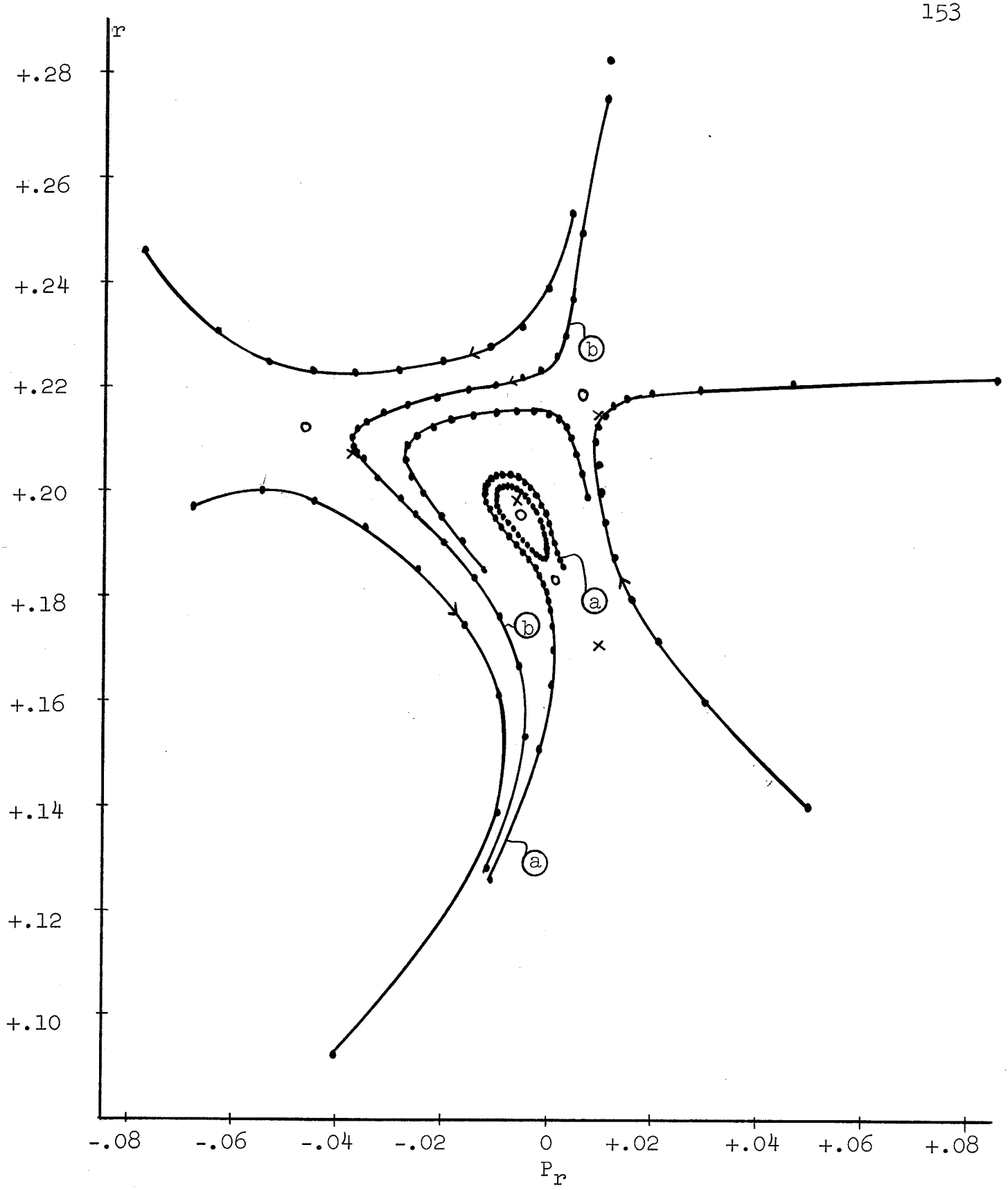

Figure 24d: Phase plot for B26A1 with: a = -.30, θ_2 = 0.

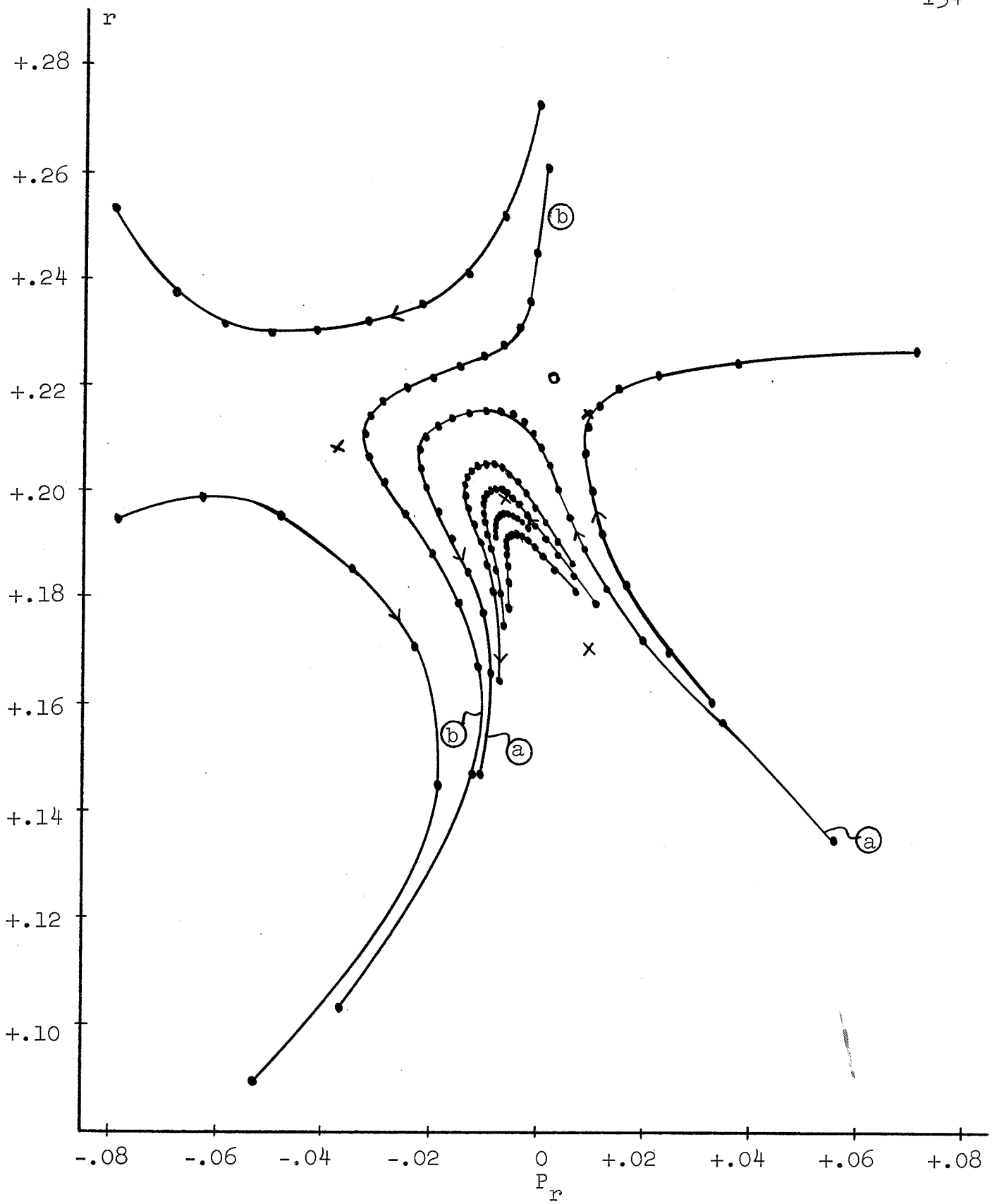

Figure 24e: Phase plot for B26A1 with: a = -.60, θ_2 = 0.

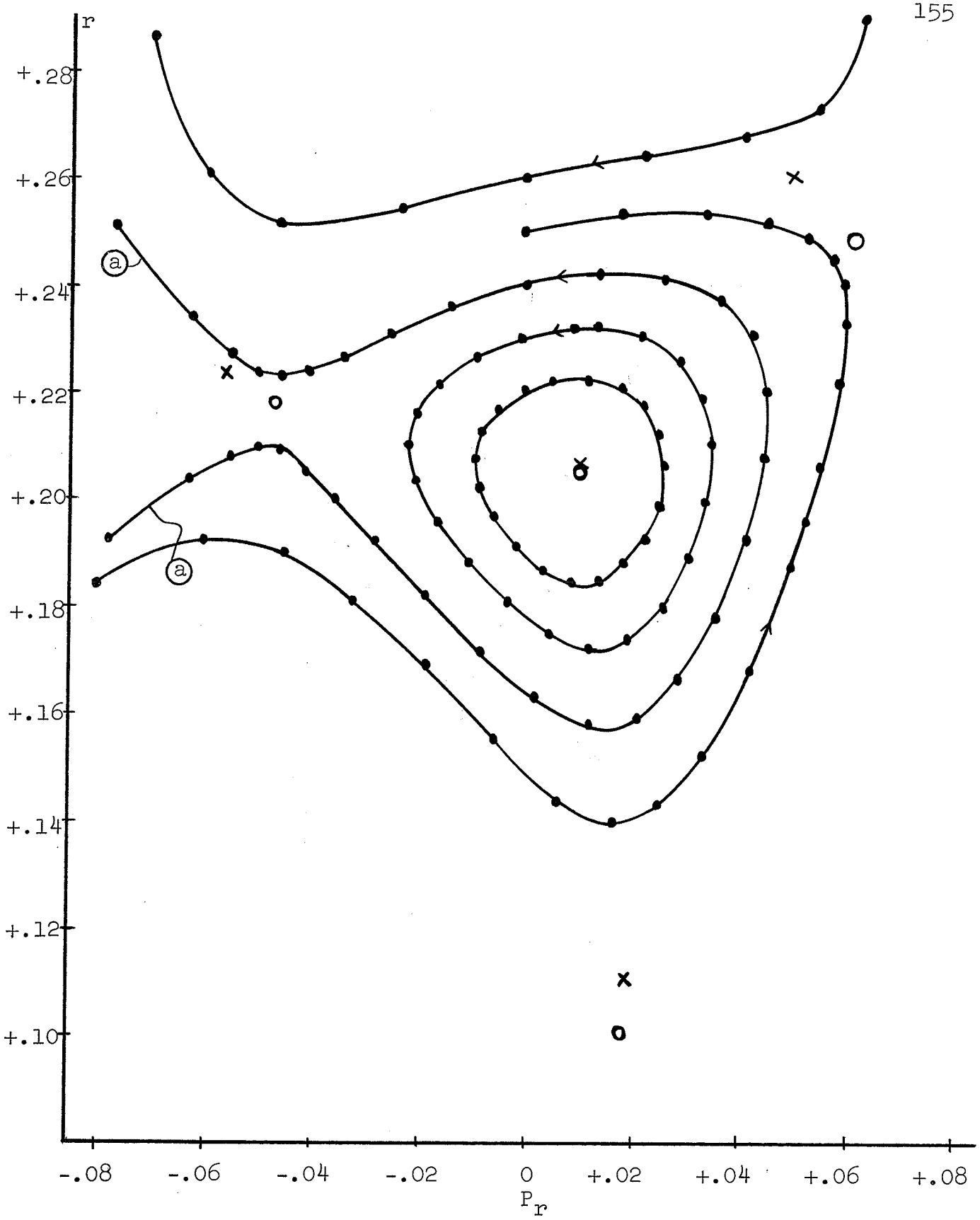

Figure 25: Phase plot of B26.29A with: a = +.30, θ_2 = 0.

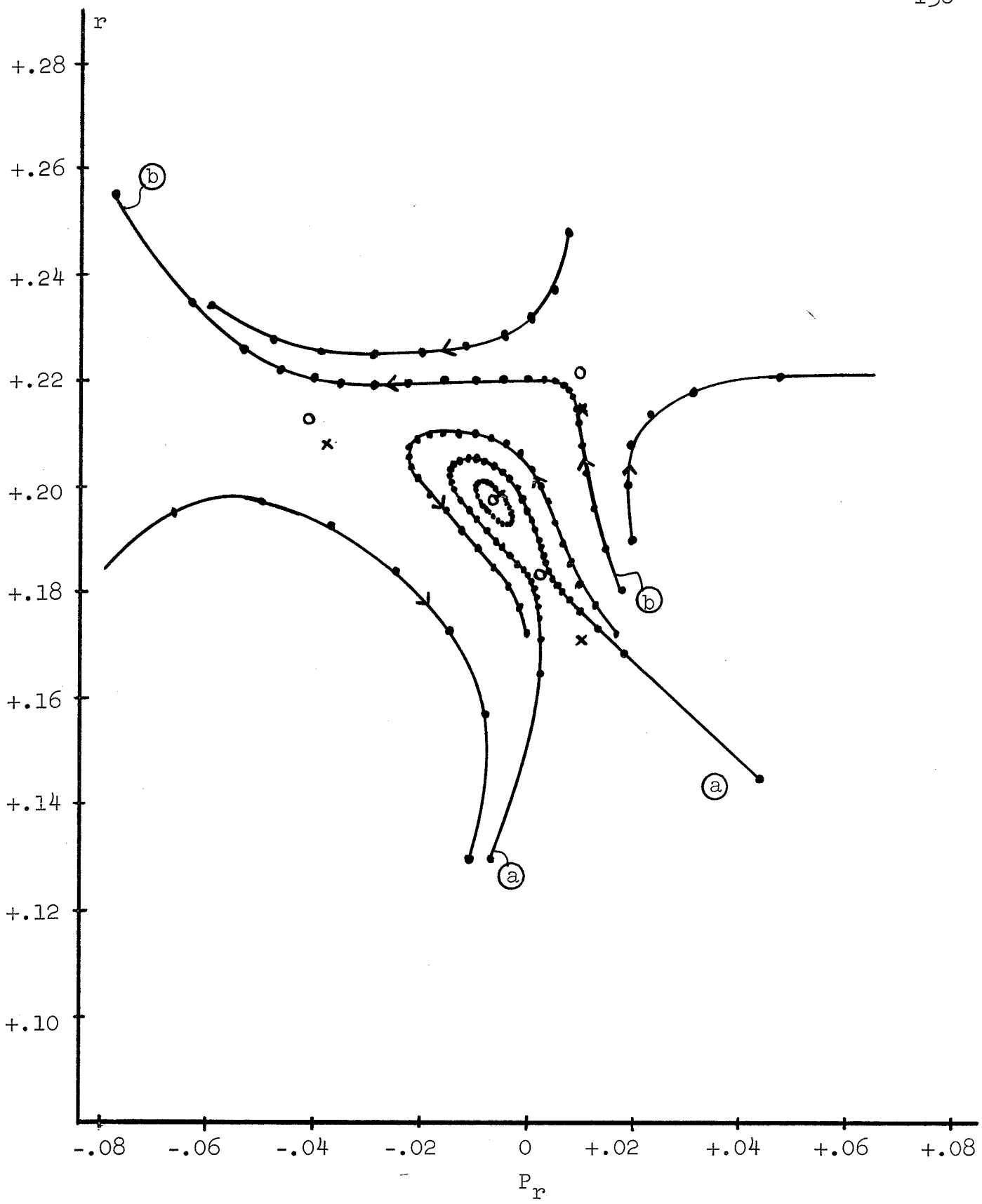

Figure 26: Phase plot for B26A1 with: a = -.30, θ_2 = -12.5°.

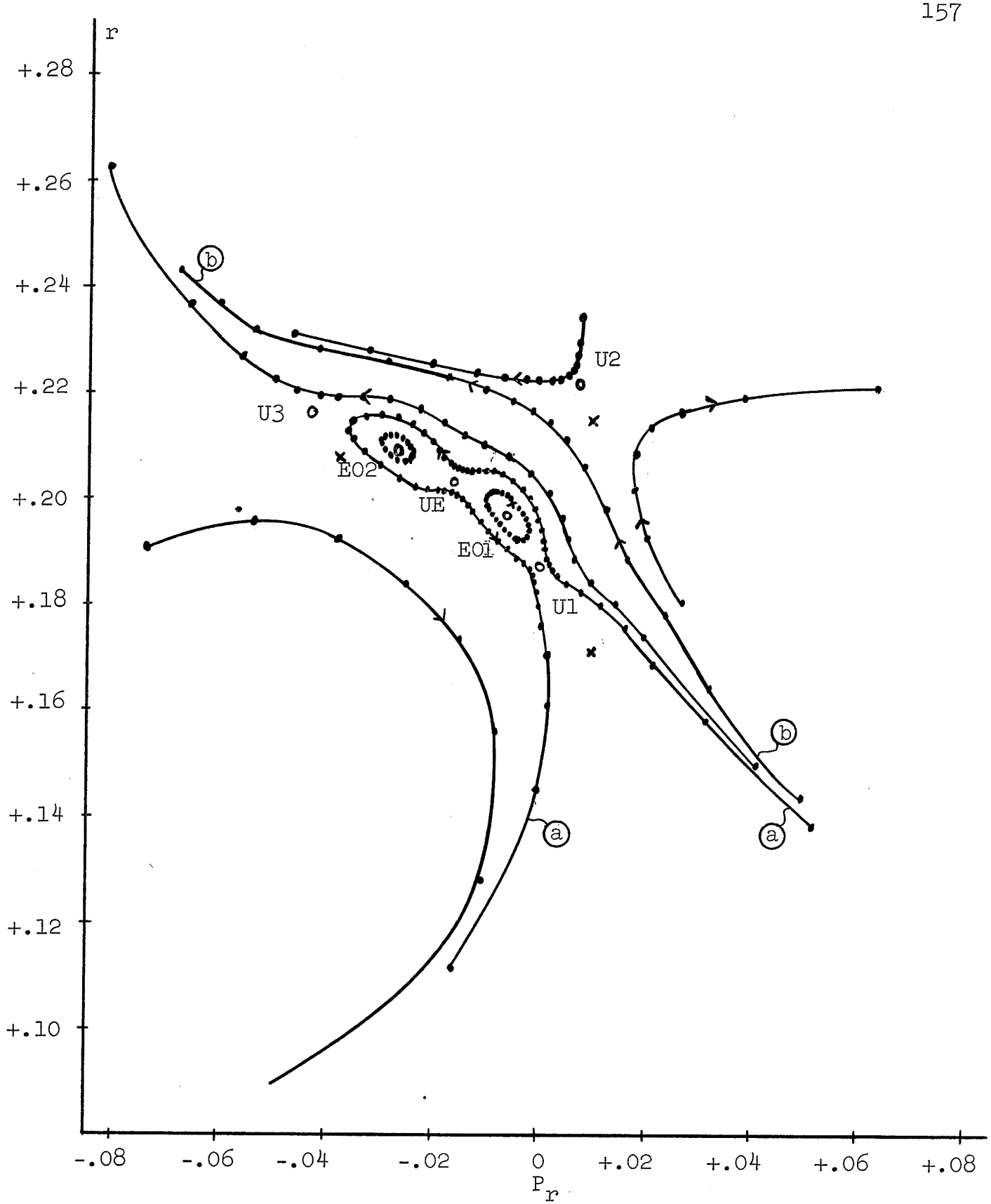

Figure 27: Phase plot for B26A1 with; a = -.30, θ_2 = -16.5°.

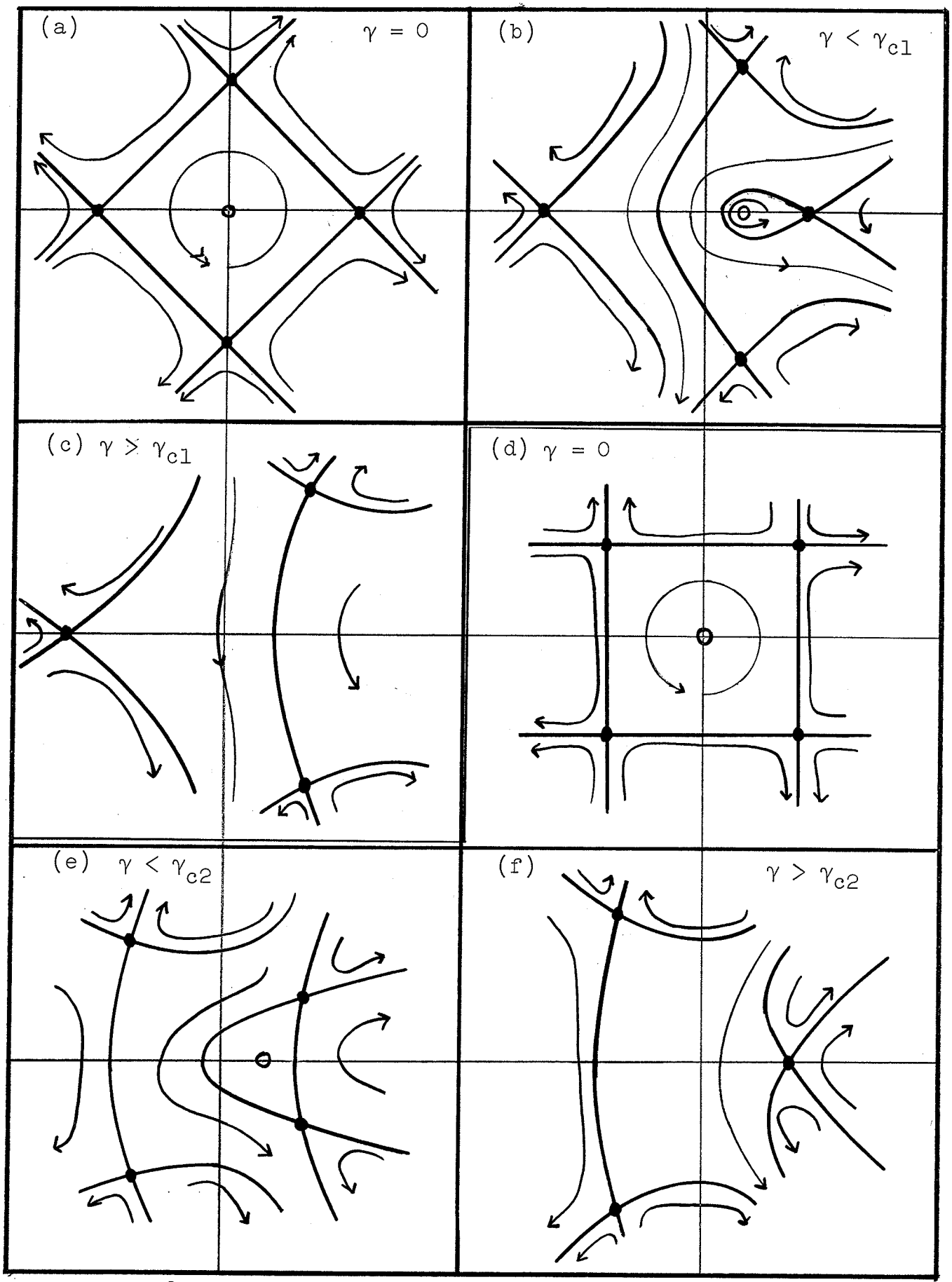

Figure 28: Evolution of four-sector phase plots with increasing one-sector perturbation: (a)-(c), $\phi_1 = \phi_o$; (d)-(f), $\phi_1 = \phi_o + 45°$.

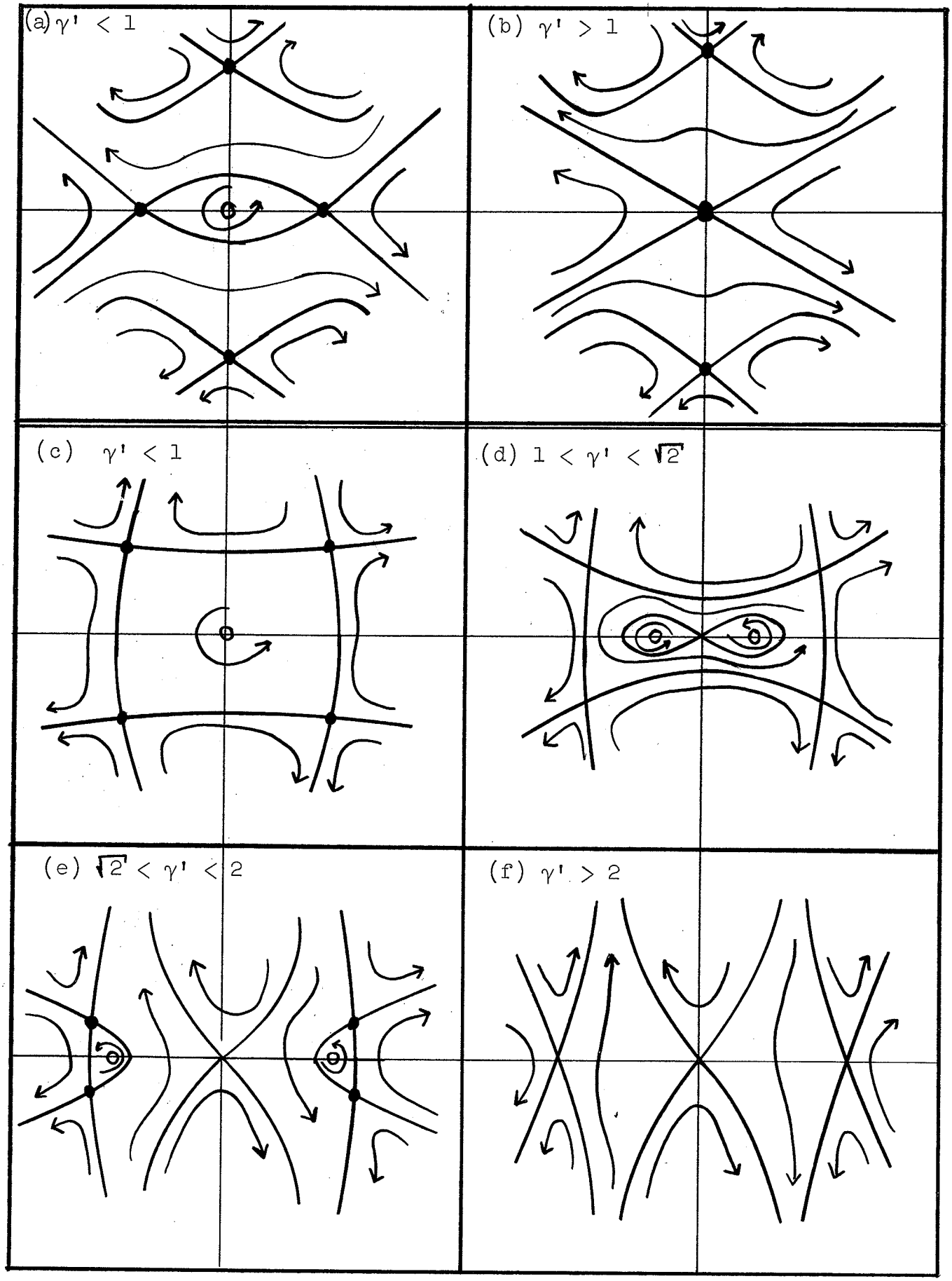

Figure 29: Evolution of four-sector phase plots with increasing two-sector gradient perturbation: (a)-(b), $\phi_2 = \phi_o$; (c) - (f), $\phi_2 = \phi_o + 45°$.

REFERENCES

[1] P.A. Sturrock, Annals of Physics 3 (1958), pp. 113-189.

[2] R. Hagedorn, M.G.N. Hine, and A. Schoch, CERN Symposium, Vol. I (Cern, Geneva, 1956), pp. 237-253.

[3] M.M. Gordon and T.A. Welton, Nuclear Instruments and Methods 6 (No. 3, 1960), pp. 221-233.

[4] P. Stähelin, Technical Report No. 1, Physics Department, University of Illinois, Urbana, Illinois.

[5] L. Smith and A.A. Garren, "Orbit Dynamics in the Spiral-Ridged Cyclotron," (Lawrence Radiation Laboratory, Berkeley, Jan. 12, 1961).

[6] N.F. Verster and H.L. Hagedoorn, Nat. Lab., Verslag Nr.3623 (Philips Res. Lab., Eindhoven-Netherlands 1960).

[7] L. Smith, Sector-Focused Cyclotrons NAS-NRC 656 (Washington: National Academy of Sciences-National Research Council, 1959), pp. 45-47.

[8] H.G. Blosser, Sector-Focused Cyclotrons NAS-NRC 656 (Washington: National Academy of Sciences-National Research Council, 1959), pp. 59-65.

[9] L.J. Laslett and K.R. Symon, "Computation Results Pertaining to Use of Time-dependent Magnetic Field Perturbation to Implement Injection or Extraction in a FFAG Synchrotron" (MURA, Madison, Wisconsin).

[10] L.J. Laslett and S.J. Wolfson, MURA-497, Aug. 17, 1959.

[11] M.M. Gordon, Bulletin of the American Physical Society Vol. 5 (series 2, Jan. 27, 1960), pp. 37.

[12] H.G. Blosser and M.M. Gordon, MSUCP-9 (Michigan State University Publication, Jan. 1961).

[13] T.K. Khoe, Report TKK-2, (Argonne National Laboratory, Argonne, Illinois, April 7, 1961).

[14] L. Teng, Proceedings of 1961 International Conference on High Energy Accelerators (to be published).

[15] H.G. Blosser, "Summary of Model Magnet and Orbit Study Results for University of Michigan 83" Cyclotron" (unpublished report, Michigan State University 1961).

[16] H.G. Blosser and D.A. Flanigan, MSUCP-5, (Michigan State University Publication, October 1960).

[17] T.I. Arnette, MSUCP-10, (Michigan State University Publication, September 1961).

[18] M.M. Gordon and T.A. Welton, ORNL-2765, (Oak Ridge National Laboratory, September. 1959).

[19] Mrs. R.D. Spence (unpublished report, Michigan State University, 1960).

[20] T.I. Arnette and T.A. Welton (private communication).

[21] M.M. Gordon and H.G. Blosser, MSUCP-7 (Michigan State University Publication, September 1961).

[22] H. Margenau and G.M. Murphy, The Mathematics of Physics and Chemistry (second edition; Princeton: D. Van Nostrand Co., 1956), pp. 80-81.

[23] S. Steinberg (private communication).